Summer 2011

Hardened concrete properties and durability assessment of high volume fly ash concrete

Kyle Marie Marlay

Department:

HARDENED CONCRETE PROPERTIES AND DURABILITY ASSESSMENT OF HIGH VOLUME FLY ASH CONCRETE

by

KYLE MARIE MARLAY

A THESIS

Presented to the Faculty of the Graduate School of the

MISSOURI UNIVERSITY OF SCIENCE AND TECHNOLOGY

In Partial Fulfillment of the Requirements for the Degree

MASTER OF SCIENCE IN CIVIL ENGINEERING

2011

Approved by

Jeffery S. Volz, Advisor
John J. Myers
David Richardson

ABSTRACT

Concrete is produced more than any other material in the world. Sustainable construction is extremely important in today's industry and fly ash is the leading material for sustainable concrete design. The addition of fly ash improves many fresh and hardened concrete properties. However, the slow hydration process associated with fly ash makes the use of the material in large amounts undesirable in conventional construction. This study evaluated the hardened concrete and durability performance of several high-volume fly ash (HVFA) concrete mixes.

The various HVFA concrete mixes evaluated within this study consisted of 70 percent replacement of portland cement by weight of cementitious material and water-to-cementitious ratios (*w/cm*) ranging from 0.30 to 0.45. Studies were conducted on hardened properties including: compressive strength, flexural strength, splitting tensile strength, and modulus of rupture. A shrinkage analysis was also performed to evaluate drying and free shrinkage. The durability performance of the HVFA concrete was also evaluated.

Results obtained from the tests revealed that compressive strengths of HVFA concrete are comparable to portland cement concrete with a reduced *w/cm*. Also, a reduction in concrete shrinkage was observed for HVFA concrete. The durability testing showed HVFA concrete increased the corrosion resistance and decreased the chloride penetration. Finally, existing relationships for hardened material properties and durability of conventional concretes are applicable to HVFA concretes.

ACKNOWLEDGMENTS

First and foremost, I would like to thank my advisor Dr. Jeffery S. Volz, for the time and effort in which he has spent in making this research endeavor as successful as it is today. I respect his professional understanding of not only my own, by my team's research material and all the guidance he has provided. I would like to express great gratitude of his character and personality, for it truly has made my graduate experience at Missouri S&T wonderful.

I would like to thank Ameren UE in Labadie, Missouri for financially supporting this project in which I was able to take part in. I have greatly enjoyed the experience and the knowledge gained from this project.

I would like to thank the members of my committee, Dr. John J. Myers and Dr. David Richardson, for their guidance and the time in which they had spent reviewing my thesis.

I would like to thank John Bullock, Jason Cox, Michael Lusher, Carlos Ortega, Michael Wolfe, Mark Ezzell, Lindsey Chaffin, and Krista Porterfield for their assistance in constructing, testing, maintaining and all processes in between with my specimens when I was unable to do so.

The best for last, I would like to thank my parents, Jerry and Leanne, and younger sister Alexis, for the love and encouragement they have shown me throughout my life. Without their support I would not have been as successful and proud of myself as I am today for my accomplishments.

Kyle Marie Marlay

TABLE OF CONTENTS

LIST OF ILLUSTRATIONS

Page

LIST OF TABLES

Page

1. INTRODUCTION

1.1. BACKGROUND, PROBLEM, & JUSTIFICATION

Concrete is produced more than any other material in the world. It is used in many applications such as road, dams, bridges, and buildings because of its versatility, strength, and durability. Fly ash from coal-burning electric power plants became readily available in the 1930s. Around that same time in the United States, studies began on use of fly ash in hydraulic cement concrete. In 1937, results of research on concrete containing fly ash were published [Davis et al., 1937]. This work served as the foundation for early specifications, methods of testing, and use of fly ash.

The production of portland cement, the binder in concrete, requires significant energy and emits enormous amounts of carbon dioxide (CO_2) as well as numerous other pollutants. The construction industry currently uses fly ash to partially replace cement, but only at modest levels ranging from 15 to 30 percent [Hopkins et al., 2003]. Using fly ash more frequently or in larger amounts, such as in high-volume fly ash (HVFA) concretes, would reduce the environmental impacts of concrete production.

Aside from the environmental standpoint of fly ash, this material has undergone extensive studies to better understand chemical compositions and reactions. Using fly ash to reduce CO_2 emissions and energy consumption when producing concrete are great advantages, but from a construction and fresh/hardened property perspective, this material requires some special consideration due to its inherent natures. Fly ash is generally a low reactive material compared to portland cement, thus requiring some additional curing time for adequate strength gain. The addition of chemical admixtures or activators assist in initiating the hydration process allowing for a shorter curing period, while still gaining sufficient strength. Further studies using HVFA concrete, consisting of greater than 50 percent fly ash replacement, are showing positive results in terms of strength and durability. Fly ash concrete is proving to be a viable contender to conventional concrete.

Although fly ash is a recycled material, it not only decreases the environmental footprint of concrete, but can have other characteristic benefits when used as a cement replacement in concrete. Fly ash is now used in concrete for many reasons, including:

improvements in workability of fresh concrete, reduction in temperature rise during initial hydration, improved resistance to sulfates, reduced expansion due to alkali-silica reaction, and increases in durability and strength of hardened concrete [Huffman, 2003].

1.2. OBJECTIVES & SCOPE OF WORK

The main ***objective*** of this study is to illustrate the behavior of hardened properties and to characterize the relative corrosion resistance of high-volume fly ash (HVFA) concrete compared to that of conventional concrete.

The following scope of work was implemented in an effort to attain this objective: (1) review applicable and relevant literature; (2) develop a research plan; (3) evaluate the hardened properties of several high-volume fly ash concrete mixes; (4) evaluate the corrosion resistance performance of the above concrete mixes with embedded reinforcement through designing, constructing, and monitoring of several reinforced concrete ponding specimens; (5) verify the validity of using the current hardened property tests on high-volume fly ash concrete; (6) quantify the high-volume fly ash concrete's ability to resist the onset of corrosion when subjected to a chloride induced environment; (7) conduct a forensic investigation upon the reinforced concrete ponding specimens; (8) analyze the information gathered throughout the testing to develop findings, conclusions, and recommendations; and (9) prepare this thesis in order to document the findings of information obtained during the study.

1.3. RESEARCH PLAN

The research plan entailed investigating concrete mixture proportioning with portland cement and various amounts of fly ash, ultimately developing a mix design to be tested that is categorized as high-volume fly ash, as described in Section 3. A number of hardened concrete property tests were completed to evaluate the performance of the high-volume fly ash concrete mix and determine the validity of using these tests to predict the performance of concretes containing high volumes of fly ash. Shrinkage specimens were also constructed to evaluate the shrinkage of the high-volume fly ash concrete as the hydration period progressed.

Specimens were constructed to evaluate the concrete durability in terms of chloride penetration by electrical and ponding methods, freeze-thaw resistance, concrete resistivity, and corrosion potential. The HVFA concrete was compared against the portland cement concrete to better understand the effects each test had on the HVFA concrete. A forensic evaluation of steel reinforcement was also performed on those specimens containing steel reinforcement to further identify the validity of using concrete resistivity and corrosion potential on HVFA concrete.

1.4. OUTLINE

This thesis consists of six sections and three appendices. Section 1 briefly explains the industry history of using fly ash and common benefits for its implementation in concrete design. Also within Section 1 are the objectives, scope of work, and research plan.

Section 2 summarizes the origin and properties of fly ash and in such applications the advantages from an environmental standpoint. Also discussed are the processes by which steel corrodes within concrete, methods that are commonly used to evaluate the condition of the steel embedded in concrete, and the test that may be used to evaluate the durability in terms of concrete resistivity of a high-volume fly ash cementitious material. Lastly, Section 2 consists of the background and correlation on using hardened concrete property testing to evaluate high-volume fly ash concrete mixes and the basis of modifying the standard shrinkage test that predicts shrinkage.

Section 3 explains the composition and chemical attributes of the Class C fly ash used. Also within Section 3 are the methods and procedures used to determine applicable high-volume fly ash concrete mix designs to be used for subsequent testing.

Section 4 pertains to hardened property tests including; compressive strength, flexural strength, modulus of rupture, modulus of elasticity and shrinkage. Each section within Section 4 covers specimen details, test procedures, results, and findings.

Section 5 explains the several methods used to evaluate the durability of HVFA concrete. Specimen details and testing procedures are also included. Evaluation of durability resilience is also discussed.

Section 6 restates the findings that were established during the course of the study that leads to the conclusions and recommendations presented therein.

There are three appendices contained within this thesis. Appendix A contains additional information associated with the hardened concrete property testing. Appendix B contains test data related with the shrinkage analysis performed for evaluating concrete shrinkage of the high-volume fly ash concrete mixes. Appendix C contains additional information, test data, and photographs associated with the durability tests.

2. LITERATURE REVIEW

Concrete is produced more than any other material in the world. It is used in many applications such as road, dams, bridges, and buildings because of its versatility, strength, and durability. Fly ash from coal-burning electric power plants became readily available in the 1930s. Around that same time in the United States, studies began on use of fly ash in hydraulic cement concrete. In 1937, results of research on concrete containing fly ash were published [Davis et al., 1937]. This work served as the foundations for early specifications, methods of testing, and use of fly ash.

2.1. FLY ASH

Fly ash is an incombustible byproduct from burning coal mainly in electric generating power plant facilities. The most common production of fly ash is from a dry-bottom boiler which burns pulverized coal. In this process, about 80 percent of all ash leaves the furnace as fly ash and is entrained in the flue gas. The fly ash is then collected in hoppers by means of an electrostatic precipitator as shown in Figure 2.1 or a mechanical precipitator. Both collection processes can generate fineness, density, and carbon content variations in the fly ash from hopper to hopper. Although, typical particle size can range from 0.00004 in. (1 μm) to more than 0.008 in. (200 μm) and density of individual particles from less than 62.4 lb/ft^3 (1000 kg/m^3) hollow spheres to more than 187 lb/ft^3 (3000 kg/m^3), coal burned from a uniform source generally produces very consistent fly ash [Huffman, 2003]. A more homogenous material is created when the hoppers are emptied and the fly ash is conveyed to storage.

2.1.1. Chemical Composition and Reactivity. Since, the composition of fly ash is controlled primarily from the source of coal, there are two types of fly ash generated for concrete, Class C and Class F. Class F fly ash is derived from bituminous coals and Class C fly ash is derived from sub-bituminous coals. The formation of the fly ash particles comes from the high temperatures caused by the combustion which liquefies the incombustible minerals. Rapid cooling as the minerals leave the boiler causes the glassy structure of spherical particles to form [Huffman, 2003]. Fly ash primarily consists of silica (SiO_2), alumina (Al_2O_3), iron (Fe_2O_3), and calcium (CaO) with smaller amounts of

magnesium, sulfates and other compounds. The greater amount of silica alumina, calcium in Class C fly ash is what mainly sets these types apart. Other differences include higher amounts of alkalis and sulfates in Class C fly ash. The combination of silica, alumina and iron must exceed 70 percent to be classified as Class F fly ash and the combination must only exceed 50 percent to be classified as Class C fly ash according to ASTM C618 [2004] "Coal Fly Ash and Raw or Calcined Natural Pozzolan for Use in Concrete". Table 2.1 shows the percentage by weight of chemical variations between bituminous (Class F) and sub-bituminous (Class C) fly ash.

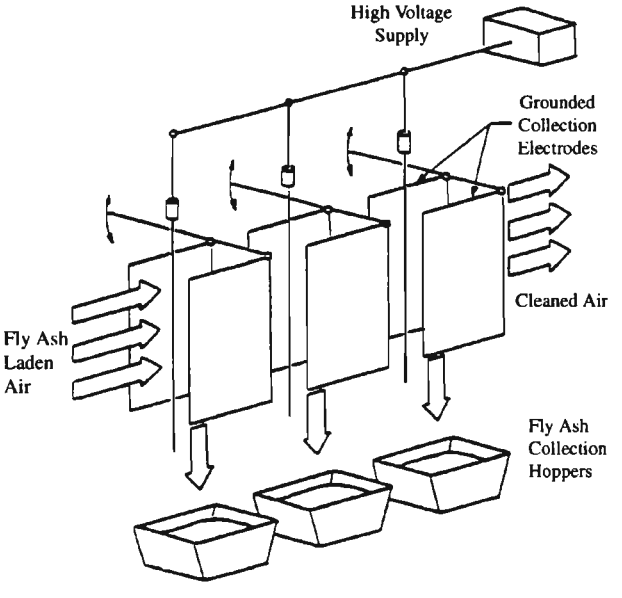

Figure 2.1: Electrostatic precipitator fly ash collection process [Huffman, 2003].

Fly ash is defined as a pozzolanic material, "a siliceous or siliceous and aluminous material that in itself possesses little or no cementitious value but that will, in finely divided form and in the presence of moisture, chemically react with calcium

hydroxide at ordinary temperatures to form compounds having cementitious properties; there are both natural and artificial pozzolans" [Huffman, 2003]. The use of fly ash proves beneficial in combination with portland cement concrete. As normal hydration occurs in a portland cement concrete mix, the hydrates as previously mentioned, will react with the calcium hydroxide, thus producing additional cementitious material in the hardened concrete. Reaction will continue to occur as long as calcium hydroxide and water is present in the pore fluid of the cement paste. At lower water-to-cement ratios (less than 0.40 by mass), it is indicated there will be more voids available during reactions [Philleo, 1991].

Table 2.1: Fly ash chemical differences expressed as percent by weight [Office, 1997].

Component	*Class F (Bituminous)*	*Class C (Sub-bituminous)*	*Lignite*
SiO_2	20 – 60	40 – 60	15 – 45
Al_2O_3	5 – 35	20 – 30	10 – 25
Fe_2O_3	10 – 40	4 – 10	4 – 15
CaO	1 – 12	5 – 30	15 – 40
MgO	0 – 5	1 – 6	3 – 10
SO_3	0 – 4	0 – 2	0 – 10
Na_2O	0 – 4	0 – 2	0 – 6
K_2O	0 – 3	0 – 4	0 – 4
LOI	0 – 15	0 – 3	0 – 5

Fly ash has been found to produce very little immediate chemical reaction when mixed with water and will increase when additional alkali, calcium hydroxides or sulfates are available for reaction. This leads to a reduced amount of heat produced initially during the hydration process when fly ash is combined with portland cement. Studies have shown that hydration reactions can vary ranging from the chemical composition to

the morphology of fly ash particles and the fineness of particles to the water-to-cement ratio. Predicting concrete performance solely through characterization of fly ash is difficult and it is suggested that acceptability be investigated by trial mixtures of concrete containing fly ash and taken in regard to workability, strength characteristics, and durability [Huffman, 2003].

2.1.2. Physical Properties. As with any material used in concrete, the shape, size, particle-size distribution, and even density influence the properties of freshly mixed, unhardened concrete, the strength development, and other properties of hardened concrete. As previously mentioned, fly ash properties can vary based on the combustion process used or the coal being burned. Color variations are also another aspect in physical properties. While color is of no engineering concern, unless aesthetics is a consideration, this can indicate changes in the carbon content, iron content, burning conditions, and coal source. These color indicators can be useful in detecting possible fly ash property variances.

Fly ash consists largely of glassy spheres that can be solid or hollow and slightly to highly porous. Figure 2.2 shows a microscopic view of fly ash particles. Reactivity of fly ash is highly dependent on the glass content and glass composition. Smaller amounts of calcium present from bituminous coals versus larger amounts of calcium present from sub-bituminous coals are the major difference of the fly ash glass composition. The fineness of individual particles also affects the reactivity and performance in concrete. Porous particles are more prevalent in a coarse fly ash and are less reactive than a finer fly ash with particle sizes ranging from 5 to 30 micron. Coarse fly ash is generally from a mechanical separator whereas an electrostatic precipitator collects finer fly ash particles [Huffman, 2003].

2.1.3. Effects of Fly Ash in Concrete. The use of fly ash in combination with portland cement in producing concrete is not uncommon to the industry and has been a practice for nearly 100 years. Using fly ash in concrete has grown dramatically over the years and the United States alone currently is estimated usage somewhere in excess of 6 million tons per year. Due to this increase, extensive applied and fundamental research has been performed to support that appropriate uses of fly ash in concrete can result in technical and economic benefits. Currently a limitation of fly ash amounts in concrete is

set by the American Concrete Institute (ACI) Building Code [ACI 318, 2008], allowing only a maximum of 25 percent by mass of total cementitious material. Even with this limitation applied to the concrete and construction industry, researchers are investigating the possibilities of concrete designed with larger amounts of fly ash. It is suggested that concrete with a minimum of 50 percent by mass of total cementitious material is considered a high-volume fly ash (HVFA) concrete [Hopkins, 2003]. When concrete begins to exceed the allowable 25 percent and beyond to greater than 50 percent, concrete characteristics differs from portland cement concrete and may require special consideration.

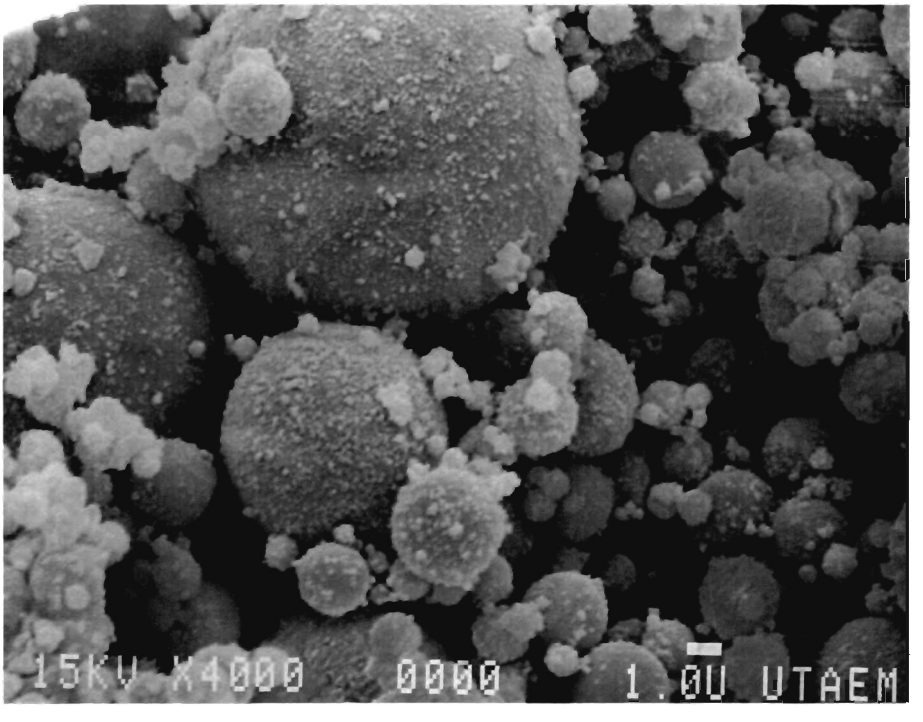

Figure 2.2: Fly ash at 4000x magnification [Huffman, 2003].

As fly ash is used as a replacement and/or additional material the paste volume will increase for a given water content. Typically an increase in paste volume will produce greater plasticity and better cohesiveness. The shape of the fly ash particles is what really makes this material advantageous in concrete. Workability can greatly be increased as the water-to-cement ratio is reduced; the fly ash particles act as "ball bearings" making the concrete more fluid-like. Improved pump ability will also result with the use of fly ash. This may be desirable for such placement of concrete. Finishing, however, has slight effects from the use of fly ash in concrete. Due to the chemical composition of fly ash, as previously mentioned, a slower rate of hydration will occur, which in turn causes a slower setting time. Concrete of this nature should be finished at a later time to avoid possible surface weaknesses [Huffman, 2003]. Not only does fly ash ensue slower setting, stickiness and consequent difficulties in finishing may also be apparent as a result of the increased fines in the concrete.

Compressive strength is nearly the most important attribute when it comes to evaluating properties of concrete. Form removal and construction progress depends largely on the concrete strength gained by certain days. The slow rate of hydration of HVFA concrete has the tendency to affect the compressive strength at 3 or 7 days. By using accelerators, activators, water reducers, or by changing the mixture proportions, equivalent 3 or 7 day strength may be achieved [Bhardwaj, 1980]. Increased early strengths can also be achieved by reducing the water-to-cement ratio to nearly 0.30. After the rate of strength gain of hydraulic cement slows, the continued pozzolanic activity of fly ash provides strength gain at later ages if the concrete is kept moist; therefore, concrete containing fly ash with equivalent or lower strength at early ages may have equivalent or higher strength at later ages than concrete without fly ash. This strength gain will continue with time and result in higher later-age strengths [Huffman, 2003].

Concrete is a porous material and therefore permeable to water. Many factors affect permeability including: cementitious material, water content, aggregate gradation, and consolidation to list a few. Calcium hydroxide present during the hydration process of concrete may leach out of hardened concrete, leaving voids for the penetration of water. The pozzolanic properties of fly ash, chemically combines with calcium

hydroxide and water to produce C-S-H, which reduces the possibility of leaching calcium hydroxide. Additionally, the prolonged hydration of fly ash enhances the pore structure of the concrete reducing the possible ingress of water containing chloride ions. The leaching of calcium hydroxide to the surface of concrete can also cause an external reaction between the calcium hydroxide and carbon dioxide in the air forming calcium carbonate ($CaCO_3$). This reaction is the formation of efflorescence, a white discoloration on the concrete [Huffman, 2003]. Since fly ash is used to reduce permeability and maintain a high- alkaline environment, as a result, efflorescence is reduced. However, it has been stated that certain Class C fly ashes of high-alkali and sulfate contents can increase efflorescence.

2.1.4. Sustainability. Fly ash is a byproduct from burning coal and thus is considered a recyclable resource. Current production of conventional concrete consumes large quantities of raw materials and the principle binder, cement, contributes significantly to carbon dioxide emissions and energy consumption. Also, longevity of a structure is an important sustainable design consideration. The Environmental Protection Agency (EPA) states that green building complements the classical building design concerns: economy, utility, durability, and comfort. The use of fly ash in concrete addresses such sustainability issues making it a viable contender to cement in the concrete industry.

Despite the economic and environmental advantages of using fly ash it still suffers from impacts brought on by changing environmental regulations. It is suggested that nitrous oxide emissions contribute to the production of acid rain and that nitrous oxide emissions be reduced. Nitrous oxide reduction systems have had a negative impact on the utilization of fly ash due to increased amounts of unburned carbon and other chemical residuals left in the ash. These systems reduce the burning temperature and also reduce the excess oxygen. Such change in the coal burning process greatly affects the characteristics of the fly ash. Lower burning temperatures can affect the particle-size distribution, particle morphology, glass content, and composition of fly ash. However, depending on the combustion modification systems used, effects can vary from significant to negligible.

2.2. CORROSION OF STEEL IN CONCRETE

When steel is embedded in concrete there is a dense, impenetrable film known as a "passive" layer to provide protection against corrosion. The "passive" layer is established and maintained in high alkali environments, such as concrete, which prevents further corrosion of steel. Concrete contains high concentrations of soluble calcium, sodium and potassium oxides within the pore structure. Those concentrations within the pore structure form hydroxides which cause the highly alkali environment of the material when water is present. Despite the regenerating process, this passive layer is still susceptible to damage, allowing corrosion to penetrate the embedded steel [Broomfield, 2007]. Destruction of the passive layer occurs when a sufficient amount of chlorides are located at the steel-concrete interface and/or when the concrete at a depth equal to that of the embedded steel becomes carbonated.

2.2.1. Carbonation. Interaction between carbon dioxide gas contained in the atmosphere and alkaline hydroxides in the concrete form carbonation, which is carbonic acid (H_2CO_3). Carbonic acid is formed when carbon dioxide gas (CO_2) diffuses through concrete and dissolves within its pore solution:

$$CO_2 + H_2O \rightarrow H_2CO_3 \tag{1}$$

The diffusion of carbon dioxide through concrete closely follows that of Fick's first law of diffusion and can be approximated by:

$$\frac{dx}{dt} = \frac{D_o}{x} \tag{2}$$

where x is the distance to the surface, t is time, and D_o is a diffusion coefficient that accounts for the quality of the concrete [Broomfield, 2007]. The carbonic acid is not an attacking substance, but simply neutralizes the alkaline environment of the concrete by reacting with available calcium hydroxide ($Ca(OH)_2$) within the pore solution forming calcium carbonate ($CaCO_3$):

$$H_2CO_3 + Ca(OH)_2 \rightarrow CaCO_3 + 2H_2O \quad (3)$$

Calcium hydroxide helps to maintain the pH level, which is typically between 12 and 13, to prevent corrosion. This additional calcium hydroxide comes from within the concrete and dissolves into the surrounding pore solution. Eventually all the calcium hydroxide reacts and the pH level begins to drop. Once the pH level falls and the passive layer can no longer be maintained, the steel becomes prone to corrosion. Carbonation damage progresses most rapidly in low concrete cover areas of the reinforcing steel and in very porous concrete structures.

2.2.2. Chloride Attack. There are several sources in which chlorides are introduced into concrete. Chlorides cast into the concrete can originate from calcium chloride (CaC_{l2}), a chemical admixture used to accelerate the hydration of portland cement, the use of seawater, or contaminated aggregates. Chlorides are more commonly from external sources which diffuse into concrete, such as seawater and deicing salts. A large portion of the chlorides that are cast into concrete will react with tricalcium aluminate ($Ca_3A_{l2}O_6$ or C_3A), a compound within portland cement, to form chloroaluminates. As chloride ions contribute towards the destruction of the passive layer, the reaction removes those chloride ions from the concrete's pore solution. However, carbonation of concrete is known to break down these chloroaluminates, which in turn releases the bound chlorides into the concrete's pore solution [Broomfield, 2007]. The chlorides, which were once bound, are now free to disseminate through the concrete and attack the passive layer. This action is similar to the chlorides that were externally introduced to the concrete.

Transport of externally generated chlorides through concrete is commonly carried out by three specific mechanisms: absorption/capillary action, permeation, and diffusion. Absorption is the initial process in which chlorides from saltwater are transported several millimeters below the concrete's surface when saltwater is placed upon dry concrete. Hydraulic pressure may cause further permeation of the chlorides into the concrete if there is an accumulation of water present on the surface of the concrete. When a chloride gradient exists within the concrete and pore solution is present, chloride ions may then

diffuse through the concrete following Fick's second law of diffusion, which is represented by Broomfield (2007) as:

$$\frac{C_{max} - C_d}{C_{max} - C_{min}} = \text{erf}\left(\frac{x}{\sqrt{4D_c t}}\right) \tag{4}$$

where variables within the error function (erf) correspond to the depth of C_d (x), time (t), and the concrete's diffusion coefficient (D_c). Variables C_{max} and C_{min} relate to the maximum and baseline chloride concentrations within the concrete, respectively. Variable C_d corresponds to the chloride concentration within the concrete at a certain distance (x) from the surface.

Chloride attack begins when unbound chloride ions reach the passive layer of an embedded bar and promote the release of ferrous (Fe^{2+}) ions by forming an iron-chloride complex ($FeCl_2$):

$$Fe^{2+} + 2Cl^- \rightarrow (FeCl_2) \tag{5}$$

As the complex migrates away from the steel it reacts with water (H_2O) molecules contained in the concrete's pores:

$$(FeCl_2) + 2H_2O \rightarrow Fe(OH)_2 + 2H^+ + 2Cl^- \tag{6}$$

This reaction causes the formation of ferrous hydroxides ($Fe(OH)_2$) and hydrogen (H^+) ions that locally reduce the pH of the pore solution surrounding the embedded bar, aiding in the destruction of the passive layer [Song et al., 2010]. This chemical reaction at the steel surface will infinitely reoccur as long as chloride ions are released back into the pore solution. However, as researched by Delbert A. Hausmann [Hausmann, 1967], the hydroxide ions within the concrete continually compete to repair the chlorides' attempt in the destruction of a passive layer.

Through mathematical calculations and laboratorial experiments involving bare steel bars contained in a simulated porous, chloride contaminated, concrete environment, Hausmann discovered that the chlorides' success in breaking down a passive layer depended upon the ratio of chloride ions to hydroxide ions at the steel-concrete interface. He concluded that the ratio of chloride ions to hydroxide ion had to be greater than 0.6 in order for the bar to actively corrode. This ratio corresponds to 0.4 percent chlorides by weight of cement when the chlorides are cast into the concrete during batching. This percentage decreases by 50 percent when the chlorides are introduced to the concrete through external sources [Broomfield, 2007].

2.2.3. Corrosion Process. Once the passive layer has been comprised, areas of corrosion will begin to appear on the surface of the steel. Corrosion from chloride attack or carbonation produces the same chemical reaction. The actual degradation of a bar takes place at an area known as the anode. Steel corrodes in concrete by dissolving in the pore water giving up electrons. The anodic reaction creates two electrons (2e-) that are released into the surrounding concrete. To maintain electrical neutrality the electrons must be consumed elsewhere on the surface of the steel.

$$Fe \rightarrow Fe^{2+} + 2e^{-} \tag{7}$$

The site at which the electrons are consumed is known as the cathode. The cathode reaction uses the electrons provided by the anode in addition to the consumption of water and oxygen (O_2), to create hydroxyl ions (OH^-):

$$2e^{-} + H_2O + \frac{1}{2}O_2 \rightarrow 2OH^{-} \tag{8}$$

Once formed, the hydroxyl ions flow through the concrete, back to a location near the anode, to react with the ferrous ions and initiate the formation of rust. When in contact with one another, the ferrous and hydroxyl ions react to form ferrous hydroxide ($Fe(OH)_2$):

$$Fe^{2+} + 2OH^- \rightarrow Fe(OH)_2 \quad (9)$$

Two additional reactions are required before the commonly seen red rust is created. First, the newly formed ferrous hydroxide reacts with water and oxygen to form ferric hydroxide ($Fe(OH)_3$):

$$4Fe(OH)_2 + O_2 + 2H_2O \rightarrow 4Fe(OH)_3 \quad (10)$$

Unhydrated ferric oxide (Fe_2O_3) has a volume of about twice that of the iron it replaces. Once hydrated, ferric oxide is known to have a volume that is typically six times that of the iron in which it had replaced [Broomfield, 2007]. The volume relationship between iron and other various forms of its oxides may be seen in Figure 2.3.

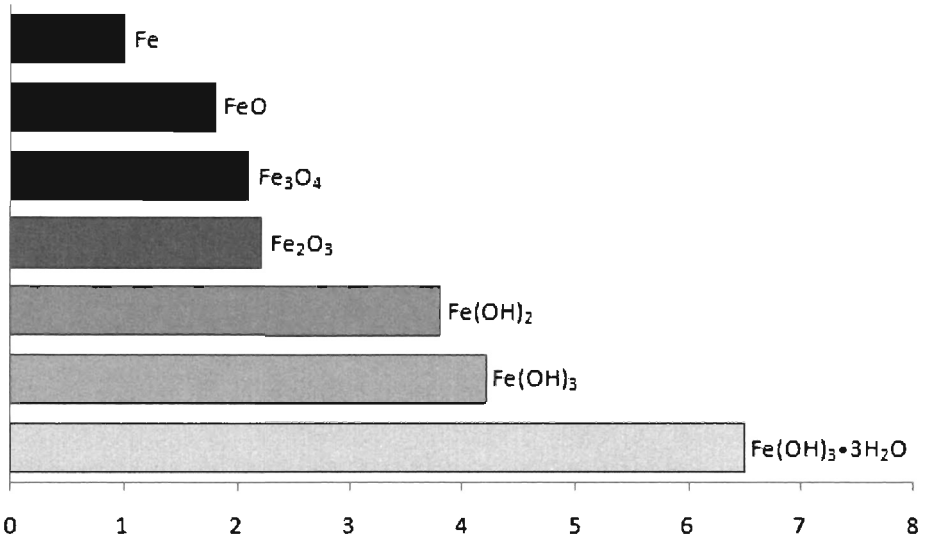

Figure 2.3: The relative volumes of various iron oxides from Mansfield (1981), Corrosion 37(5), 301-307.

As the volume at the steel-concrete interface increases, the tensile stresses formed within the concrete increase as well. Due to the corrosion forming, cracks and spalling will begin to appear along the surface of the structure. In some cases, spalling of the concrete may be observed. An alternative to the formation of red rust, known as black rust (Fe_3O_4), may form on the steel. Black rust is less expansive than red rust, as shown in Figure 2.3 and as a result no visual signs of cracking may be seen along the concrete surface.

Starvation of oxygen to the anode and distances of several hundred millimeters between the anode and cathode keeps the iron as Fe^{2+} and will stay in solution. Under these circumstances the steel is susceptible to corrosion, but no expansive forces will cause cracks and spalling and corrosion may not be detected [Broomfield, 2007]. Damaged waterproofing membranes placed along the surface of the concrete may cause a lack of oxygen within the concrete. Reinforcing steel embedded in marine structures are susceptible to black rust due to the continual saturation environment in which they are exposed.

2.3. CONDITION EVALUATION

This section addresses three procedures that are commonly used to evaluate the corrosion condition of steel embedded in concrete. Also discussed within the section are results and/or interpretation of each test and factors that may affect those outcomes.

2.3.1. Concrete Resistivity. Electrical resistivity is important as a measure of the ability of concrete to resist the passage of electrical current. Rate of corrosion on embedded reinforcing steel is dependent on the electrical resistivity of concrete. In turn, this relates electrical resistivity to the permeability of fluids and diffusion of chloride ions through concrete. Hydroxyl ions (OH^-) promote the corrosion process as long as there is an available source. The quicker the ions can flow from the cathode to the anode, the quicker the corrosion process may proceed, provided that the cathode is supplied with a sufficient amount of oxygen and water. The transport of electricity through concrete closely resembles that of ionic current; therefore it is possible to classify the rate of corrosion of a bar embedded within concrete by quantifying the electrical resistance of the concrete surrounding it [Whiting and Nagi, 2003].

Many factors have affects on concrete's electrical resistivity. In the consideration and evaluation of the study conducted on concrete resistivity it is significant to make note of two effecting factors: water-to-cement ration and the addition of fly ash. The water-to-cement ratio is inherently the most important of all parameters in controlling the performance of concrete. The microstructure development of the cement paste and the ionic concentration of its pore solution are highly dependent on the water-to-cement ratio. Monfore (1968) has studied the relationship between the water-to-cement ratio and resistivity in cement paste and has found an increase in resistivity of cement paste as the water-to-cement ratio decreases. Case in point, a water-to-cement ratio of 0.40 has a resistivity of about twice that of paste having a water-to-cement ratio of 0.60. Although this evaluation of resistivity was conducted on paste and it should be noted that concrete made of the same paste is higher [Whiting and Nagi, 2003].

Technology for field concrete resistivity measurements is currently available by means of using one of the three following methods: single-electrode method, two-probe method, or the four-probe method. Of the three methods, the two-probe is the least accurate and at times the most labor intensive [Broomfield, 2007]. The two-probe resistivity meter operates by measuring the potential between two electrodes while an alternating current is passed from one electrode to the other. Significant limitations arise from the errors that may occur through measurements. Aggregate has a higher resistivity than the surrounding microstructure; therefore, aggregate near the location of the electrode can produce a reading much higher than the actual concrete resistivity. It has also been indicated that 90 percent of the resistivity reading represents an area with a diameter equivalent to 10 times the contact radius of the electrode tip [Whiting and Nagi, 2003]. In an attempt to achieve a more accurate reading, the two electrodes may be placed within shallow pre-drilled holes [Broomfield, 2007], making the two-probe method more labor intensive.

The single-electrode method is a newer, more advanced method in measuring a concrete's resistivity. The single-electrode method is based on using a small metallic disc placed on the concrete surface as an electrode and a steel reinforcing bar as a counter-electrode. This method specifically measures the resistance of the concrete cover by applying the following equation:

$$\text{Resistivity } (\Omega\,\text{cm}) = 2RD \tag{12}$$

where R is the iR drop between the rebar cage and the surface electrode and D is the surface electrode's diameter. This method is susceptible to contact resistance problems and is most accurate when the surface electrode is placed between embedded bars as opposed to directly over them [Broomfield, 2007].

Originally developed in 1916 by Frank Wenner, the four-probe method was initially designed for geophysical studies. The method has been adopted for field use and today the four-probe method (or Wenner method) is the most widely used and researched method for in-situ evaluation of concrete resistivity. The four probe resistivity meter, also known as the Wenner probe, contains four equally spaced electrodes that are positioned within a straight line. The two outer electrodes send an alternating current through the concrete while the inner electrodes measure the drop in potential. The resistivity is then calculated using the following equation:

$$\rho = \frac{2\pi sV}{I} \tag{13}$$

where ρ is the resistivity (Ωcm) of the concrete, s is the spacing of the electrodes (cm), V is the recorded voltage (V), and I is the applied current (A).

As the applied current passes through the concrete it travels in a hemispherical pattern as shown in Figure 2.4. An immediate advantage of the four-probe method over the two-probe method is the concrete area between the inner electrodes that is measured for resistivity. This allows for a larger area to be measured and also avoids the influence aggregate may have on readings.

As with any method used to measure concrete resistivity there are factors that influence errors in readings recorded. The four-probe method is based on the theory that resistivity values obtained from equation (13) are accurate if current and potential fields exist in a semi-infinite volume of material [Whiting and Nagi, 2003]. This also implies structures with larger dimensions will have more accurate resistivity readings. It has also been found that measuring thin concrete or near edges produce significant errors and is

recommended that spacing between electrodes not exceed ¼ of the minimum concrete section dimensions.

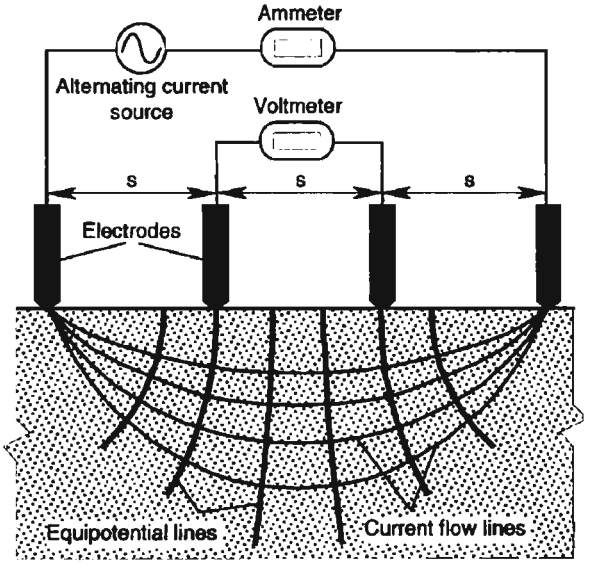

Figure 2.4: Schematic representation of the four-probe resistivity method [Broomfield, 2007].

Another assumption associated with the four-probe Wenner method is the type of material tested. The material is assumed to be homogenous, which concrete is not and would otherwise be believed to affect the electrical resistivity measurements. The non-homogenous nature of concrete is defined by a high-resistivity aggregate surrounded by low-resistivity cement paste. This effect can be alleviated by increasing the spacing between the inner electrodes and research has found that increasing the spacing greater than 1.5 times the aggregate maximum size will not exceed a coefficient of variation in resistivity measurements of 5 percent [Whiting and Nagi, 2003].

The presence of steel is an important factor influencing the electrical resistivity of reinforced concrete. Measurements taken directly over reinforcement show the significance reinforcement can have on errors. The reinforcing steel provides a 'short circuit' path and may give misleading readings. It is suggested the errors in measurements can be minimized if measurements are taken between bars or perpendicular to the bar [Broomfield, 2007].

In 1987, Langford and Broomfield first published a relationship between the corrosion rate for a depassivated steel bar embedded within a concrete of known resistivity, as may be seen in Table 2.2. Since then Broomfield further claimed that a concrete resistivity of greater than 100 kΩcm will essentially prevent any steel reinforcement from corroding [Broomfield, 2007]. The information gathered by Richard Stratfull, during his 1957 field investigation of San Francisco's San Mateo-Hayward Bridge, was compared alongside additional information that was collected while monitoring the bridge after his initial study. The results showed that areas along the structure which reported resistivity values between 50 and 70 kΩcm possessed reinforcement that was corroding at a very low (almost negligible) rate [Sengul and Gjørv, 2009]. Today, Table 2.2 has been widely accepted as a quick and approximate way to correlate the rate at which a depassivated steel bar corrodes in a concrete of known resistivity.

Table 2.2: Correlation between concrete resistivity and the rate of corrosion for a depassivated steel bar embedded within the concrete [Broomfield, 2007].

Concrete Resistivity	*Rate of Corrosion*
> 20 kΩcm	Low
10-20 kΩcm	Low to Moderate
5-10 kΩcm	High
< 5 kΩcm	Very High

2.3.2. Corrosion Potential Measurements. As was stated earlier, the corrosion process is dependent upon the ability of steel to dissolve into the surrounding concrete upon the availability of oxygen and water at the steel-concrete interface. The standard reference electrode or half cell is a simple device consisting of a piece of metal in a fixed concentration solution of its own ions, such as copper in saturated copper sulfate. When this half cell is connected to another metal in solution of its own ions, such as iron in $Fe(OH)_2$, the measurement is the potential difference between the two 'half cells'. Rebar within concrete has anodic (corroding) areas and cathodic (passive) areas. The two cells are connected to an embedded steel bar using a high impedance voltmeter, as shown in Figure 2.5, which allow the measurement of the corrosion risk when the external reference electrode of copper/saturated copper sulfate is moved along the surface of the concrete. Establishing this corrosion cell, the ferrous ions may be released into the concrete, while the electrons created during the reaction are free to travel to the reference electrode (via wiring) where a reduction reaction may occur.

The voltmeter reads a voltage as electrons travel from the steel to the reference electrode. If the section of steel beneath a copper/copper sulfate electrode (CSE) is still protected by the passive layer, a voltage reading above -200 mV will be indicated on the voltmeter, according to Broomfield [2007]. A reading between -200 mV and -350 mV means the passive layer is damaged or has begun to breakdown. A voltage reading below -350 mV indicates the steel is usually actively corroding within the concrete [Broomfield, 2007]. In the 1970's, field and laboratory studies were conducted and an empirical relationship between a bar's potential (mV) and its risk of corrosion was developed. Table 2.3 illustrates this correlation. However, care should be taken when interpreting results, for the correlation between a bar's true corrosion risk and that of its potential may not necessarily agree with the relationship shown in Table 2.3. This may be due to a number of factors such as, but not limited to: oxygen concentration, carbonation/concrete resistance, and protective steel coatings [Gu and Beaudoin, 1998].

Highly negative potential values may reach beyond -350 mV when a steel bar is placed within an oxygen deprived environment. A potential this low corresponds to a 90 percent probability that the steel is corroding. However, due to lack of oxygen, the cathodic reaction may not be established and the corrosion process may not proceed.

Therefore, a bar may report a highly negative potential with no evident corrosion occurring.

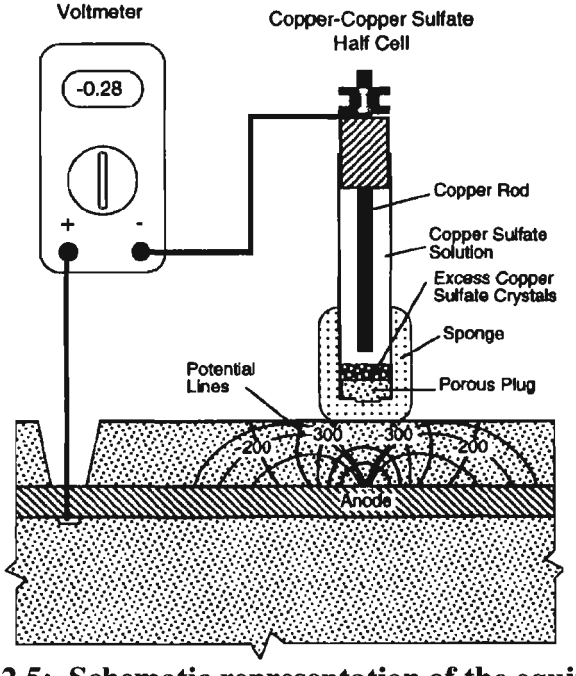

Figure 2.5: Schematic representation of the equipment and procedure used when conducting a half-cell. potential measurement [Broomfield, 2007].

Table 2.3: Correlation between the corrosion potential of a steel bar embedded within concrete and risk of corrosion [Broomfield, 2007].

Potential (CSE)	*Corrosion Risk*
> -200 mV	Low (< 10%)
-200 to -350 mV	Intermediate
-350 to -500 mV	High (> 90%)
< -500 mV	Severe

The opposite of the above occurrence may happen when the bars are embedded within a carbonated concrete environment. This may cause the reported potential to be more positive than its actual value. A more positive potential value may be attributed to the dry nature of carbonated concrete as well as the formation of calcium carbonate within the concrete's pore structure. These two factors are known to increase a concrete's resistance, which in turn increases (more positive) a bar's reported potential as may be seen within the following equation:

$$V_{measured} = V_{actual} \times \frac{\Omega_{voltmeter}}{\Omega_{voltmeter} + \Omega_{concrete}} \quad (14)$$

where $V_{measured}$ is the reported potential of the bar, V_{actual} is the actual potential of the bar, $\Omega_{voltmeter}$ is the resistance of the voltmeter, and $\Omega_{concrete}$ is the resistance of the concrete. A more uniform corrosion along the bar tends to occur in dry carbonated concrete. This is a result from the anodic (active) and cathodic (non-active) areas along the bar being closely spaced. Therefore, the potential of a uniformly corroded bar tends to be more positive, due to the averaging of the active and non-active sites along the bar.

2.3.3. Chloride Content Analysis. As previously mentioned, the passive layer protects a steel bar from corrosion and chlorides are the cause of destroying the passive layer. However, to destroy this passive layer, a sufficient amount of chlorides are required to be present at the steel-concrete interface. Therefore, chloride analyses are conducted upon reinforced concrete structures to determine whether a sufficient amount of chlorides are present at a depth equal to that of embedded steel and/or how quickly the chlorides are diffusing through the concrete.

Chloride profiles are a common development that aid in the calculation of the rate at which chloride ions penetrate through a concrete element. A chloride profile represents the chloride concentration at various depths within the concrete. According to Broomfield [2007], it is recommended that a minimum of four data points be used in developing a chloride profile in order to obtain an accurate representation of the chloride distribution. The rate at which the chlorides penetrate through the concrete is determined from the mentioned data points and Equation (4) in Section 2.2.2 of this section. The

diffusion rate is a time approximation associated as to when a sufficient amount of chlorides become present at the steel-concrete surface to induce corrosion.

Currently, the American Society for Testing and Materials (ASTM) International has a published standard procedure for testing the acid-soluble (ASTM C1152-04) and water-soluble (ASTM C1218-08) chloride concentrations within concrete. The acid-soluble chloride test represents to the concentration of both the bound and free chlorides; whereas, the water-soluble chloride test represents the concentration of only the free chlorides within the concrete. The free chlorides are those that contribute to the destruction of the passive layer. Therefore, ASTM standard C1218 is considered to be more informative than that of ASTM C1152 standard; however, the results obtained from the water-soluble test are known to be less accurate and difficult to reproduce. Both standards are commonly carried out in the lab and involve subjecting a concrete powder sample to an acid which is then followed by titration. Results from the acid-soluble (total) test can then be correlated to the values shown in Table 2.4 so that the corrosion risk of the embedded bars may be classified [Broomfield, 2007].

Table 2.4: Correlation between percent chloride by mass of concrete and corrosion risk [Broomfield, 2007].

% CL by Mass of Concrete	*Corrosion Risk*
< 0.03	Negligible
0.03-0.06	Low
0.06-0.14	Moderate
> 0.14	High

To conduct the chloride test, concrete powders are typically collected by drilling or pulverizing cores. Both the ASTM and AASHTO standards require the test sample to

be 10 grams in size and capable of passing a No. 20 (850 μm) or No. 50 (300 μm) sieve, respectively. For most standards a required overall sample size of 20 grams is needed. When collecting a powder sample from a specimen at a fitted depth, multiple drilling locations are recommended. To reduce the likelihood of a piece of aggregate influencing the results, mixing the powder of several drilled locations will increase the statistical accuracy. A sample's fine powder is known to posses high chloride concentrates and care should be taken to avoid loss of this powder. Contact between exposed skin and a powder sample may contaminate the sample therefore, handling with bare hands shall be held to a minimum [Broomfield, 2007].

2.4. TESTING METHODS

Understanding hardened concrete properties is the basis for using concrete in construction and design. Many ASTM standards are used in the concrete industry and these tests ensure the quality and control of concrete production. Results from these tests are used in hopes to establish the validity and/or correlation of the current standards for use on high-volume fly ash concrete. Corrosion is a complex and highly unpredictable process which is often affected by numerous factors. These factors are often difficult to quantify and/or account for, which makes classifying and understanding a material's corrosion resistance extremely difficult. Therefore, when trying to characterize a material's ability to postpone the corrosion process, it may be beneficial to conduct a series of tests in hope that the results may lead to a clear and indisputable conclusion. This section describes the various ASTM concrete property tests used to study the hardened properties and the AASHTO T259 Resistance of Concrete to Chloride Ion Penetration ponding test to evaluate the durability and corrosion protection of high-volume fly ash concrete.

2.4.1. Hardened Concrete Property Tests. The behavior of hardened concrete is an essential tool when designing with concrete. When concrete mixes are specified in design, there is slight variability as the properties the concrete is expected to have are supported by previously tested performance of similar concrete mixes. These values used in design have been developed through extensive testing. Because of this testing, the American Standards of Testing Materials (ASTM) has created standards which enable

these tests to be reproduced and performed not only in the laboratory, but in the field as well. Using the standard test methods for determining hardened concrete properties reassures the predicted and expected performance of concrete. These standard test methods were used to evaluate and compare the high-volume fly ash concrete. Also, the results from the standard tests are used to determine the applicability of using specific hardened concrete prediction functions to predict concrete properties and performance of high-volume fly ash concrete. All tests were performed in compliance with the ASTM associated with each test. The tests performed are summarized in Table 2.5.

Table 2.5: ASTM standard test methods used for high-volume fly ash concrete evaluation.

ASTM C39	Standard Test Method for Compressive Strength of Cylindrical Concrete Specimens
ASTM C78	Standard Test Method for Flexural Strength of Concrete
ASTM C469	Standard Test Method for Static Modulus of Elasticity and Poisson's Ratio of Concrete in Compression
ASTM C496	Standard Test Method for Splitting Tensile Strength of Cylindrical Concrete Specimens
ASTM C157	Standard Test Method for Length Change of Hardened Hydraulic Cement Mortar and Concrete

2.4.2. Shrinkage Analysis. Shrinkage is an inevitable phenomenon that occurs within concrete. The amount concrete may shrink depend on the specimen or structure size, type of concrete used, and the conditions in which the concrete will be cured. Shrinkage is observed at a micro level and may or may not cause effects to the concrete's

change in size. There are three basic types of shrinkage, when considering why shrinkage may occur: autogenous shrinkage, which is caused by the absence of moisture exchange due to the hydration reactions of the cement; carbonation shrinkage, which results as the various cement hydration products are carbonated in the presence of carbon monoxide (CO); and drying shrinkage, which is due to moisture loss in the concrete from environmental exposure [Rhodes, 1992].

ASTM C157-08 "Standard Test Method for Length Change of Hardened Hydraulic Cement Mortar and Concrete" [ASTM C157, 2008], is used to measure free shrinkage of concrete. This method uses rectangular concrete prisms with gage studs at each end and a mechanical dial gage length comparator is used to measure length change over time [Deshpande et al., 2007]. Shrinkage is a relative measure corresponding to the type of specimen used to conduct the test and influenced by many factors, including those mentioned above. Increasing or decreasing the water-to-cement ratio influences the volume of paste and amount of aggregate in a concrete mix. ACI Committee 232 on use of fly ash in concrete reports that where the addition of fly ash increases the paste volume in a concrete mix, shrinkage may be increased slightly if the water content remains constant. If the water content is reduced, shrinkage should be about the same as concrete without fly ash [Deshpande et al., 2007].

A study done by Cabrera and Atis [1999] reported a decrease in drying shrinkage with the use of fly ash. This study evaluated 50 and 70 percent fly ash replacements of portland cement. To note, although, about this study is that Class F fly ash was used. This aside, it is still very similar to the fly ash approach conducted within this research study to provide a relevant perspective of the effect high volumes of fly ash in concrete have on shrinkage. The specimens were demolded after one day of curing and a lower shrinkage was observed for the high-volume fly ash concrete over the conventional concrete. The 70 percent exhibited less shrinkage than that of even the 50 percent fly ash concrete. However, some studies show little to no difference in shrinkage between conventional concrete and concrete containing fly ash.

2.4.3. Durability Tests. In terms of durability when designing a structure, understanding a concrete's resistance toward the ingress of destructive chloride ions is highly beneficial. Among the many factors of concrete design, the environment in which

the structure will be exposed must be considered when determining the resistance concrete may have against chlorides. For testing such durability and chloride penetration, both the American Association of State Highway and Transportation Official's (AASHTO) and (ASTM) International have established standard concrete durability tests.

Many tests have been developed to aid in the understanding and prediction of potential durability issues that concrete may experience during its lifetime. There are tests that analyze chloride penetration and concentration, which is then related to a scale estimating the potential risk for corrosion of embedded steel reinforcement. Other tests include using electrical resistance and potential difference to predict the resistance concrete may have against the onset of corrosion and how much corrosion damage may be present. Climate variations are also studied through freezing and thawing cycles to illustrate the damaging effects of such environments on concrete. Table 2.6 lists the durability tests used and performed to evaluate the particular concrete mixes within this research study.

Table 2.6: Standard tests performed to evaluate the durability of high-volume fly ash concrete.

Durability Characteristics	***Test***
Chloride Permeability	
Electrical Method	ASTM C 1202
Ponding Method	ASTM C 1543 / AASHTO T 259
Freeze-Thaw Resistance	ASTM C 666 (Test Procedure A)
Corrosion Resistance	
Concrete Resistivity	ASTM C 1543 / AASHTO T 259
Corrosion Potential	ASTM C 1543 / AASHTO T 259

3. MIX DESIGN

3.1. INTRODUCTION

This section describes the process that was carried out to develop a concrete mix design using a high volume of cement replacement with fly ash. The objective of this process was to maximize the percentage of fly ash in the mix, yet still fulfill the strength and workability requirements. A target strength of 5,000 psi at 28 days was selected to perform the mix development based on the ACI 211.1, Title (ACI 211.1, 1991) document. Class C fly ash donated by Ameren UE was used as replacement of the portland cement due to its high level of calcium. This part of the study used mortar and paste mixes to arrive at the optimum combinations and percentages of several powder additions to maximize the amount of fly ash. The primary criteria to select such percentages were the set time and the rate of strength gain. The main goal was to develop a mix that could fulfill a minimum strength requirement of 1,000 psi at 1 day in addition to the requisite 5,000 psi at 28 days. Attainment of this goal would prove that the use of HVFA concrete in construction is viable. Rheological composition of the fly ash, mix design development, and compressive strength results are contained in the following sections.

3.2. FLY ASH CHEMICAL COMPOSITION

Fly ashes are subdivided into two main classes, C and F, which reflect the composition of the inorganic fractions. Class F fly ashes are produced from either anthracite bituminous or sub-bituminous coals. Class C fly ashes are derived from sub-bituminous or lignitic coals. In other words, the two classes of fly ash are distinguished by the silica oxide and calcium contents of the type of coal burned. Fly ash can be cementitious, pozzolanic, or both. Class F fly ash is pozzolanic while Class C fly ash is often cementitious and pozzolanic. Cementitious fly ash hardens when wetted while pozzolanic fly ash requires a reaction with lime before hardening. Both classes of fly ash are used as a cement replacement in concrete.

The fly ash used in this study was an ASTM Class C fly ash produced in the coal-fired electrical generating plant of Ameren UE located in Labadie, Missouri. The

chemical composition of the fly ash is given below in Table 3.1. Four samples of fly ash were tested for chemical composition. The amount of each oxide represents the range of the four samples expressed as a percent by weight. Table 3.2 shows the typical ranges of the chemical composition of a Class C fly ash. The chemical oxide quantities reported in Table 3.1 coincide with those listed in Table 3.2. All requirements are also in accordance with ASTM C618, Title (ASTM C618, 2007).

Table 3.1: In-house chemical analysis of Ameren UE fly ash.

Oxide	*%*
Silicon Oxide (SiO_2)	30.45 – 36.42
Aluminum Oxide (Al_2O_3)	16.4 – 20.79
Iron Oxide (Fe_2O_3)	6.78 – 7.73
Calcium Oxide (CaO)	24.29 – 26.10
Magnesium Oxide (MgO)	4.87 – 5.53
Sulfur (SO_3)	2.18 – 6.36
Sodium Oxide (Na_2O)	1.54 – 1.98
Potassium Oxide (K_2O)	0.38 – 0.57
Titanium Oxide (TiO_2)	1.42 – 1.56
Phosphorus Oxide (P_2O_5)	1.01 – 1.93
Manganese Oxide (MnO)	0.028 – 0.036
Strontium Oxide (SrO)	0.40 – 0.44
Barium Oxide (BaO)	0.68 – 0.99
LOI	0.24 – 1.15

3.3. ACTIVATORS

Although certain fly ashes exhibit some cementitious properties, the main contribution to the hardened concrete properties results from the pozzolanic reaction of the fly ash with the calcium hydroxide released by the portland cement. The pozzolanic reaction typically occurs more slowly than cement hydration reactions and consequently

concrete containing fly ash requires more curing during early ages. Previous research has shown that fly ash has very little immediate chemical reaction when it is only mixed with water. There are enough oxides and aluminates within the portland cement to provide sufficient reaction in the process of hydration, whereas, fly ash requires the addition of activators to initiate the hydration process. The activators used in the HVFA concrete for this study were calcium hydroxide and gypsum, selected based on previous research. Appropriate proportions were determined to ensure a proper hydration process. Insufficient amounts of activators may generate a delay in reaching adequate early-age strengths. Excess amounts of activators may generate a rapid set or false set that may not develop the required densification of the microstructure, also affecting the concrete strength.

Table 3.2: Fly ash chemical differences expressed as percent by weight (ASTM C618-07).

Component	*Class F (Bituminous)*	*Class C (Sub-bituminous)*	*Lignite*
SiO_2	20 – 60	40 – 60	15 – 45
Al_2O_3	5 – 35	20 – 30	10 – 25
Fe_2O_3	10 – 40	4 – 10	4 – 15
CaO	1 – 12	5 – 30	15 – 40
MgO	0 – 5	1 – 6	3 – 10
SO_3	0 – 4	0 – 2	0 – 10
Na_2O	0 – 4	0 – 2	0 – 6
K_2O	0 – 3	0 – 4	0 – 4
LOI	0 – 15	0 – 3	0 – 5

3.3.1. Gypsum. Calcium sulfate dihydrate (gypsum) is added to portland cement to limit the vigorous initial reaction of the tricalcium aluminate (C_3A) with water, which can lead to a flash set. However, fly ash has a slower initial setting time. When fly ash is used in large amounts, such as in a HVFA concrete consisting of 70 percent fly ash

replacement, additional gypsum may be required to prevent sulfate depletion and promote the immediate start of the hydration process.

The gypsum used in this study was obtained from the company USA Gypsum located in Reinholds, PA, where it is produced from recycled gypsum boards. Gypsum board, otherwise known as dry wall, is regularly used as a building interior lining and partitioning where structural requirements are low. The panels of dry wall are made of gypsum plaster pressed between two thick sheets of paper. The gypsum used in this study was ground to an ultra-fine consistency with a 96% pure content of calcium sulfate ($CaSO_4$). Figure 3.1 shows the packaging and gypsum material used in this study.

Figure 3.1: Gypsum material sample.

The mixture proportion for gypsum was determined from a previous study carried out by Bentz [2010]. Bentz studied a 50:50 ratio of portland cement to fly ash, and found that at least 2 percent additional gypsum by mass of total cementitious materials was required for a proper hydration. The mix was based on a total cementitious material amount of 400 grams (0.882 lb). Having higher fly ash content would likely require

more than two percent of gypsum, so it was decided to use a 4 percent replacement of the fly ash with gypsum. This amount proved to be effective in testing of paste and mortar cubes, the results of which will be discussed later in this section.

3.3.2. Calcium Hydroxide. In conventional concrete, the tricalcium silicate (C_3S) and dicalcium silicate (C_2S) react individually with water to produce the principal hydration product of calcium silicate hydrate (C-S-H) and calcium hydroxide (CH) in varying amounts. This reaction will be repeated over time producing an excess of CH. The fly ash will then consume the excess CH and continue to hydrate, forming additional C-S-H, and gaining additional strength over time. In a HVFA concrete, additional calcium hydroxide is required to ensure a more complete hydration process for the fly ash.

The hydrated lime (calcium hydroxide) used in this study was purchased from the Mississippi Lime company located in Sainte Genevieve, MO. A standard hydrated lime material of 96% purity was added to the HVFA mixture. Figure 3.2 shows the packaging and calcium hydroxide material.

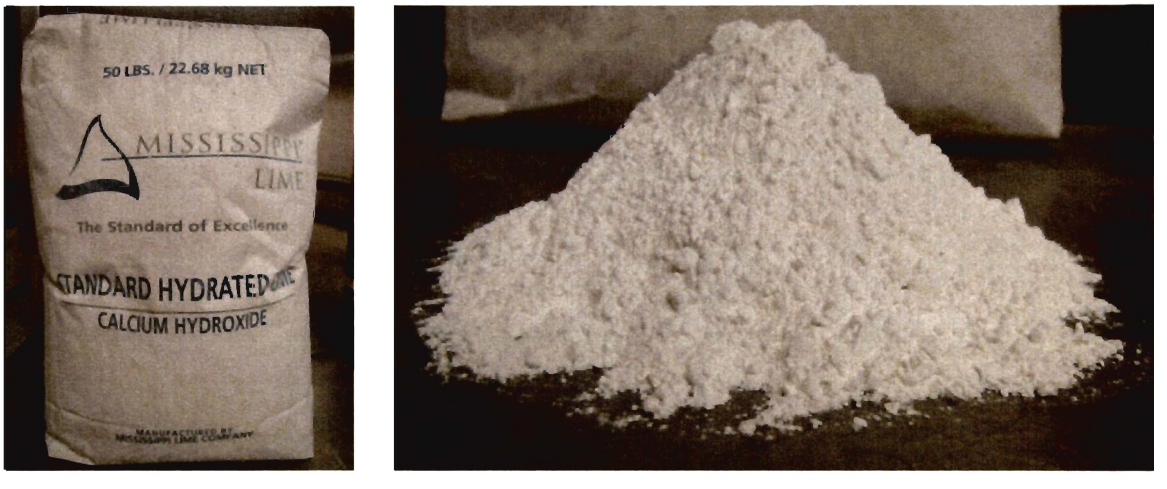

Figure 3.2: Calcium hydroxide material sample.

The same method used for the selection of the amount of gypsum was repeated to determine the proportions for calcium hydroxide. Bentz found that at least 5 percent of calcium hydroxide by weight of cementitious material was sufficient for early and later strength gain in cement pastes containing a 50:50 ratio of portland cement to fly ash. The mix was based on a total cementitious material amount of 400 grams (0.882 lb). Having higher fly ash content would likely require more than 5 percent calcium hydroxide, so it was decided to use a 10 percent replacement of fly ash with calcium hydroxide. A higher amount of calcium hydroxide (15 percent) was also tested and initial results showed an increase in the compressive strength compared to the paste containing only 10 percent calcium hydroxide. However, results of compressive strength at later ages showed no advantageous increase, concluding that a 10 percent replacement with calcium hydroxide was sufficient for this particular fly ash.

3.4. PASTE AND MORTAR CUBES

3.4.1. General. The purpose of testing paste and mortar cubes was to optimize the constituent percentages for a control and experimental HVFA mix using a specimen that is smaller and more cost-effective to construct before advancing to larger specimen tests. Cubes made from paste (water, cementitious materials, and activators only) were used to determine what percentages of fly ash substitution, gypsum, and calcium hydroxide were optimal to achieve practical early-age compressive strengths. Mortar cubes, including sand supplied by Capital Sand in Jefferson City, were used to determine a plausible water to cement ratio that would allow for a sufficient balance between workability and compressive strength.

3.4.2. Paste Cubes Procedure. Each specimen was constructed and tested following the guidelines set forth in ASTM C109-08 using 2 in. (50 mm) cube specimens. The specimens were moist cured until the day of testing. The paste cubes, with a 0.40 *w/cm*, were tested at 1, 3, and 7 days in order to determine the early strengths of the mix, since early form removal is a concern when using HVFA concrete for construction. The 0.40 w/cm was selected based on previous research and the desired objectives of this stage of the research as mentioned previously. Several modifications were made to the ASTM C109-08 procedure in order to account for the low paste

viscosity and the addition of activators in the mixing phase. These modifications were as follows:

- To ensure that no paste would leak through the joints in the cube molds, the molds were caulked with silicon on the outside (Figure 3.3)
- A 5 gallon (19 L) bucket with lid was modified to accommodate a drill-driven paddle by cutting a hole in the lid (Figure 3.4)
- One half of the required mixing water was added to the bucket
- Cementitious materials were then added to the bucket (first the fly ash, then the cement) while stirring the mixture
- The activators (CH and gypsum) were mixed with the remaining half of the required water in a separate container to form a light slurry
- The activator slurry was then added to the cementitious mixture and mixed with the drill paddle for 5 minutes
- After mixing, the sides and lid of the bucket were checked for excess and unmixed material
- The mix was then transferred to a pitcher with a pouring spout for ease of placement into the cube molds
- The paste was then poured into the molds in one lift via the pitcher
- The molds were then vibrated with a rubber mallet for consolidation purposes and the excess paste was struck off with a polypropylene straight edge
- The molds were then placed in a moist cure chamber
- The cubes were de-molded at 1 day with the exception of the 100 percent fly ash specimens which had not set
- The demolded cubes were placed back in the moist cure room until the test dates

Every specimen was tested on a 600,000 lb. (2,670 kN) capacity Forney compression machine until failure. The test matrix for this phase of the study is shown below in Table 3.3.

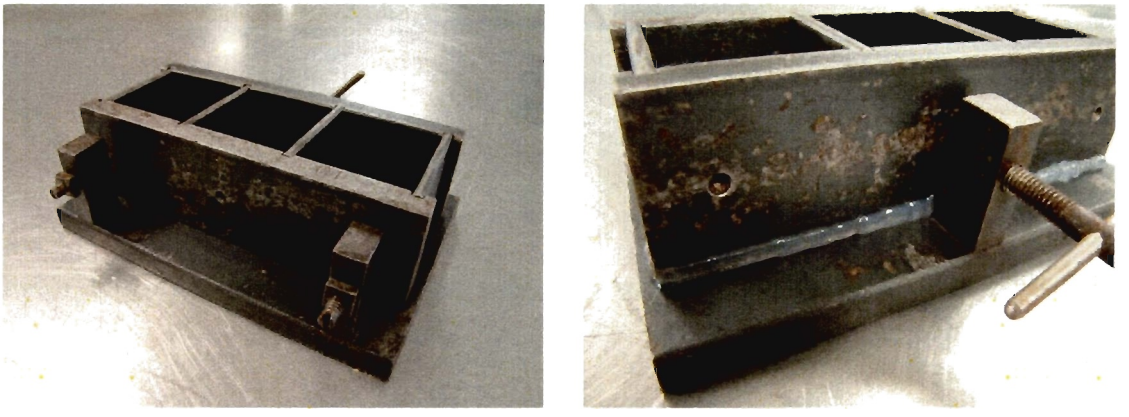

Figure 3.3: Caulked cube molds.

Figure 3.4: 5 gallon bucket and mixer set-up.

Table 3.3: Test matrix for paste cubes.

	% of Cementitious Material			
Specimen Set	***Cement***	***Fly Ash***	***Gypsum***	***Calcium Hydroxide***
Control	100	0	-	-
50/50	50	50	-	-
40/60	40	60	-	-
27/75	25	75	-	-
100 % FA	0	100	-	-
50/50 - G	50	50	4	-
40/60 - G	40	60	4	-
25/75 - G	25	75	4	-
100 % FA - G	0	100	4	-
50/50 - G - 10 CH	50	50	4	10
40/60 - G - 10 CH	40	60	4	10
25/75 - G - 10 CH	25	75	4	10
100 % FA - G - 10 CH	0	100	4	10
50/50 - G - 15 CH	50	50	4	15
40/60 - G - 15 CH	40	60	4	15
25/75 - G - 15 CH	25	75	4	15
100 % FA - G - 15 CH	0	100	4	15

3.4.3. Mortar Cubes Procedure. The mortar cubes, with *w/cm* values of 0.30 and 0.40, were tested at 3, 7, and 28 days (moist cured until test date) to predict the effects that the *w/cm* would have on the mix from the early strengths up until the design strength of 28 days. The mortar cube fabrication process more closely followed the ASTM C109-08 standard. Due to a more manageable mix viscosity, actual mixing was performed using a Hobart mixer. The activators were added, as they were for the paste cubes, as part of the second water addition, and the sand-to-cementitious material ratio used was 0.33. The sand gradation is shown in Table 3.4.

Table 3.4: Sand gradation performed at Missouri S&T.

Sieve Size	⅜"	#4	#8	#16	#30	#50	#100	#200
Total % Passing	100	99	92	79	48	9	1	0.2

Every specimen was tested on a 600,000 lb. (2,670 kN) capacity Forney compression machine until failure. The test matrix for this experiment is shown below in Table 3.5.

Table 3.5: Test matrix for mortar cubes.

		% of Cementitious Material	
Specimen Set	***w/cm***	***Cement***	***Fly Ash***
Control	0.40	100	0
50/50		50	50
25/75		25	75
100 % FA		0	100
Control	0.30	100	0
50/50		50	50
25/75		25	75
100 % FA		0	100

3.4.4. Results. The results recorded from the mortar and paste cube tests were organized into Tables 3.6 and 3.7. Each value in the tables represents the average of three replicate specimens.

Table 3.6: Compressive strengths for mortar cubes.

		Compressive Strength (psi)		
Specimen Set	***w/cm***	***Day 3***	***Day 7***	***Day 28***
Control	0.40	3435	5275	5506
50/50		2726	4079	5368
25/75		1003	1906	2909
100% FA		74	313	520
Control	0.30	2905	4695	5105
50/50		2106	2176	3926
25/75		1434	1824	2384
100% FA		218	468	881

(1 psi = 6.89 kPa)

Table 3.7: Compressive strengths for paste cubes.

	Compressive Strength (psi)		
Specimen Set	***Day 1***	***Day 3***	***Day 7***
Control	1748	3919	5255
50/50	558	1920	3594
40/60	439	1571	2136
27/75	0	740	1266
100 % FA	0	35	53
50/50 - G	981	2500	3540
40/60 - G	793	1701	2469
25/75 - G	339	1271	1646
100 % FA - G	0	0	71
50/50 - G - 10 CH	1063	2529	2943
40/60 - G - 10 CH	953	2243	2708
25/75 - G - 10 CH	554	1219	1314
100 % FA - G - 10 CH	671	670	748
50/50 - G - 15 CH	1708	2649	3804
40/60 - G - 15 CH	890	2390	3701
25/75 - G - 15 CH	980	1075	1551
100% FA - G - 15 CH	624	616	580

(1 psi = 6.89 kPa)

3.4.5. Analysis and Conclusions. The test results from the mortar cubes suggest that using a *w/cm* of 0.30 can increase the specimen strength in some cases, such as with the 25/75 mix, but the loss of workability outweighs the minimal strength gain. This is evident with the 0.30 *w/cm* control specimens, which yielded lower results due to compaction problems caused by the lack of water. Therefore, a *w/cm* of at least 0.40 was selected for further testing. A graphical representation of this tests data is shown in Figures 3.5 and 3.6.

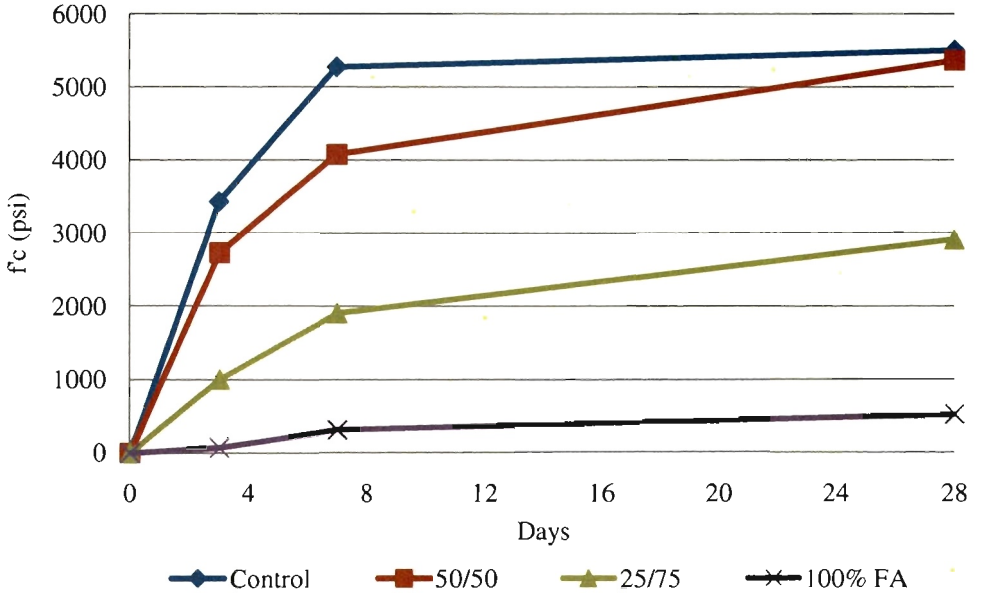

(1 psi = 6.89 kPa)

Figure 3.5: Mortar cube compressive strengths on test days (w/cm = 0.40).

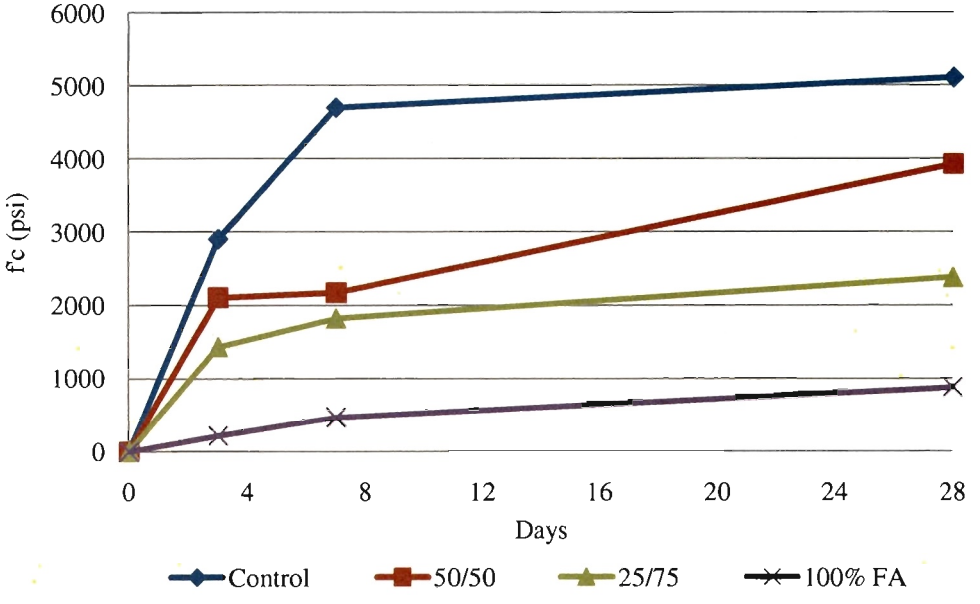

(1 psi = 6.89 kPa)

Figure 3.6: Mortar cube compressive strengths on test days (w/cm = 0.30).

A number of conclusions can be drawn from the paste cube test data (Figures 3.7 to 3.10). The data shows that adding 15 percent calcium hydroxide and 4 percent gypsum (by weight of cementitious material) results in the highest compressive strengths for the HVFA mixes. The two best performing HVFA mixes were the 50 percent and 60 percent fly ash mixes with nearly identical 7 day strengths. The 75 percent fly ash mix did not perform as well as the 50 percent and 60 percent mixes, but exhibited sufficient strength at 7 days. The poorest performing mix was the 100 percent fly ash mix. Since the objective of this study was to push the bounds of fly ash substitution in concrete, the 75 percent fly ash mix was selected for further testing. The 75 percent fly ash mix including 10 percent calcium hydroxide was used since there was little difference in the results between this mix and the mix including 15 percent calcium hydroxide.

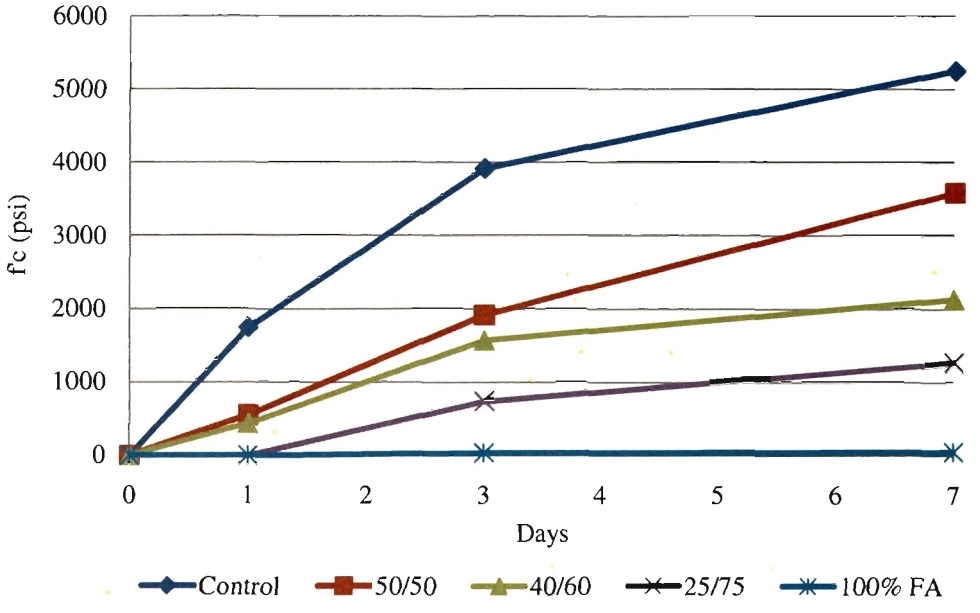

(1 psi = 6.89 kPa)

Figure 3.7: Paste cubes with no admixtures.

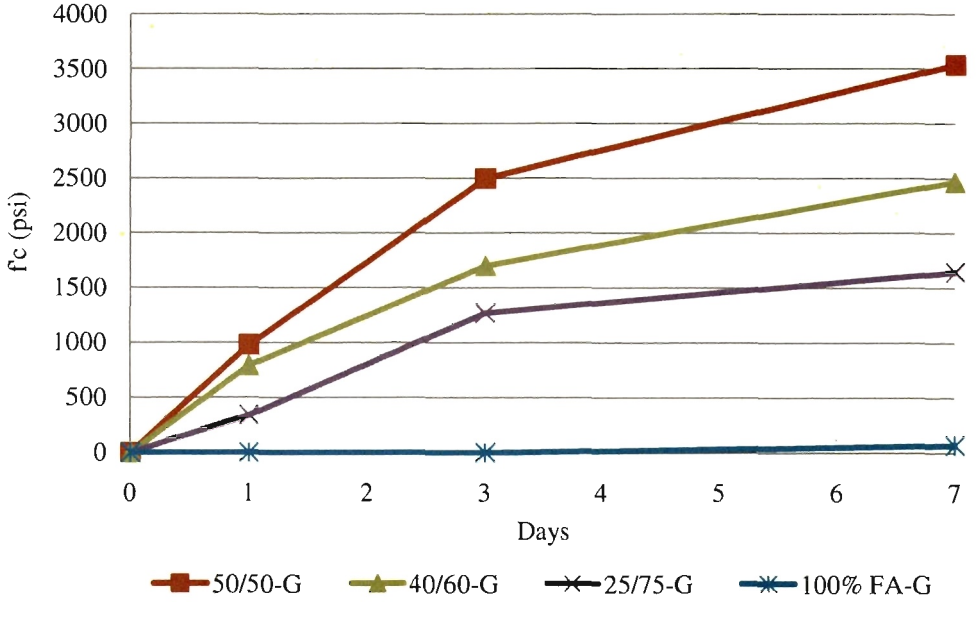

(1 psi = 6.89 kPa)

Figure 3.8: Paste cubes with 4 percent gypsum.

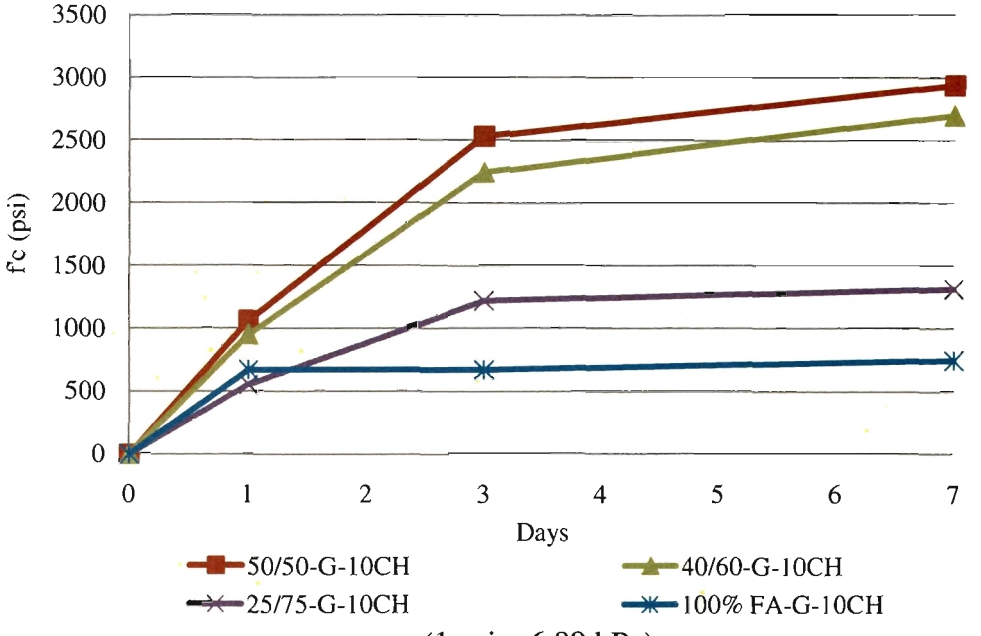

(1 psi = 6.89 kPa)

Figure 3.9: Paste cubes with 4 percent gypsum and 10 percent calcium hydroxide.

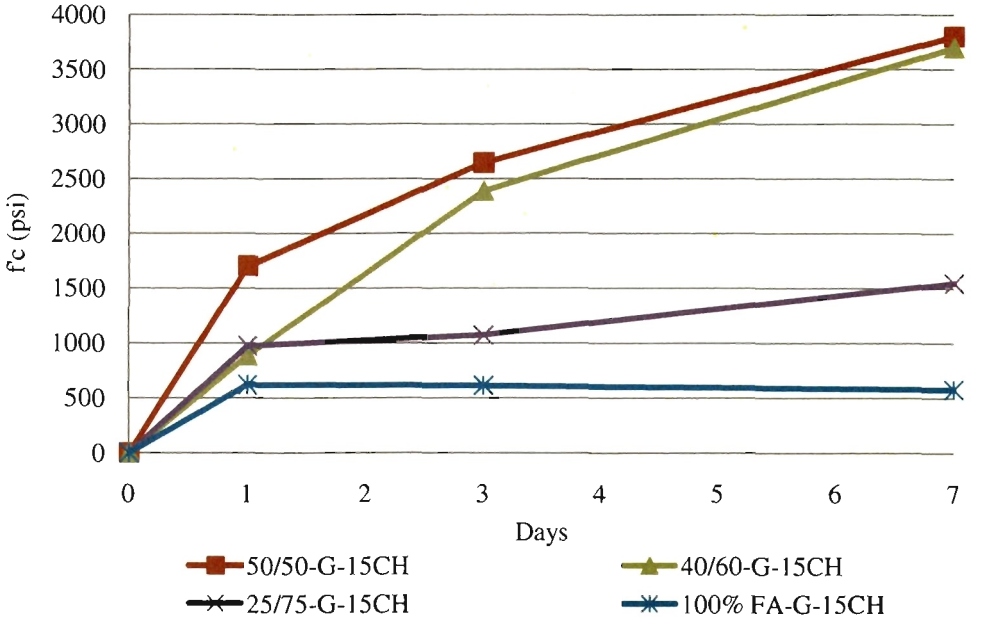

(1 psi = 6.89 kPa)

Figure 3.10: Paste cubes with 4 percent gypsum and 15 percent calcium hydroxide.

3.5. CONCRETE MIX DESIGN

The HVFA concrete mix design was developed using the procedure outlined in Section 6 of the ACI 211.1-91 document. The procedure for selection of mix proportions given in this document is applicable to normal weight concrete. Estimating the required batch weights for the concrete involves a sequence of logical, straightforward steps to fit the characteristics of the materials into a mixture suitable for a specific application. Expected 28-day target strength of 5,000 psi (34.5 MPa) was considered. The solution approach used during the mix development is summarized below.

3.5.1. Slump Selection. If slump is not specified, a value appropriate for the work can be selected from Table 3.11. These slump ranges shown apply when vibration is used to consolidate the concrete.

Table 3.8: Recommended slump for various types of construction [ACI 211.1-91].

Types of construction	*Slump (in.)*	
	Maximum	*Minimum*
Reinforced foundation, walls, and footings	3	1
Plain footings, caissons, and substructure walls	3	1
Beams and reinforced walls	4	1
Building columns	4	1
Pavements and slabs	3	1
Mass concrete	2	1

(1 in = 25.4 mm)

The slump may be increased when chemical admixtures are used, provided that the admixture-treated concrete has the same or lower water-to-cement or water-to-cementitious materials ratio and does not exhibit segregation potential or excessive bleeding. For this research, a slump of 4 in. (102 mm) was selected.

3.5.2. Maximum Aggregate Size Selection. The maximum aggregate size was determined based on the gradation of the materials available locally. A gradation of the coarse aggregate is shown in Table 3.9. Generally, the nominal maximum aggregate size should be the largest that is economically available and consistent with the dimensions of the structure. Large nominal maximum sizes of well graded aggregates have fewer voids than smaller sizes. For this research, a coarse aggregate having a nominal maximum size of ¾ in. (19 mm) was considered.

Table 3.9: Coarse aggregate gradation performed at Missouri S&T.

Sieve Size	1"	¾"	½"	⅜"	#4	#8	#30	#100	#200
Total % Passing	100	89	59	47	16	7	4	4	3

3.5.3. Mixing Water and Air Content Estimation. The quantity of water per unit volume of concrete required to produce a given slump is dependent on: the nominal maximum size, particle shape, and gradation of the aggregates; the concrete temperature; the amount of entrained air; and the use of chemical admixtures. Slump is not significantly affected by the quantity of cement or cementitious materials within normal levels. The selection of the required mixing water was made based on Table 3.10.

Slump values of more than 7 in. (178 mm) are only obtained through the use of water-reducing chemical admixtures. For this research, a value of 340 lb/yd^3 (1978 N/m^3) of water was obtained from this table. This value was defined as the optimum value for this mix design. However, for concrete ordered from the local ready mix supplier, approximately 8 gallons per yd^3 (40 L/m^3) of water was held in abeyance for subsequent slump adjustment at the lab prior to placement. Water was then added at the lab until the desired slump was reached, but never exceeding the amount of water held back initially.

This approach also helped to adjust the overall mixing water content based on the actual water content of the aggregate for each particular placement.

Table 3.10: Approximate mixing water and air content requirements for different slumps and nominal maximum sizes of aggregates (ACI 211.1-91).

Water (lb/yd^3) of concrete for indicated nominal maximum sizes of aggregate								
Slump (in.)	*⅜ in.*	*½ in.*	*¾ in.*	*1 in.*	*1½ in*	*2 in.*	*3 in.*	*6 in.*
Non-air-entrained concrete								
1 to 2	350	335	315	300	275	260	220	190
3 to 4	385	365	340	325	300	285	245	210
6 to 7	410	385	360	340	315	300	270	-
More than 7	-	-	-	-	-	-	-	-
Approximate amount of entrapped air in non-air-entrained concrete (%)	3.0	2.5	2.0	1.5	1.0	0.5	0.3	0.2
Air-entrained concrete								
1 to 2	305	295	280	270	250	240	205	180
3 to 4	340	325	305	295	275	265	225	200
6 to 7	365	345	325	310	290	280	260	-
More than 7	-	-	-	-	-	-	-	-
Recommended averages total air content, percent for level of exposure								
Mild exposure	4.5	4.0	3.5	3.0	2.5	2.0	1.5	1.0
Moderate exposure	6.0	5.5	5.0	4.5	4.5	4.0	3.5	3.0
Severe exposure	7.5	7.0	6.0	6.0	5.5	5.0	4.5	4.0

(1 in = 25.4 mm)

3.5.4. Water-to-Cementitious Materials Ratio Selection. The *w/cm* is determined not only by strength requirements, but also by factors such as durability. In the absence of data to develop a relationship between strength and this ratio for the materials to be used, a set of approximate and relatively conservative values for concrete containing Type I portland cement can be taken from Table 3.11.

Table 3.11: Relationship between water-to-cement or water-to-cementitious materials ratio and compressive strength of the concrete (ACI 211.1-91).

Compressive strength at 28 days (psi)	*Water-to-cement ratio by weight*	
	Non-air-entrained concrete	*Air-entrained concrete*
6,000	0.41	-
5,000	0.48	0.40
4,000	0.57	0.48
3,000	0.68	0.59
2,000	0.82	0.74

(1 psi = 68.9 kPa)

These values are estimated average strengths for concrete containing no more than 2 percent air for non-air-entrained concrete and 6 percent total air content for air-entrained concrete. Strength is based on 6 × 12 in. (152 mm x 305 mm) cylinders moist-cured for 28 days. The relationship in Table 3.14 assumes a nominal maximum aggregate size of about ¾ (19 mm) to 1 inch (25 mm). For this research, two water-to-cement ratios were used. A water-to-cement ratio (*w/c*) of 0.45 was selected for the conventional mix, and a water-to-cementitious materials ratio (*w/cm*) of 0.40 was selected for the HVFA mix.

This difference in these ratios is due to reports of previous research showing that when fly ash is incorporated into the mix, the water demand is lower for the same level of workability.

3.5.5. Cement Content Calculation. The amount of cement per unit volume of concrete is fixed by the determinations made in Section 3.5.3 and 3.5.4 above. The required cement is equal to the estimated mixing-water content divided by the water-to-cement ratio. Equation 3-1 shows how to calculate the amount of cement.

$$Amount\ of\ cement = \frac{340}{0.40} = 850\ {}^{lb}/_{yd^3} \qquad (3\text{-}1)$$

3.5.6. Coarse Aggregate Content Estimation. Aggregates of essentially the same nominal maximum size and gradation will produce concrete of satisfactory workability when a given volume of coarse aggregate is used per unit volume of concrete. Appropriate values for this aggregate volume are given in Table 3.12. The volume of coarse aggregate in a unit volume of concrete is dependent only on its nominal maximum size and the fineness modulus of the fine aggregate. The fineness modulus of the fine aggregate available from the local supplier was 2.60.

Volumes are based on aggregates in oven-dry-rodded conditions. These volumes are selected from empirical relationships to produce concrete with a degree of workability suitable for usual construction.

Table 3.12: Volume of coarse aggregate per unit of volume of concrete (ACI 211.1-91).

Nominal maximum size of aggregate (in.)	*Volume of oven-dry-rodded coarse aggregate per unit volume of concrete for different fineness moduli of fine aggregate*			
	2.40	***2.60***	***2.80***	***3.00***
⅜	0.50	0.48	0.46	0.44
½	0.59	0.57	0.55	0.53
¾	0.66	0.64	0.62	0.60
1	0.71	0.69	0.67	0.65
1½	0.75	0.73	0.71	0.69
2	0.78	0.76	0.74	0.72
3	0.82	0.80	0.78	0.76
6	0.87	0.85	0.83	0.81

(1 in = 25.4 mm)

For this research, the available coarse aggregate had a unit weight of 101.5 lb/ft^3 (591 N/m^3). The amount of coarse aggregate is calculated from the value obtained in Table 3.15 multiplied by 27 and the unit weight. Equation 3-2 shows how to calculate the amount of coarse aggregate.

$$Amount\ of\ coarse\ aggregate = 0.64 \times 27 \times 101.5 = 1754\ ^{lb}/_{yd^3} \quad (3\text{-}2)$$

3.5.7. Fine Aggregate Content Estimation. After the completion of the previous step, all ingredients of the concrete have been estimated except for the fine aggregate. Either of two procedures may be employed to estimate the fine aggregate content, the weight method or the absolute volume method. For this research, the weight method was used.

The required weight of the fine aggregate is simply the difference between the weight of fresh concrete calculated using Table 3.13 and the total weight of the other ingredients. Equation 3-3 shows how to calculate the amount of fine aggregate.

Table 3.13: First estimate of weight of fresh concrete (ACI 211.1-91).

Nominal maximum size of aggregate (in.)	*First estimate of weight of fresh concrete (lb/yd^3)*	
	Non-air-entrained concrete	*Air-entrained concrete*
⅜	3840	3710
½	3890	3760
¾	3960	3840
1	4010	3850
1½	4070	3910
2	4120	3950
3	4200	4040
6	4260	4110

(1 in = 25.4 mm, 1 lb/ft^3 = 16 kg/m^3)

$$Amount\ of\ fine\ aggregate = 3960 - (340 + 850 + 1754) = 1016\ ^{lb}/_{yd^3} \quad (3\text{-}3)$$

3.5.8. Aggregate Moisture Adjustments. The aggregate quantities to be weighed out for the concrete must allow for moisture in the aggregates. Generally, the aggregates will be moist and their dry weights should be increased by the percentage of water they contain, both absorbed and surface. The mixing water added to the batch must be reduced by an amount equal to the free moisture contributed by the aggregate.

During the casting of the beams, periodic measurements of moisture content and percentage of absorption were carried out on the coarse and fine aggregates to maintain the same conditions for all castings. The moisture content was measured following the standard described in ASTM C566, Title (ASTM C 566, 1997). The percentage of absorption was measured following the standards described in ASTM C127, Title (ASTM C127, 2007) for the coarse aggregate and ASTM C128, Title (ASTM C128, 2007) for the fine aggregate. Equations 3-4 to 3-6 show how to adjust the amount of water due to moisture contents. As an example, data measured in the first and second castings of the control specimens will be used, the moisture contents for the coarse aggregate and fine aggregate measured 2.3 percent and 1.7 percent, respectively. The percentages of absorption were found to be 0.5% and 0.9% for the coarse and fine aggregate, respectively. Absorbed water does not become part of the mixing water, therefore, it is excluded from the adjustment in the water as shown below.

$$Adjustment\ of\ water\ for\ coarse\ aggregate = 1754 \times 0.023 = 40.34\ ^{lb}/_{yd^3} \quad (3\text{-}4)$$

$$Adjustment\ of\ water\ for\ fine\ aggregate = 1016 \times 0.017 = 17.27\ ^{lb}/_{yd^3} \quad (3\text{-}5)$$

$$Amount\ of\ water\ (adjusted) = 340 - (40.34 + 17.27) = 282.40\ ^{lb}/_{yd^3} \quad (3\text{-}6)$$

3.5.9. Fly Ash, Calcium Hydroxide, and Gypsum Amount Estimations. This step does not apply to the control specimens that were cast using a conventional mix. The purpose of this research was to evaluate the effectiveness of a concrete containing a high

amount of fly ash. After some batching and testing of different mixes using cubes and cylinders, a 70 percent replacement of portland cement with fly ash was selected as the target. Additional powder activators to improve the early strength were also considered in the mix design. Calcium hydroxide and gypsum were selected for their favorable contribution to the development of early strength in a high-volume fly ash concrete mix. A 10 percent replacement with calcium hydroxide and a 4 percent replacement with gypsum were incorporated to the mix design. The amount of these activators was based on the amount of fly ash, but it was deducted from the total amount of the cementitious materials to maintain the ratio between the fly ash and portland cement (70/30). Equations 3-7 to 3-11 show how to calculate the weight of these admixtures. From equation 3-1, a total amount of cement equal to 850 lb/ft^3 (13616 kg/m^3) was determined for the base (control) mix design.

$$Amount\ of\ fly\ ash\ (not\ final) = 850 \times 0.70 = 595\ {}^{lb}/_{yd^3} \quad (3\text{-}7)$$

$$Amount\ of\ calcium\ hydroxide = 595 \times 0.10 = 59.50\ {}^{lb}/_{yd^3} \quad (3\text{-}8)$$

$$Amount\ of\ gypsum = 595 \times 0.04 = 23.80\ {}^{lb}/_{yd^3} \quad (3\text{-}9)$$

$$Amount\ of\ fly\ ash\ (final) = \left(850 - (59.50 + 23.80)\right) \times 0.70 = 536.70\ {}^{lb}/_{yd^3} \quad (3\text{-}10)$$

$$Amount\ of\ cement = \left(850 - (59.50 + 23.80)\right) \times 0.30 = 230\ {}^{lb}/_{yd^3} \quad (3\text{-}11)$$

3.5.10. Mix Designs Summary. Tables 3.14 and 3.15 present a summary of the final amount of each ingredient for the mixes used in this research. Table 3.14 presents the final design of a conventional mix used in the control specimens with a *w/cm* equal to 0.45. Table 3.15 presents the final design of the HVFA concrete mix used in this research with a *w/cm* equal to 0.40. The values contained in these tables are given in saturated surface dry (SSD) conditions.

Table 3.14: Conventional mix description.

Ingredient	*Amount (lb/ft^3)*
Water	340
Portland cement	756
Coarse aggregate	1750
Fine aggregate	1110
w/c	0.45

(1 lb/ft^3 = 16 kg/m^3)

Table 3.15: HVFA mix description.

Ingredient		*Amount (lb/ft^3)*
Water		340
Cementitious materials	Portland cement	230
	Fly ash	537
	Calcium hydroxide	59.5
	Gypsum	23.8
Coarse aggregate		1750
Fine aggregate		1110
w/cm		0.40

(1 lb/ft^3 = 16 kg/m^3)

3.6. CYLINDER COMPRESSION TESTING

3.6.1. General. Cylinder compression tests were used to test the strengths of the mixes utilizing the proportions from the compression cube tests in conjunction with the other concrete constituents, such as coarse and fine aggregate. A mix with a fly ash replacement value of 70 percent was selected for testing based on the success of the 75 percent fly ash paste cube specimens. This design allows the mix to have a fly ash percentage closer to that of the top performing HVFA paste cube specimens as well as a fly ash content twice the ACI recommended maximum of 35 percent (ACI Committee 232, 2003). Four other sets of cylinders were constructed using fly ash replacement contents of 0, 50, 60, and 75 percent for comparison purposes.

3.6.2. Procedure. Each cylinder specimen was constructed in accordance with ASTM C192, Title (ASTM C192, 2007). Mixing was performed in a 6 cubic foot (0.17 cubic meter) drum mixer (Figure 3.11). The fly ash was added with the cement at the ASTM designated time for addition of cementitious material and the activators were added using the second specified water addition as a vehicle. The concrete was then mixed for 5 minutes, poured, and cured as per ASTM C192 (2007). The specimens were moist cured for 1, 3, 7, or 28 days, depending on the designated test day for each specimen, before they were tested until failure using a 600,000 lb. (2,670 kN) capacity Forney compression machine in accordance with ASTM C39-09. The test matrix for the cylinder tests is shown in Table 3.19.

Figure 3.11: Large drum mixer.

Table 3.16: Test matrix for cylinder compression tests.

		Cementitious Materials (%)			
Specimen Set *	***w/cm***	***Fly Ash***	***Cement***	***Gypsum***	***CH***
Control	0.40	0	100	4	10
HVFA (50%)	0.40	50	50	4	10
HVFA (60%)	0.40	60	40	4	10
HVFA (70%)	0.40	70	30	4	10
HVFA (75%)	0.40	75	25	4	10

3.6.3. Results. The results from the cylinder compressive strength tests are shown in Table 3.17. As with the compression cube tests, each specimen set consists of the average of three replicate specimens.

Table 3.17: Test results from cylinder compression tests.

		Compressive Strength (psi)			
Specimen Set *	***w/c***	***Day 1***	***Day 3***	***Day 7***	***Day 28***
Control	0.40	3090	4540	5180	6190
HVFA (50%)	0.40	1190	2460	3980	5360
HVFA (60%)	0.40	1240	2670	3990	5480
HVFA (70%)	0.40	1120	1850	2880	4430
HVFA (75%)	0.40	660	1230	2000	3020

*Each set is comprised of the average of three specimens

(1 psi = 6.89 kPa)

3.6.4. Analysis and Conclusions. The test results, as shown in Figure 3.12, suggest that the highest strength HVFA concrete mixes are the 50 and 60 percent fly ash proportions with nearly identical results. The 70 percent fly ash mix, however, yielded a reasonable 1-day compressive strength of over 1100 psi (metric), a 3-day compressive strength of nearly 2000 psi (13.8 MPa), and 28-day strength of nearly 4500 psi (31 MPa). Since these values are acceptable when designing concrete for normal construction, the final HVFA concrete mix chosen for this study was the 70 percent fly ash mix with 4 percent gypsum and 10 percent calcium hydroxide.

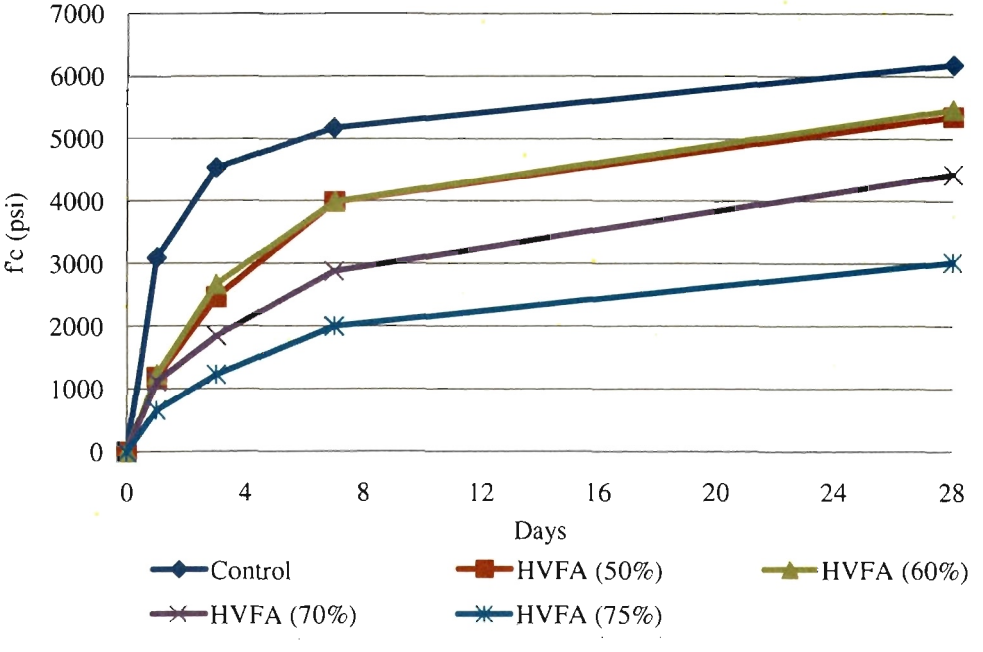

(1psi = 6.89 kPa)

Figure 3.12: Compressive strength vs. test day plot for all cylinder mixes.

3.7. FINAL MIX DESIGN AND MIXING DETAILS

Concrete for this study was provided by a ready mix plant, Rolla Ready Mix, in order to emulate field construction practices. The mix design provided to Rolla Ready Mix was decided upon based on the results described in Sections 3.4 and 3.6, only batched at a higher quantity, but using the same constituent proportions. The control mix was a 100 percent portland cement mix that was completely batched at the ready mix plant. The high-volume fly ash concrete mix featured a 70 percent replacement of cement with fly ash. The quantities used for each pour are shown in Tables 3.13 and 3.14 with only a difference in the amount of water that was adjusted based on the moisture content and percentage of absorption measured in both fine and coarse aggregates. While the fly ash was added at the ready mix plant, the required amounts of gypsum and calcium hydroxide, as per Section 3.4, were added directly to the truck upon arrival to the lab. Once mixed thoroughly for a minimum of 5 minutes at high speed, the concrete placement commenced. During each placement, a slump tests was performed to ensure the workability of the concrete. A 6-inch (152 mm) slump was the typical target value. Unit weight was also performed on the concrete as part of fresh concrete property testing. A summary of fresh property values are shown in Table 3.18. Also, as a part of the concrete placement, cylinders were cast in order to test the compressive strength at 28 days and on the day of testing of the full-scale specimens. Figure 3.13 presents a summary of images showing the construction process followed during each casting.

Table 3.18: Test results from cylinder compression tests.

Fresh Concrete Property Test	***Measurement Value***	
	Fly Ash (*w/cm* = 0.40)	Control (*w/cm* = 0.45)
Slump	6.5 in.	6 in.
Air Content	2.5 %	2 %
Unit Weight	138 lb/ft^3	141 lb/ft^3

(1 in. = 25.4 mm, 1 lb/ft^3 = 16 kg/m^3)

(a) Adding gypsum.

(b) Adding calcium hydroxide.

(c) Concrete placement.

Figure 3.13: HVFA concrete procedures.

4. HARDENED CONCRETE PROPERTY TESTS

4.1. INTRODUCTION

This section discusses the testing and evaluation of the hardened concrete properties of several high-volume fly ash (HVFA) concrete mix designs. All testing was performed in accordance with the applicable ASTM standards. A concrete mix of 100 percent portland cement was used as a baseline reference and to aid in the correlation of current test data. The tests conducted included: compressive strength, flexural strength, splitting tensile strength, modulus of elasticity, and shrinkage. Specimens were constructed and tested within the parameters of the standards associated with each of the tests conducted.

4.2. MIX DESIGNS EVALUATED

Table 4.1 contains the material weights for each of the mix designs evaluated within this section.

4.3. COMPRESSIVE STRENGTH TEST

Using ASTM C39-09 "Standard Test Method for Compressive Strength of Cylindrical Concrete Specimens" [ASTM C39, 2009], as a guideline, concrete cylinders were cast to evaluate the compressive strengths for each of the concrete mix designs. Mix No. 1 was used as a baseline reference for comparison with Mix Nos. 2 through 5, which consisted of 70 percent fly ash at varying water-to-cementitious ratios (*w/cm*). The test consisted of subjecting the concrete cylinders to a uniform compressive load at the ends of the cylinders as designated by the ASTM standard.

4.3.1. Preparation and Testing. Each specimen was 4 in. (102 mm) in diameter and 8 in. (204 mm) in length. There were 15 cylinders constructed for each mix design in order to obtain compressive strength data at 1, 3, 7, 28, and 56 days. All specimens were cast in plastic cylinder molds with caps and moist cured for 7 days, except for those tested at 1 day and 3 days. The specimens were then stripped from the plastic molds, marked and stored in the moist cure chamber until their intended test date. Prior to testing, each cylinder was capped in accordance with ASTM C617-09 "Standard Practice

for Capping Cylindrical Concrete Specimens" [ASTM C617, 2009]. The 1, 3, 7, 28, and 56-day strengths were determined through testing three replicate cylinders. The various concrete mixes were chosen to explore the different strengths that can be gained by decreasing the water-to-cementitious ratio (*w/cm*). The *w/cm* for each mix can be referenced previously in this section in Section 4.2. A typical specimen being tested for compressive strength is shown in Figure 4.1.

Table 4.1: Material weights of each mix design.

Materials (lb/yd^3)	*Mix Design*				
	No. 1	*No. 2*	*No. 3*	*No. 4*	*No. 5*
Water	345	345	345	345	345
Cement	850	196	222	256	301
Fly Ash	–	457	519	598	703
Calcium Hydroxide	–	53	60	68	79
Gypsum	–	49	49	49	49
Coarse Aggregate	1754	1754	1754	1754	1754
Fine Aggregate	1016	1016	1016	1016	1016
w/c	0.45	0.45	0.40	0.35	0.30

(1 lb/ft^3 = 16 kg/m^3)

Figure 4.1: Compressive strength performed on concrete specimen.

4.3.2. Results. The plotted compressive strengths for each mix design are shown in Figure 4.2. Each data point in the figure represents an average value of three tested cylinders. Mix No. 2 revealed the lowest strength gain over the testing period. This result is attributed to the higher *w/cm* for this mix, 0.45. The data for Mix No. 3 shows increased strength from that of Mix No. 2, which is to be expected due to the nature of the decreased *w/cm* from 0.45 to 0.40. Mix No. 4 shows a similar increase in compressive strength with the change in *w/cm* from 0.40 to 0.35. However, Mix No. 5 revealed a smaller strength increase with the change in *w/cm* from 0.35 to 0.30. This behavior may be the result of a combination of a very low *w/cm* combined with the high volume of fly ash, resulting in a plateau in potential strength gain with decreased water content. It is also recognized that concrete containing fly ash will have a longer hydration period than that of a pure portland cement concrete, with a corresponding slower strength gain with age. Therefore, in the range from 7 to 56 days, the high-volume fly ash concrete shows a greater increase in compressive strength than the portland cement concrete. Conversely, at early age strengths, the high-volume fly ash

concrete shows significantly lower compressive strength values. As a result, Mix Nos. 2 and 3 attained lower strengths than the control mix, while Mix No. 4 (*w/cm* of 0.35) attained a 56-day strength approximately equal to the control mix, and Mix No. 5 (*w/cm* of 0.30) attained a 28-day strength approximately equal to the control mix with a 56-day strength exceeding the control mix. Complete compressive strength data can be found in Appendix B.

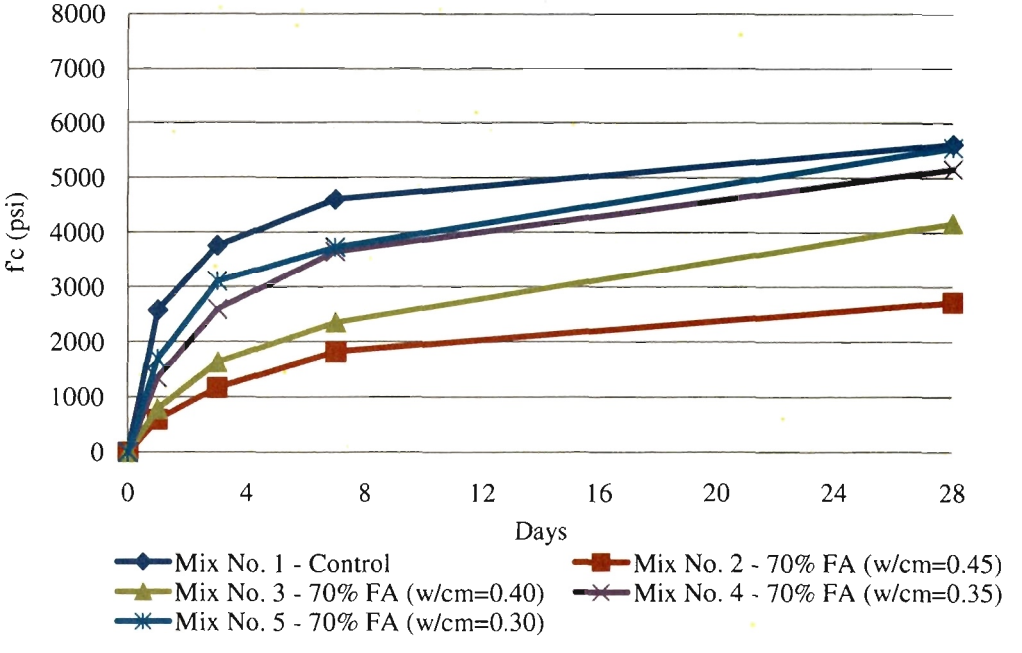

(1psi = 6.89 kPa)

Figure 4.2: The trend in the average compressive strength for each mix design.

4.3.3. Conclusions. Obtaining comparable compressive strengths at 28 days with HVFA concrete versus conventional concrete was a goal in this study. Figure 4.2 illustrates that when the *w/cm* is decreased to 0.30, HVFA concrete does exhibit identical

28-day compressive strength values. Also, at a *w/cm* of 0.30 in a HVFA concrete, the compressive strength exceeded that of the conventional concrete at 56 days. If the *w/cm* were increased slightly to 0.35, the HVFA concrete still exhibits a comparable compressive strength to that of conventional concrete at 56 days.

Early strength gain is important in construction, particularly for form removal. Figure 4.2 also shows that HVFA concrete having a w/cm consistent to a typical w/cm used in conventional concrete produces lower strengths not always suitable for normal construction practices. However, decreasing the HVFA concrete *w/cm* increases even early strength gain. HVFA concrete at 0.45 and 0.40 *w/cm* results in 1 day compressive strengths of less than 1,000 psi (6.9 MPa). Mix Design No. 1 reported a 1-day compressive strength of 2,570 psi (17.7 MPa). Although decreasing the *w/cm* to 0.35 and 0.30 does improve the 1 day compressive strengths, Mix Nos. 4 and 5 resulted in compressive strengths nearly 1,000 psi (6.9 MPa) less than that of Mix No. 1, but these strengths are likely sufficient for normal concrete construction practices.

When considering the differences in each mix design, the *w/cm* is the major factor. Each mix design was produced to investigate the effect decreasing the *w/cm* would have on the compressive strength. The behavior of the compressive strengths for the mix designs analyzed coincides with results for traditional mix designs with decreasing *w/cm*. Even with a mix consisting of 70 percent fly ash and 30 percent portland cement, it is still shown that decreasing the *w/cm* increases the compressive strength at all ages. Low early strength development is expected in HVFA concrete and the data concludes this very well. Lowering the *w/cm* in conventional concrete will also produce increased compressive strengths, but workability becomes difficult without admixtures. The advantage to using HVFA concrete is that the water-to-cement ratio can be reduced to produce compressive strengths comparable to conventional concrete while maintaining workability.

4.4. FLEXURAL STRENGTH TEST

The ASTM C78-09 "Standard Test Method for Flexural Strength of Concrete (Using Simple Beam with Third-Point Loading)" [ASTM C78, 2009], was used as a guideline to evaluate the flexural strength of simply-supported concrete beams, also

referred to as the modulus of rupture (MOR). The concrete mix design evaluated was Mix No. 3 (70% fly ash and 0.40 *w/cm*). The test consisted of subjecting the concrete simple beams to a third-point loading as designated by the ASTM standard.

4.4.1. Preparation and Testing. Each specimen measured 6 in. x 6 in. x 24 in. (153 mm x 153 mm x 612 mm). Three rectangular beams were constructed from Mix No. 3. All specimens were cast in steel beam molds covered with plastic and moist cured for 7 days. This cast was performed on October 8, 2010 and was batched at a local ready-mix plant, then delivered to the lab where it was placed indoors. The specimens were then removed from the steel molds and moist cured for 7 days. Testing was performed at 28 days and the test set up is shown in Figure 4.3.

(a) (b)

Figure 4.3: Testing specimens in flexural strength. (a) Flexural strength testing set up. (b) Failure of flexural specimen.

4.4.2. Results. The following results are from testing Mix No. 3. As stated in Section 3, this particular mix design was chosen to evaluate large scale testing. Other tests were also performed on this mix design as mentioned throughout this section. This mix design contains 70 percent fly ash by volume of cementitious material and has a

w/cm of 0.40. Chemical activators included 10 percent calcium hydroxide and 4 percent gypsum by weight of cementitious material.

The average compressive strength for Mix No. 3 was 4,180 psi (30 MPa) at 28 days. The tested flexural stress value was determined by the average of three test specimens and measured 445 psi (3.0 MPa) with a coefficient of variation (COV) of 12.5 percent. All specimens failed within the middle third region as shown in Figure 4.4.

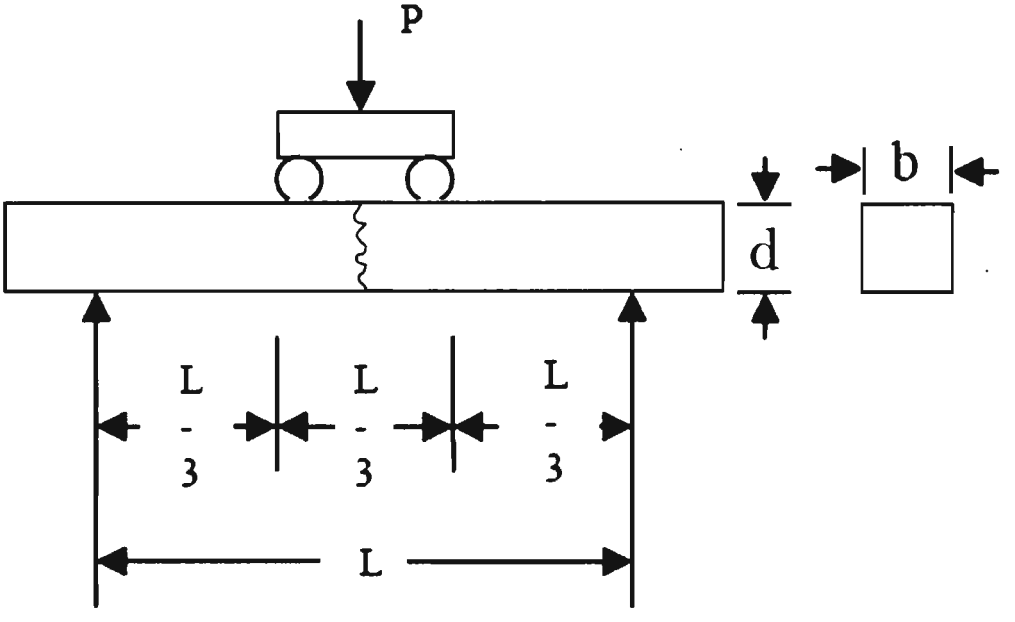

Figure 4.4: Flexural beam with failure shown at the middle third region.

4.4.3. Conclusions. The flexural strength test was performed to assist in determining the tensile strength for Mix No. 3, the production mix for the full scale specimen testing. Due to the failures occurring within the middle one-third region of the beams, the MOR can be expressed by PL/bd^2. This equation is based on the elastic beam theory which implies the tensile stress is proportional to the distance from the neutral axis. However, this is merely an estimate since the stresses induced under load generate

a parabolic relationship. Thus, the MOR overestimates the tensile strength and it is suggested that the correct value of tensile strength is about ¾ of the theoretical modulus of rupture. Even for a conventional concrete, inconsistencies occur in determining the modulus of rupture.

The variability of the MOR test is significant and strongly affected by the moisture conditions of the specimen. Additional possibilities as to the reasons why the MOR test gives a higher value of strength than a direct tension test include: accidental eccentricity in a direct tensile test, which lowers the apparent strength of the concrete: the loading arrangement in a direct tensile test where the entire volume of the specimen is subjected to the maximum stress, increasing the potential for a weak element, and crack propagation blocked by less-stressed material closer to the neutral axis for the MOR test.

ACI 318 Building Code [2008] uses the expression $7.5\sqrt{f'_c}$, where f'_c equals the average 28-day compressive strength, as the calculated MOR for building design. This expression is used for mix designs generally consisting of between 70 and 100 percent portland cement. Since Mix No. 3 is comprised of 70 percent fly ash, the applicability of using this equation in calculating the tensile strength for mixes with this magnitude of fly ash was evaluated. In using this particular approach, though, there is still some variability in calculating the MOR, even for 100 percent portland cement concrete mixes, with the actual coefficient ranging anywhere from 6 to 12. This equation showed that with the tested average stress value of 445 psi (3.0 MPa), the coefficient calculates to be 7.89. This value is well within the given range used for portland cement concrete mixes.

4.5. SPLITTING TENSILE STRENGTH TEST

Using ASTM C496-04 "Standard Test Method for Splitting Tensile Strength of Cylindrical Concrete Specimens" [ASTM C496, 2004], as a guideline, concrete cylinders were constructed to evaluate the tensile stress for each of the concrete mix designs. Mix No. 1 was used as a comparison for Mix Nos. 2 and 3 and also provided a baseline when analyzing prediction of tensile strength. The test consisted of subjecting the concrete cylinders to a uniform compressive load along the longitudinal axis as designated by the ASTM standard.

4.5.1. Preparation and Testing. Each specimen was 6 in. (153 mm) in diameter and 12 in. (306 mm) in length. There were 3 cylinders constructed for each mix design. All specimens were cast in plastic cylinder molds, covered with plastic and moist cured for 7 days. The specimens were then stripped from the plastic molds, marked and stored until their intended test date. The specimens were tested at 28 days with an axial load of 283 lb/ft (128 kg/m) and the test set up is shown in Figure 4.5.

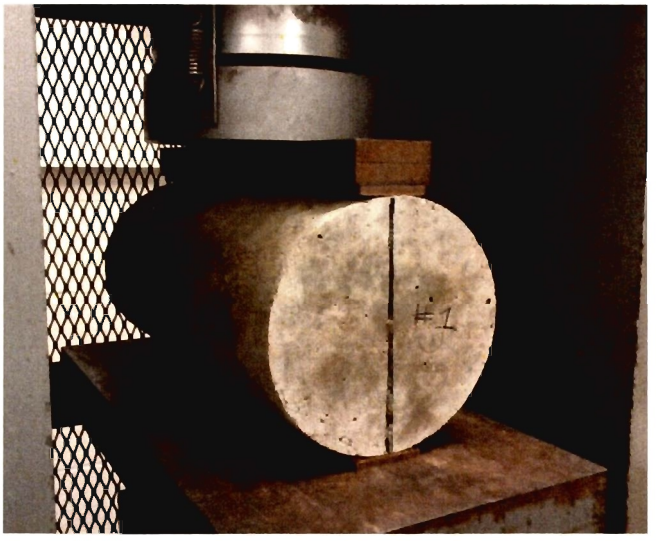

Figure 4.5: Specimen in the splitting tensile test set up.

4.5.2. Results. The average splitting tensile strength was determined for each concrete mix from the equation stated in ASTM C496. The average compressive strength and average maximum load were the values used in the above mentioned equation. The average splitting tensile strength for Mix No. 1, the control, was 477 psi (3.3 MPa) with a COV of 24 percent. Mix No. 2 was found to have an average splitting tensile strength of 356 psi (2.5 MPa) with a COV of 10 percent. Lastly, the average splitting tensile

strength of Mix No. 3 was 443 psi (3.0 MPa) with a COV of 23 percent. The above results were evaluated for direct comparison by removing the compressive strength variable contained within calculating tensile strength. The reported splitting tensile strengths were divided by the square root of f'_c, where f'_c was the compressive strength associated with each concrete mix. As shown in Figure 4.6, the results from each concrete mix are comparable to each other. Mix Nos. 2 and 3 exhibit nearly the exact same value; whereas Mix No. 1 was slightly lower. Individual test data may be found in Appendix A.

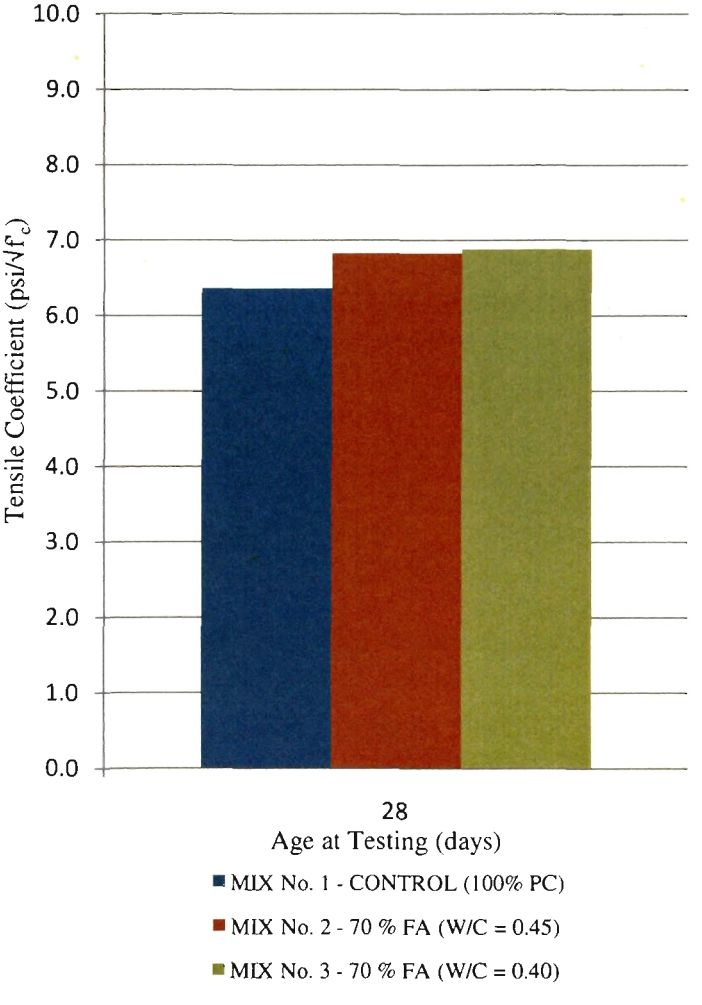

Figure 4.6: Tensile strength coefficient for each concrete mix design.

4.5.3. Conclusions. Significant variability of results from tensile testing is commonly recognized. Also, it is recognized that the MOR test rather overestimates the tensile strength of concrete, while the splitting tensile strength test determines tensile strengths closer to the direct tensile strength of concrete, only being 5 to 12 percent higher [Neville, 1997]. Mix No. 1 reported a tensile strength of $6.36\sqrt{f'_c}$ and Mix Nos. 2 and 3 reported tensile strengths of 6.83 and $6.86\sqrt{f'_c}$, respectively. The results conclude that the splitting tensile strength test produced similar tensile properties among the HVFA concretes, excluding the compressive strength variation. Also concluded was that the splitting tensile strength test generated values of nearly the same tensile properties for HVFA concrete as well as conventional concrete. According to these results, the splitting tensile strength test may be used to define tensile strength for HVFA concrete.

4.6. MODULUS OF ELASTICITY TEST

Concrete cylinders were constructed to evaluate the modulus of elasticity of Mix No. 1, Mix No. 2, and Mix No. 3. The ASTM C469-02 "Standard Test Method for Static Modulus of Elasticity and Poisson's Ratio of Concrete in Compression" [ASTM C469, 2002], was used as a guideline to perform the necessary procedures. Mix No. 1 was comprised of 100 percent portland cement and was used in conjunction with the other two mixes in evaluating the validity of using the secant modulus of elasticity equation for high-volume fly ash concrete mixes. The test consisted of subjecting the concrete cylinders to a uniform axial compressive load as designated by the ASTM standard.

4.6.1. Preparation and Testing. Each specimen was 6 in. (153 mm) in diameter and 12 in. (306 mm) in length. There were three cylinders constructed for each mix design. All specimens were cast in plastic cylinder molds, covered with plastic and moist cured for 7 days. Each mix was batched and cast within the lab. The specimens were then stripped from the plastic molds, marked and stored until their intended test date. The modulus of elasticity testing was performed at 28 days. Prior to testing, each cylinder was capped in accordance with ASTM C617-09 "Standard Practice for Capping Cylindrical Concrete Specimens" [ASTM C617, 2009]. A specimen in the test set up is shown below in Figure 4.7.

Figure 4.7: Modulus of elasticity test set up.

4.6.2. Results. The average tested modulus of elasticity for each concrete mix as performed by the ASTM C496 standard is listed below in Table 4.2, along with the average compressive strength from testing three replicate specimens. The calculated modulus of elasticity value and the compressive strength used in the equation $57{,}000\sqrt{f'c}$ is also shown in Table 4.1. The values calculated through testing are noticeably higher than the values calculated using the equation specified by ACI 318-08 [2008].

4.6.3. Conclusions. Like compressive strength, the modulus of elasticity is significantly affected by the modulus of the aggregate used in the concrete. Therefore, the modulus of elasticity is sensitive and measured values can be higher or lower than the specified calculated modulus of elasticity in accordance with ACI 318 [2008]. The percent increase typically ranges from 80 to 120 percent of the specified calculated value according to ACI 318-08 [2008]. Taking this into consideration, the average tested modulus of elasticity for Mix No. 2 falls within this range at 115 percent of the specified calculated modulus of elasticity. Mix No. 3 is slightly outside of this range at 130 percent. As for Mix No. 1, it lies significantly outside of this typical range at 150 percent of the specified calculated modulus of elasticity. Nonetheless, it appears from this

limited amount of testing that the ACI 318 [2008] equation for modulus of elasticity is as applicable to HVFA concrete as it is to conventional concrete.

Table 4.2: Modulus of elasticity test results of each mix evaluated.

Mix Design	*28-Day Compressive Strength (psi)*		*Modulus of Elasticity (ksi)*		
	Test Value	*Average*	*Test Value*	$57{,}000\sqrt{f'_c}$	$w^{1.5}33\sqrt{f'c}$
No. 1	5990	5610	5800	4300	4120
	5460				
	5380				
No. 2	2590	2720	3430	2900	4050
	2910				
	2660				
No. 3	4240	4180	4780	3680	4020
	4400				
	3900				

(1 psi = 6.89 kPa)

4.7. SHRINKAGE ANALYSIS

A modified version of ASTM C157-10 "Standard Test Method for Length Change of Hardened Hydraulic-Cement Mortar and Concrete" [ASTM C157, 2010] was used in constructing concrete cylinders to evaluate the length change known as shrinkage for Mix Nos. 1, 2, and 3. Mix No. 1, the 100 percent portland cement concrete with a *w/cm* of 0.45, was used as a baseline reference. Mix Nos. 2 and 3 contained 70 percent fly ash with *w/cm* of 0.45 and 0.40, respectively.

4.7.1. Preparation and Testing. Each specimen was 4 in. (102 mm) in diameter and 24 in. (612 mm) in length. There were four long cylinders constructed for each mix design. All specimens were cast in PVC pipes with end caps and moist cured for 1 day. The specimens for each mix design were cast on three separate days over the course of an

8 month period. The first cast was of Mix No. 1 and took place on March 15, 2010. The second cast was of Mix No. 2 and occurred on June 2, 2010. The final cast was of Mix No. 3 and took place on November 4, 2010. The specimens were removed from the PVC pipe molds and marked for identification. Concrete and steel epoxy was then used to adhere 3 equally spaced sets of 5 DEMEC points every 4 in. (102 mm) along the length of each specimen as shown Figure 4.8. The points were set using the placement bar of the DEMEC instrument.

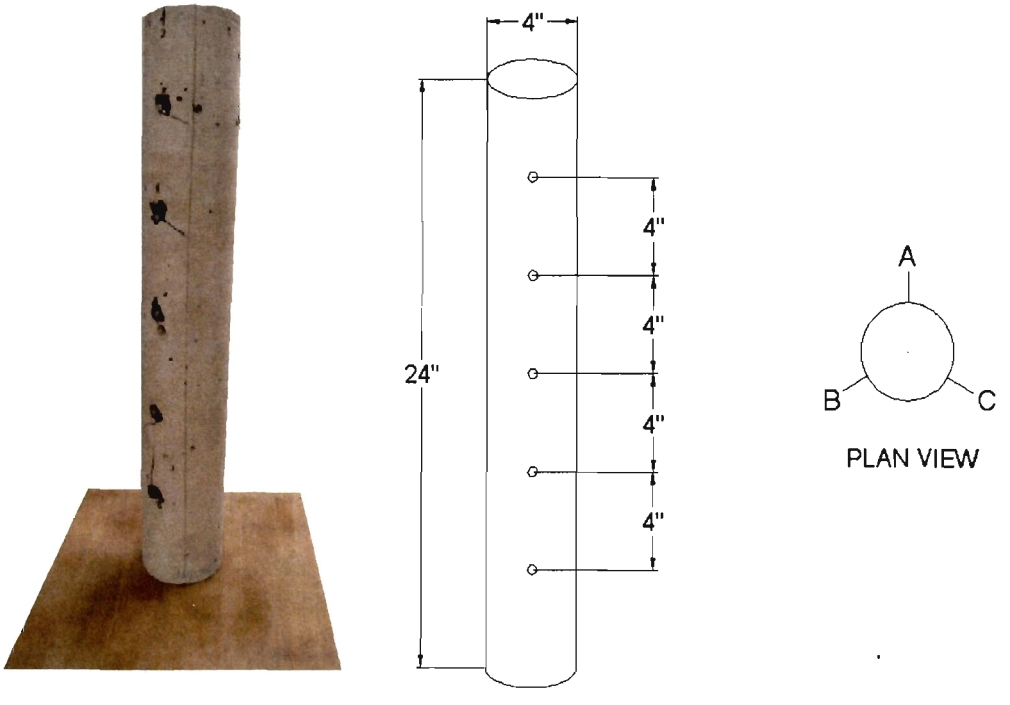

Figure 4.8: Shrinkage specimen details. (a) Concrete shrinkage specimens with DEMEC points. (b) Dimensions of shrinkage specimen and placed DEMEC points. A, B, and C are at 120° angles.

Readings on each of the specimens was taken for a period of 4 to 6 months, respectively of each mix design. A DEMEC gauge was used to take the initial reading the day the specimens were removed from the molds and then taken once daily for 2 weeks. After the specimens reached an age of 2 weeks, readings were then taken every other day for 2 months. Readings were then taken once a month for the remainder of the testing period.

4.7.2. Results. Figure 4.9 shows the average concrete shrinkage of Mix Nos. 1 through 3 over a period of approximately 120 days. As the results show, Mix No. 1 had considerably higher shrinkage strains than that of Mix Nos. 2 and 3. Mix Nos. 2 and 3 contained 70 percent fly ash and 30 percent portland cement. The shrinkage strain results of Mix Nos. 2 and 3 are very similar to one another.

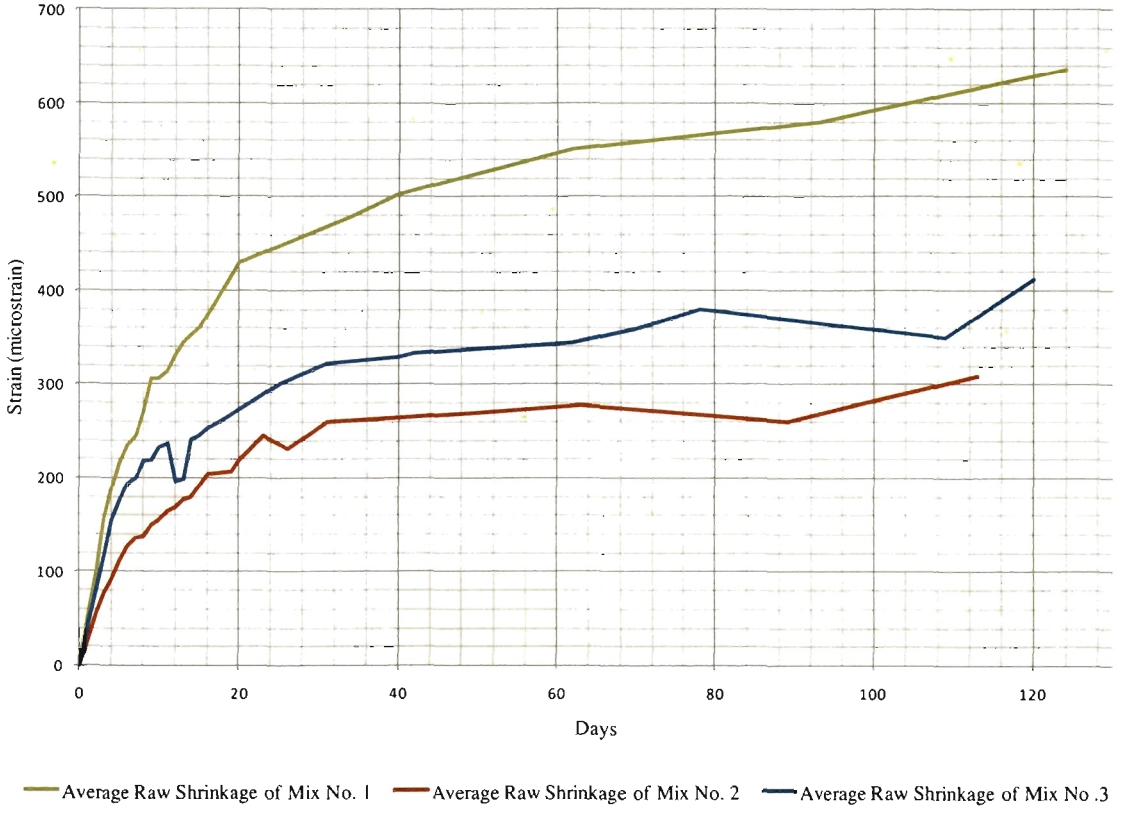

Figure 4.9: Average raw concrete shrinkage for each specimen.

4.7.3. Data Analysis and Interpretation. A standard error analysis was also performed for each of the mixes tested as shown in Figure 4.10. The standard error bars represent a 95 percent confidence interval for each set of four specimens cast for each concrete mix design. The confidence intervals were developed using the standard error of a set's mean value (SEM). A data set consisted of nine DEMEC measurements from each of the four specimens tested for each mix design, or 36 readings for each plotted point in Figure 4.10. Data values pertaining to each of the specimens tested may be found in Appendix B. The standard errors plotted for each concrete mix design show only small amounts of variation. The plotted standard error bars illustrate how comparative the shrinkage is between each mix.

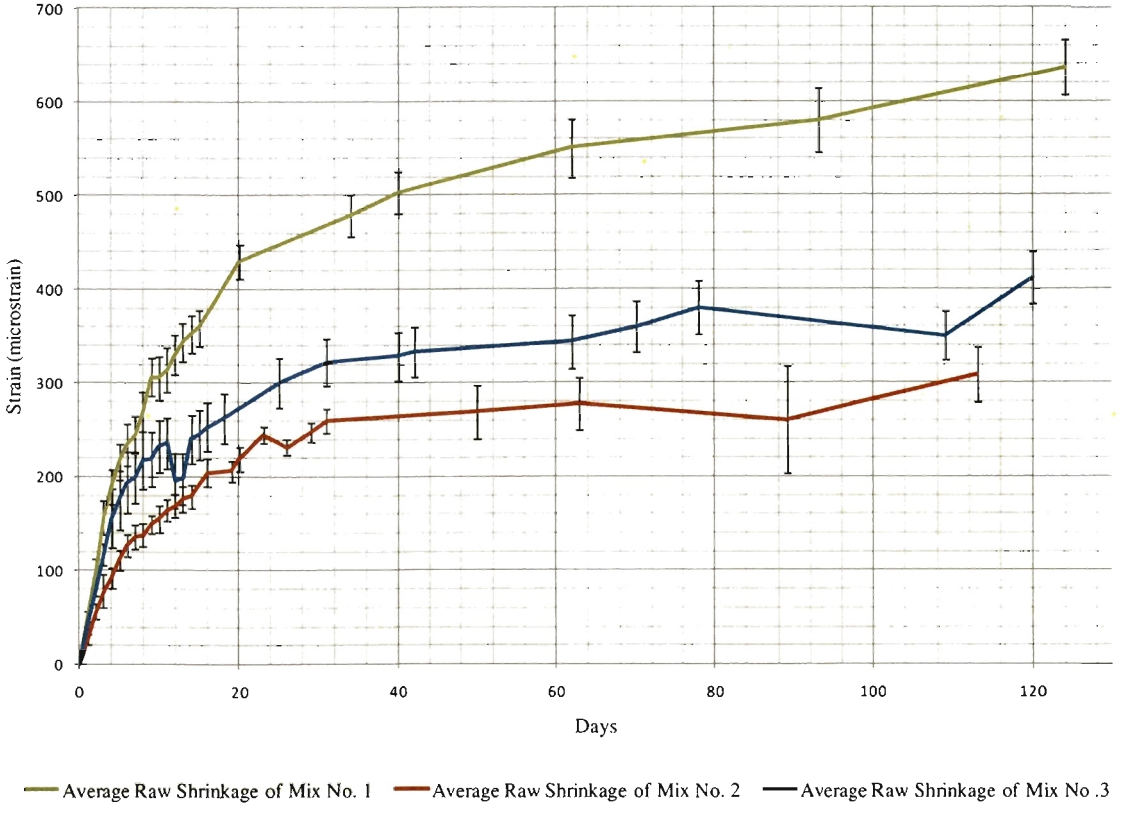

Figure 4.10: Average raw concrete shrinkage with standard error displayed for each specimen.

Also evaluated with the results from the shrinkage testing were several shrinkage prediction models discussed in a study conducted by Videla [2008]. The prediction models evaluated include: ACI 209-92 empirical model with a modified ultimate shrinkage $(\varepsilon_{sh})_u$ value; Bažant-Baweja B3 model; and CEB MC90-99 model. Various factors that affect shrinkage as stated in Videla [2008] include: age of concrete when drying starts; curing method; relative humidity; volume-surface ratio or average specimen thickness; cement type; and concrete mean compressive strength. Each prediction model is based on different variations of the factors mentioned above. Although, no particular model is considered "the best model" to use in predicting shrinkage, each model was plotted to show a comparison between predicted values and tested values. Lastly, to note from the above study, is the models were calibrated with conventional concretes and concretes containing no more than 30 percent fly ash.

The prediction models mentioned above are shown in comparison to Mix No. 1 as expressed in Figure 4.11. The ACI 209 R-92 Model over predicts the shrinkage as measured for Mix No. 1. The CEB MC90 Model under predicts the shrinkage. The B3 Model shows the nearest predicted shrinkage to Mix No. 1, although, predicting slightly lower values. The measured shrinkage of Mix No. 1 is greater than any of the prediction models for the first 30 days. After about 30 days, Mix No. 1 falls within the predicted values of the ACI 209 R-92 Model and B3 Model, although much closer to the B3 Model.

Mix No. 2 with the prediction models are shown in Figure 4.12. All three models show over prediction of shrinkage compared to the measured shrinkage values of Mix No. 2. The B3 Model exhibits values nearly 400 micro strain higher than that of Mix No. 2. However, the ACI 209 R-92 Model and CEB MC90 Model have comparable prediction results. Early values predicted by the ACI 209 R-92 Model are near that of measured shrinkage values.

Figure 4.13 shows Mix No. 3 with each shrinkage prediction model. For the first 10 days, the CEB MC90-99 and B3 models follow the measured shrinkage results very well. Although, compared to the other models at later age, the CEB MC90-99 model predicts closest with the measured shrinkage results. However, this model is still nearly 100 micro strain larger than the measured results. The other two models result in

shrinkage predictions of very similar fashion and show much larger results than the measured results, having values near 600 micro strain.

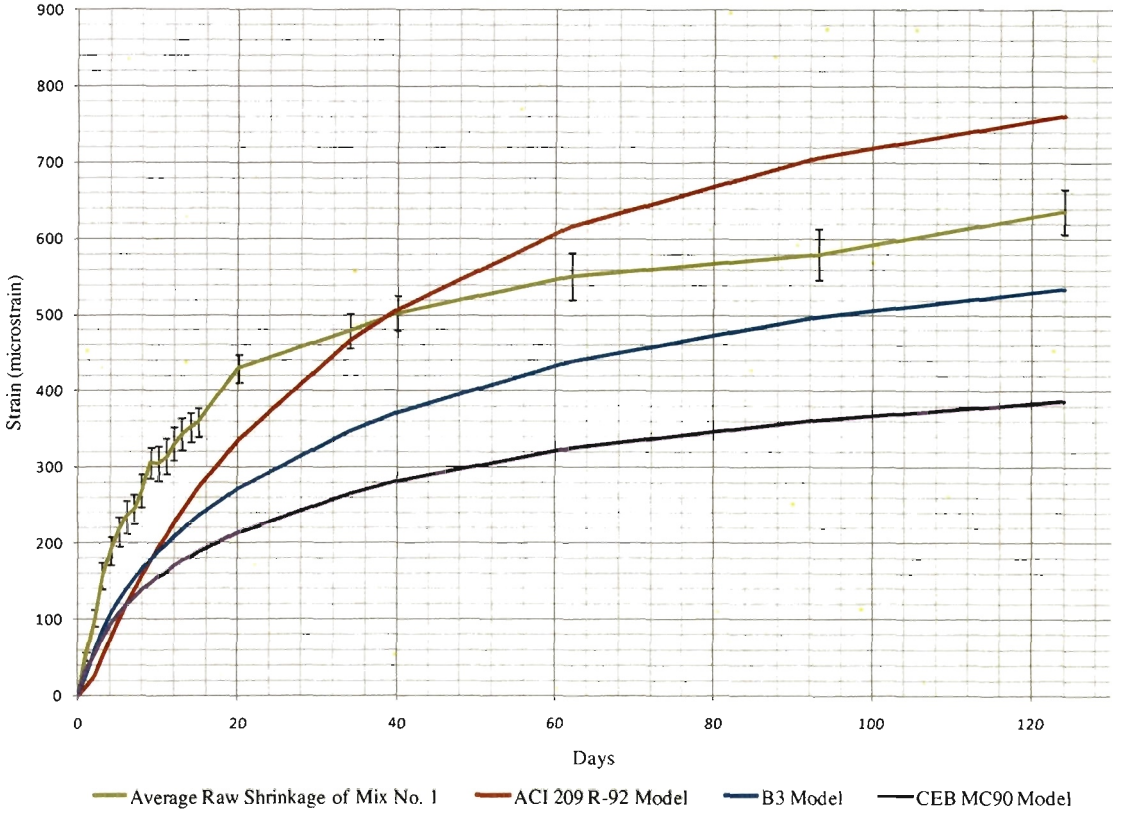

Figure 4.11: Average raw shrinkage of Mix No. 1 and shrinkage prediction models.

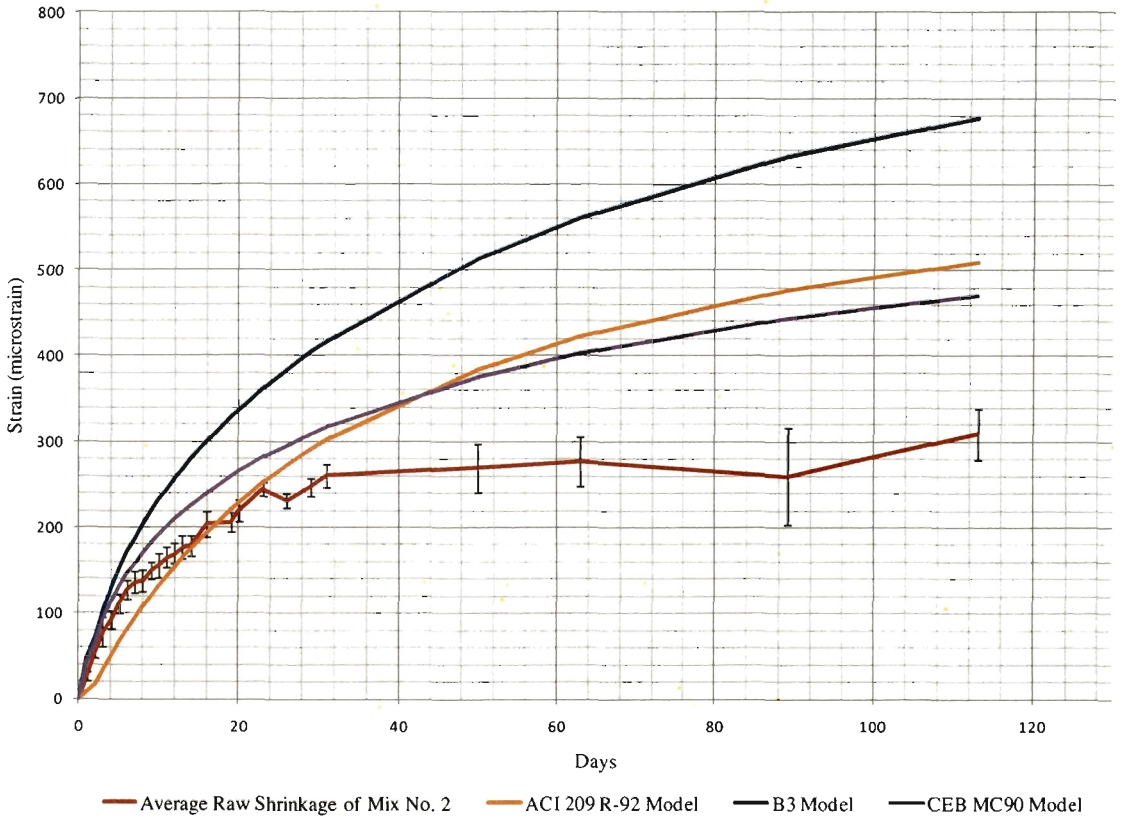

Figure 4.12: Average raw shrinkage of Mix No. 2 and shrinkage prediction models.

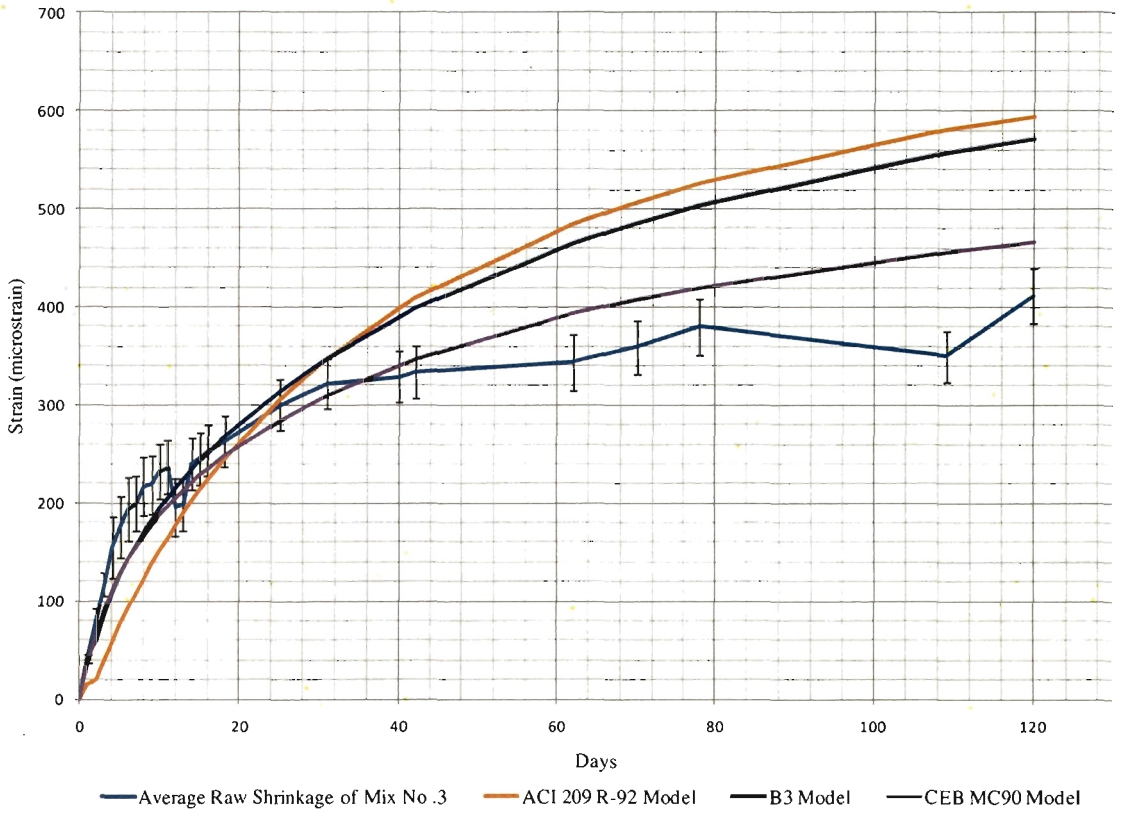

Figure 4.13: Average raw shrinkage of Mix No. 3 and shrinkage prediction models.

4.7.4. Conclusions. As stated above, the HVFA concrete mixes exhibited much lower shrinkage strains than the 100 percent portland cement concrete mix. The results of this test conclude that the addition of fly ash in the concrete has a significant effect on the shrinkage strain experienced by each specimen. Section 2.4.2 discusses that the addition of fly ash increases the volume of paste and may increase shrinkage provided the *w/cm* remains unchanged. This study examined two *w/cm* for the HVFA concrete of 0.45 and 0.40. It is to be expected that decreasing the *w/cm* from 0.45 to 0.40 in the HFVA concrete mix would reduce the shrinkage. The results of the data not coinciding with this may be attributed to the humidity conditions at which the specimens of Mix No. 3 were stored, which were indoor ambient conditions but not within a controlled environmental

chamber. Nonetheless, the HVFA concrete specimens experienced noticeably less shrinkage than the 100 percent portland cement concrete.

The standard error plots shown in Figure 4.10 indicate that each mix design has statistically different shrinkage strains from one another over the period of testing. If the results from any one mix were to fall within the standard error variation of any other concrete mix tested, this would indicate those mixes would not be statistically different. However, none of the concrete mixes exhibited this result. Tables pertaining to standard error values for a specific specimen may be found in Appendix B.

Figures 4.11 through 4.13 shows the average shrinkage of each mix and the shrinkage prediction models used. The results for Mix No. 1 indicate that the B3 Model could be used to predict an estimation of the shrinkage experienced within the concrete. As for Mix Nos. 2 and 3, the models noticeably overestimate the shrinkage. The models tended to over predict the shrinkage for Mix No. 2 more than for Mix No. 3. If any of the shrinkage prediction plots were within the standard error bar ranges of either concrete mix, then it could be concluded the model's prediction of shrinkage would not be statistically different than the reported measured shrinkage values. Previously discussed in Section 4.7.2 is the fact that these models are based on conventional concrete mixes. The models overestimating the shrinkage for Mix Nos. 2 and 3 may be attributed to this fact, indicating that a HVFA concrete mixes may use more of the available water for hydration and leave less available for shrinkage.

5. DURABILITY TESTS

5.1. INTRODUCTION

Durability is influenced by many factors and more often than not the integrity of structures or pavements are affected not only by one, but a combination of several of those factors. These factors include: strength, air content, and permeability, all of which share a common deterioration mechanism. The connecting mechanism between all the factors is water; which has significance on initial concrete mix design and provides the pathway for the ingress of other chemicals to promote deterioration when the concrete is hardened. Testing for the effects of simulated environmental wear on concrete specimens is important for designing structures and pavements with increased longevity. This section describes and explains the many tests preformed to evaluate the durability of the particular concrete mixes within this research study.

5.2. DURABILITY TESTING

Many tests have been developed to aid in the understanding and prediction of potential durability issues that concrete may experience during its lifetime. There are tests that analyze chloride penetration and concentration, which is then related to a scale estimating the potential risk for corrosion of embedded steel reinforcement. Other tests include using electrical resistance and potential difference to predict the resistance concrete may have against the onset of corrosion and how much corrosion damage may be present. Climate variations are also studied through freezing and thawing cycles to illustrate the damaging effects of such environments on concrete. Table 5.1 lists the durability tests used and performed to evaluate the particular concrete mixes within this research study.

Three concrete mixes were evaluated with the durability tests listed in Table 5.1. These concrete mixes consisted of 100 percent portland cement at a *w/cm* of 0.45 and two mixes of 70 percent replacement of cement with fly ash at a *w/cm* of 0.45 and 0.40, which are shown below in Table 5.2. Since the *w/cm* is generally related to durability, the same *w/cm* was chosen for the portland cement and HVFA concrete that would undergo the various durability tests. A second *w/cm* of 0.40 was selected for the HVFA concrete

recognizing the decreased water demand that results from incorporating fly ash in a concrete mix. Fly ash develops a more condensed microstructure during the hydration period due to the fineness of the material compared to that of portland cement. This refined microstructure reduces the potential for ingress of chemicals and other such solvents that stimulate deterioration, which should be apparent during the durability testing.

Table 5.1: Durability tests performed on concrete mixes.

Durability Characteristics	*Test*
Chloride Permeability	
Electrical Method	ASTM C 1202
Ponding Method	ASTM C 1543 / AASHTO T 259
Freeze-Thaw Resistance	ASTM C 666 (Test Procedure A)
Corrosion Resistance	
Concrete Resistivity	ASTM C 1543 / AASHTO T 259
Corrosion Potential	ASTM C 1543 / AASHTO T 259

Table 5.2: Material weights for each concrete mix evaluated.

Materials (lb/yd^3)	*Mix Design*		
	No. 1	*No. 2*	*No. 3*
Water	345	345	345
Cement	765	196	222
Fly Ash	–	457	519
Calcium Hydroxide	–	53	60
Gypsum	–	49	49
Coarse Aggregate	1754	1754	1754
Fine Aggregate	1016	1016	1016
w/cm	0.45	0.45	0.40

(1 lb/ft^3 = 16 kg/m^3)

5.3. CHLORIDE PERMEABILITY BY ELECTRICAL METHOD

5.3.1. Preparation and Testing. Two specimens were constructed for each mix design listed in Table 5.2. The specimens measured 3.75 in. (95 mm) in diameter and 2 in. (51 mm) in length and were cut from cores of cast cylinders which measured 6 in. (152 mm) in diameter. The curved surface of each specimens was coated in epoxy, and then the specimens were vacuum saturated with water for 1 hour followed by soaking in water for 18 hours.

Figure 5.1 shows the testing apparatus, where the specimen was placed with one end exposed to a solution of sodium chloride (NaCl) and the other end was exposed to a solution of sodium hydroxide (NaOH). A constant 60 V potential was applied across the specimen to increase the rate at which the chlorides would penetrate through the specimens. The test was run for 6 hours with electrical current measurements taken every 30 minutes. The total charge passing through the specimen (in coulombs) was then found by calculating the total area under the plot of time versus current. Thus, higher coulomb values indicated higher permeability.

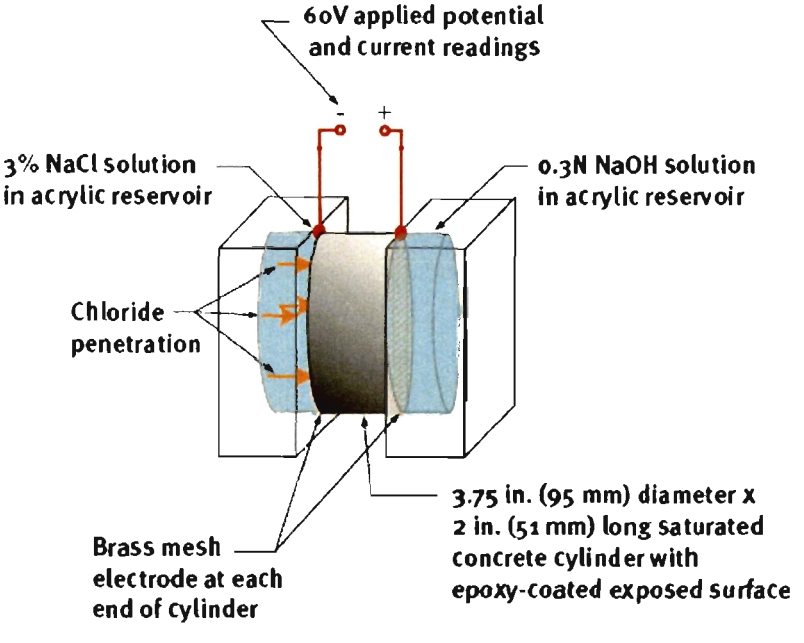

Figure 5.1: Schematic of rapid chloride permeability test set up [Hooton, 2006].

The chloride permeability test by electrical method does not directly measure the depth or rate of chloride penetration, therefore, a correlation of qualitative terms to a chloride ion penetrability has been recommended by ASTM C1202 [2009]. This correlation is shown in Table 5.3.

Table 5.3: Chloride ion penetrability based on charge passed.

Charge Passed *(Coulombs)*	***Chloride Ion Penetrability***
> 4000	High
2000 to 4000	Moderate
1000 to 2000	Low
100 to 1000	Very Low
< 100	Negligible

5.3.2. Results. The test results are shown in Table 5.4. Mix No. 1 resulted in the highest average charge passed, indicating there would be "moderate" penetration of chloride ions within a structure constructed with this concrete. The coefficient of variation was calculated to be 10 percent for the two specimens tested. Mix Nos. 2 and 3 resulted in similar average charge passed indicating there would be "low" penetration of chloride ions within a structure constructed with this concrete, with Mix No. 3 having the lowest value or highest resistance to chloride penetration. The coefficients of variation were calculated to be 11 and 12 percent for Mix No. 2 and Mix No. 3, respectively. The average charge passed for each concrete mix with the associated chloride ion penetrability rating is shown in Table 5.4.

Table 5.4: The tested concrete mixes with associated chloride ion penetrability rating.

Mix Designation	*Average Charge Passed (coulombs)*	*Chloride Ion Penetrability*
Mix No. 1	2480	Moderate
Mix No. 2	1860	Low
Mix No. 3	1590	Low

5.3.3. Conclusions. The results shown in Table 5.4 lead to the conclusion that Mix Nos. 2 and 3, each containing 70 percent fly ash replacement, would reduce the penetration of chloride ions through the concrete as compared to that of Mix No. 1. The refined microstructure of the fly ash proves to be beneficial in preventing the ingress of chloride ions, even at the same *w/cm*. The decreased *w/cm* of Mix No. 3 further reduces chloride ion penetration based on the results shown in Table 5.4.

5.4. CHLORIDE PERMEABILITY BY PONDING METHOD

5.4.1. Preparation and Testing. The AASHTO T259 standard was used as a guideline for conducting continual ponding tests of specimens from each mix design. This test standard states that continual ponding shall be maintained for 90 days. The testing carried out within this study consisted of 120 days. The ponding specimens measured 18 in. x 18 in. (457 mm x 457 mm) in plan and 3½ in. (89 mm) in height. Each specimen contained a 15 in. square (381 mm) by 1 in. deep (25 mm) reservoir along its surface, as shown in Figure 5.2.

The forms used to cast the specimens were constructed of lumber and 1 in. thick (25 mm) polyisocyanurate foam. The walls of each form were made of four pieces of 1½ in. x 3½ in. (38 mm x 89 mm) lumber. A 21 in. x 21 in. x ¾ in. (533 mm x 533 mm x 19 mm) section of plywood was used as the bottom of each form. Centrally located on the top of the plywood was a 15 in. x 15 in. x 1 in. (381 mm x 381 mm x 25 mm) section of polyisocyanurate foam. The foam was secured to the plywood using Polyurethane

Premium Construction Adhesive manufactured by Henkel Corporation. Prior to using the forms, the interior surface of each form was coated with a layer of release agent that was manufactured by Dayton Superior. A drawing of a typical form may be found within Appendix C.

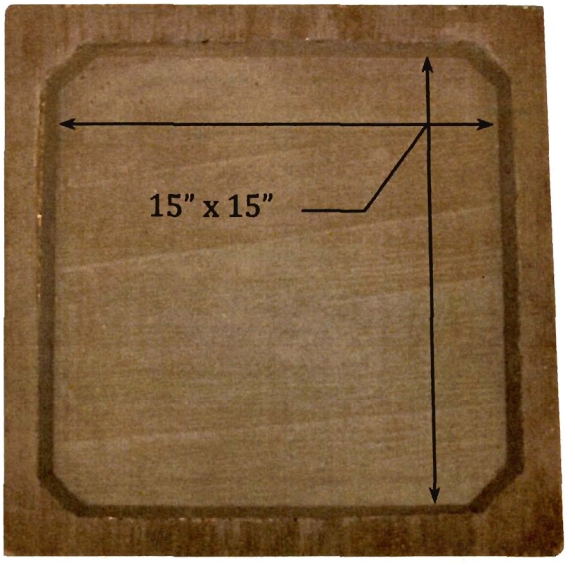

(1 in = 25.4 mm)

Figure 5.2: Typical ponding specimen.

During the 120 days of testing, specimens were stored within a room that had an average ambient temperature of 68°F (20°C) and a relative humidity of 40 to 60 percent. Specimens were placed upon shelves in an elevated position that measured approximately 1 in. (25 mm) above the underlying shelf as shown in Figure 5.3.

Figure 5.3: Typical specimen during testing.

The chloride analysis conducted upon these specimens involved determining the water soluble chloride content within multiple samples of concrete powder. The samples of powder were collected at various locations along the depth of a core. Cores were removed from the middle of each specimen's reservoir. Before a core was taken from a specimen, a concrete powder sample was collected from the surface of the specimen's reservoir at the location in which a core was going to be removed. Using a file, approximately 0.035 oz (1.0 g) of concrete paste, in a flower-like state, was gathered from a 3-in. x 3-in. (76 mm x 76 mm) area along the surface of the specimen's reservoir. Additional powder was obtained from within the same area while using a drill and a ⅝-in.-diameter (16 mm) concrete drill bit. As the drill was running, it was slowly lowered onto the concrete surface and remained there for approximately two seconds. This procedure was then repeated multiple times until approximately 0.071 to 0.106 oz (2.0 to 3.0 g) of concrete powder was obtained. The penetration of the drill bit into the concrete was less than 0.1 in. (3 mm) and did not occur twice at any one location. Cores were obtained using a 3-in.-diameter (76 mm), water-cooled, diamond core bit as shown in Figure 5.4. After a core had been labeled, it was immediately placed within a plastic bag and then stored within a dry environment.

Figure 5.4: Coring of a specimen.

Before collecting concrete powder samples from a core, elevations along its height were marked which indicated the elevations at which the concrete powder samples were to be collected. Those elevations were at distances of 0.25 in. (6 mm), 0.75 in. (19 mm), 1.5 in. (38 mm), and 2 in. (51 mm) from the top surface, as shown in Figure 5.7. The top of the core was considered to be the area in which the surface powder sample was collected prior to coring. After the core was properly marked, it was placed within a vise that was securely attached to a drill press. As shown in Figure 5.5, a steel disk was positioned between the top of the core and the vise. This was done to prevent any spalling of the core while collecting the powder sample located at a distance of 0.25 in. (6 mm) from the top of the core. The alignment of the vise and the platform of the drill press were then adjusted so that the 0.25 in. (6 mm) mark coincided with the ⅜-in.-diameter (10 mm) concrete drill bit. Once the mark was in line with the drill bit, a portion of the core's outer edge was removed by drilling to a depth of approximately 0.25 in. (6 mm). This initial amount of powder was removed with compressed air. A paper plate was then attached to the perimeter of the core using scotch tape, as shown in Figure 5.5. The drill bit was then reinserted into the 0.25 in. (6 mm) deep hole that was

previously drilled and 0.053 to 0.071 oz (1.5 to 2.0 g) of concrete powder was collected by drilling to a depth of approximately 2 in. (51 mm). The powder sample was then placed within a labeled plastic bag and the surrounding surfaces were cleaned using compressed air. This procedure was then repeated until concrete powder samples were collected from each of the four elevations marked along the depth of a core.

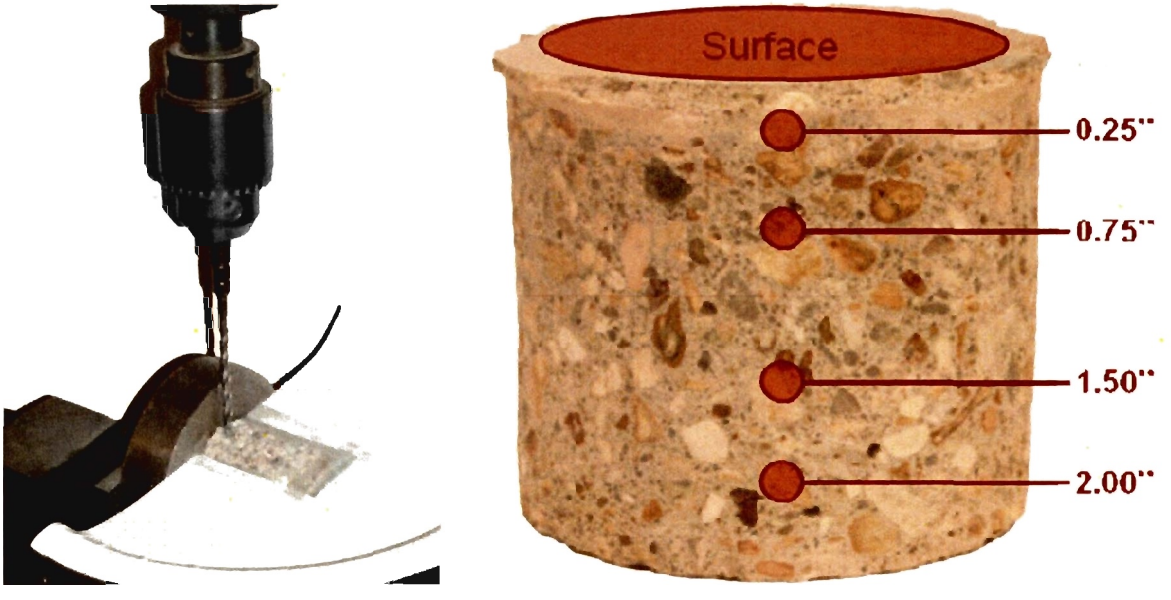

(a) (b)

Figure 5.5: Powder sample collection process. (a) Collecting powder samples along the height of a concrete core. (b) Locations along the height of a core where concrete powder samples were collected.

Using Rapid Chloride Testing (RCT) equipment manufactured by Germann Instruments, Inc., the concentration of water soluble chlorides contained within each powder sample was determined. Using the graduated ampoule and compression pin that were included within the RCT kit, 0.053 oz (1.5 g) of concrete powder, which pertained

to a single location along the height of a core, was measured. The powder was then transferred to a vial containing 0.304 fl-oz (9 mL) of an extraction liquid that was composed of 96 percent deionized water and 4 percent hydrogen peroxide (H_2O_2). The vial was then shaken for a period of 5 minutes. After a vial had been shaken, the contents within the vial were then filtered into a vial containing 0.034 fl-oz (1 mL) of a buffer solution. The buffer solution consisted of 24 percent hepes ($C_8H_{18}N_2O_4S$) and 76 percent deionized water. While filtering the contents from one solution to the other, the chloride selective electrode was prepped and calibrated according to the directions provided by the manufacturer.

Prepping of the electrode consisted of filling it with a wetting agent that contained 2 percent potassium nitrate (KNO_3), 3 percent potassium chloride (KCl), and 95 percent deionized water. Any air bubbles entrapped within the electrode were removed by gently taping the exterior surface of the electrode with a finger. Once prepped, the electrode was then connected to a voltmeter and inserted into one of four vials containing a solution with a known chloride concentration. The four calibration liquids included within the RCT kit contained chloride concentration levels of 0.005, 0.020, 0.050, and 0.500 percent. Those four chloride concentrations produced voltage readings of approximately 100 mV, 72 mV, 49 mV, and -5 mV respectively. After removing the electrode from a vial, it was rinsed off using distilled water and then blotted dry with a tissue. The recorded voltage readings were then plotted upon a log chart that contained units of voltage in the x-axis and percent chlorides by weight of concrete in the y-axis. The four points were then connected by three straight lines which were drawn with the use of a straight edge. A data sheet containing this log chart is located in Appendix C.

After successfully filtering the solution from one vial to the other, the solution was then quickly shaken for 1 to 2 seconds. The calibrated electrode was then inserted into the vial and remained there until the voltage reading stabilized to within 0.2 mV. Once stable, the voltage reading was then recorded and the chloride content was determined by using the log chart that contained the data which was previously obtained from the calibration liquids. The electrode was then removed from the vial, rinsed with distilled water and blotted dry with a tissue.

5.4.2. Results. Chloride profiles for the specimens are shown in Figures 5.6 and 5.7. Two specimens from each concrete were used to obtain cores and conduct chloride content sampling. The results indicate that the cores from identical concrete mixes contain similar chloride concentrations. The chloride profile for all specimens followed the typical shape of highest concentration at the surface with a decreasing concentration as a function of depth. Figure 5.6 shows Mix Nos. 2 and 3, those containing high volumes of fly ash, have lower chloride concentrations than that of Mix No. 1, the 100 percent portland cement mix. The same trend is noticed in Figure 5.7. Set A and Set B were cast at different times.

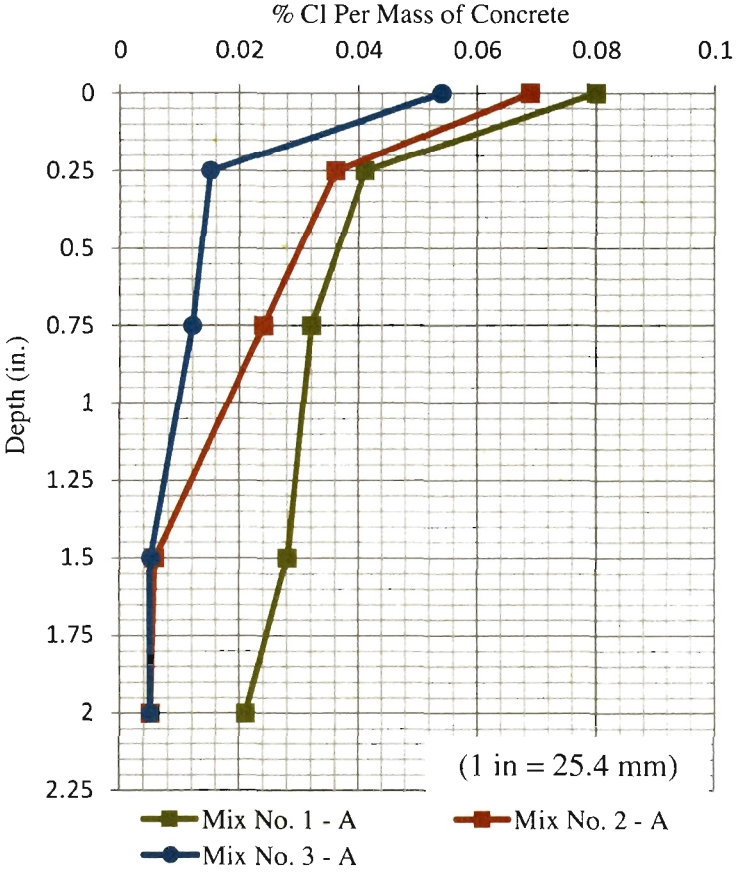

Figure 5.6: Typical chloride profiles for Set A ponding specimens.

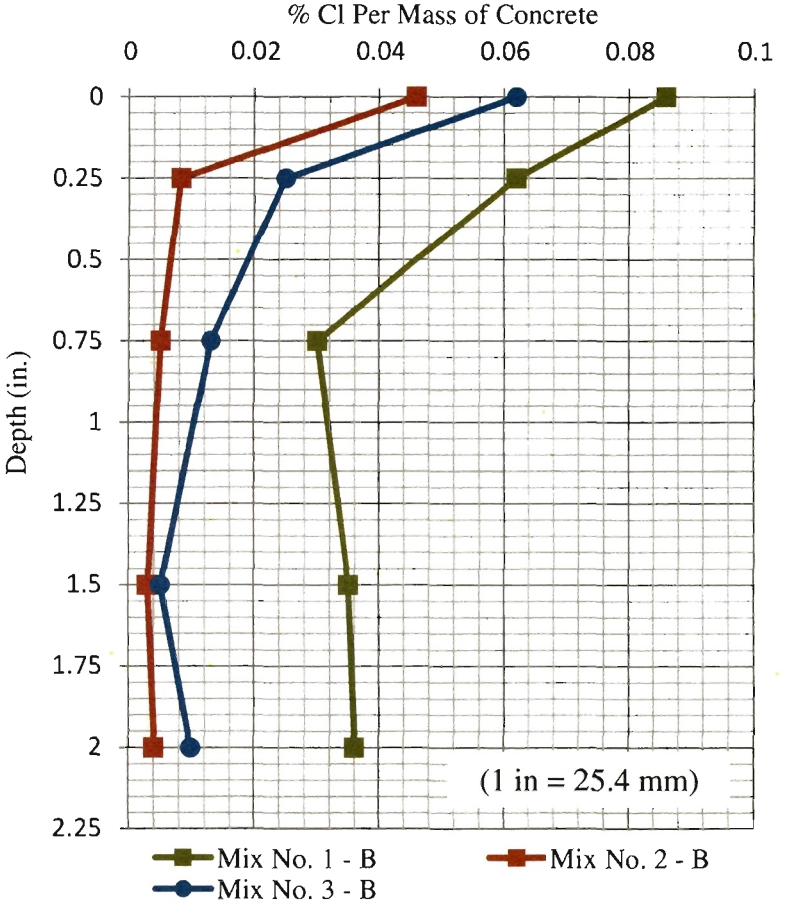

Figure 5.7: Typical chloride profiles for Set B ponding specimens.

5.4.3. Conclusions. The results shown in Figure 5.6 and 5.7 lead to the conclusion that all the chloride profiles are consistent with the chloride penetration within the specimens; the highest concentration at the surface and decreasing in chloride concentration with depth. The HVFA concrete of Mix Nos. 2 and 3 show lower chloride concentrations at the decreasing depths, thus, indicating a lower permeability and greater resistance to chloride penetration. Mix No. 1 resulted in higher chloride concentrations at the decreasing depths than that of Mix Nos. 2 and 3, therefore, concluding Mix No. 1 has a greater permeability and lower resistance to chloride penetration.

5.5. FREEZE-THAW RESISTANCE – TEST PROCEDURE A

5.5.1. Preparation and Testing. Test specimens were constructed in the laboratory and measured 3 in. x 4 in. x 16 in. (76 mm x 102 mm x 406 mm). Two specimens were constructed for each concrete mix design evaluated. All specimens were moist-cured for 28 days, tested at 28 days, and contained 5±1 percent air entrainment.

Test procedure A of the freeze-thaw resistance test consisted of a rapid freezing and thawing cycle within water. The specimens were placed in the bath of water and subject to a temperature change from 40°F (4.4°C) to 0°F (-17.7°C) then from 0°F (-17.7°C) back up to 40° (4.4°C). The temperature decrease and increase represented one freeze-thaw cycle. The cycle was within ASTM specifications lasting no longer than 5 hours, but no less than 2 hours. The dynamic modulus of elasticity was recorded at several intervals, though not to exceed 36 cycles of freeze-thaw throughout the testing. An oscillator with ranging values of frequencies was used to find the lowest frequency at which each specimen would resonate. A conversion equation was then used to convert the fundamental transverse frequency to dynamic modulus of elasticity. This procedure was repeated until each specimen had undergone 300 freeze-thaw cycles.

5.5.2. Results. The results from the freeze-thaw testing are shown in Table 5.5. A reported durability factor greater than 80 percent classifies a concrete mix as having "good" freeze-thaw resistance. Overall, the specimens representing Mix Nos. 1 through 3 show results very near or above the 80 percent mark. Mix No. 1, containing 100 percent portland cement, reported the highest durability factors at nearly 90 percent. Mix No. 3 reported the next highest durability factors at around 85 percent. Lastly, Mix No. 2 reported durability factors right at 80 percent. There is a significant difference in reported durability factors between Mix Nos. 2 and 3. However, Mix Nos. 1 and 3 show more similar results in the durability factors reported.

5.5.3. Conclusions. The results from Table 5.5 lead to the conclusion that Mix No. 3 is comparable to Mix No. 1 in terms of reported durability factors. The increased durability factors of Mix No. 3 over Mix No. 2 are likely attributed to the decreased w/cm from 0.45 to 0.40. The reduction in w/cm decreases the amount of free voids within the pore structure of the concrete. Mix No. 2, containing 70 percent fly ash at the same w/cm as Mix No. 1, did not perform as well as Mix Nos. 1 and 3, although it still indicated

"good" resistance to freeze-thaw damage. In general, the test results indicated that the HVFA concrete was able to develop an adequate air-void system to resist freeze-thaw damage.

Table 5.5: Reported durability factor (%) from freeze-thaw tests for each concrete mix.

Mix Designation	*Durability Factor (%)*
Mix No. 1	
Specimen No. 1	91
Specimen No. 2	87
Mix No. 2	
Specimen No. 1	81
Specimen No. 2	79
Mix No. 3	
Specimen No. 1	87
Specimen No. 2	84

5.6. CONCRETE RESISTIVITY

5.6.1. Preparation and Testing. The concrete resistivity test consisted of subjecting a total of 18 reinforced concrete ponding specimens to a continuous two week wet / one week dry cycle, for a period of 24 to 30 weeks. The 18 reinforced concrete ponding specimens were divided into two groups based on 2 and 4 bar reinforcement arrangements. The two groups then had three sets, one for each mix design, with three specimens in each set. The group of specimens containing 2 bars was cycled for a period of 30 weeks and the group of specimens containing 4 bars was cycled for a period of 24 weeks.

The ponding specimens measured 18 in. x 18 in. (457 mm x 457 mm) in plan and 3½ in. (89 mm) in height. Each specimen contained a 15 in. square (381 mm) by 1 in. deep (25 mm) reservoir along its surface, as shown in Figure 5.8.

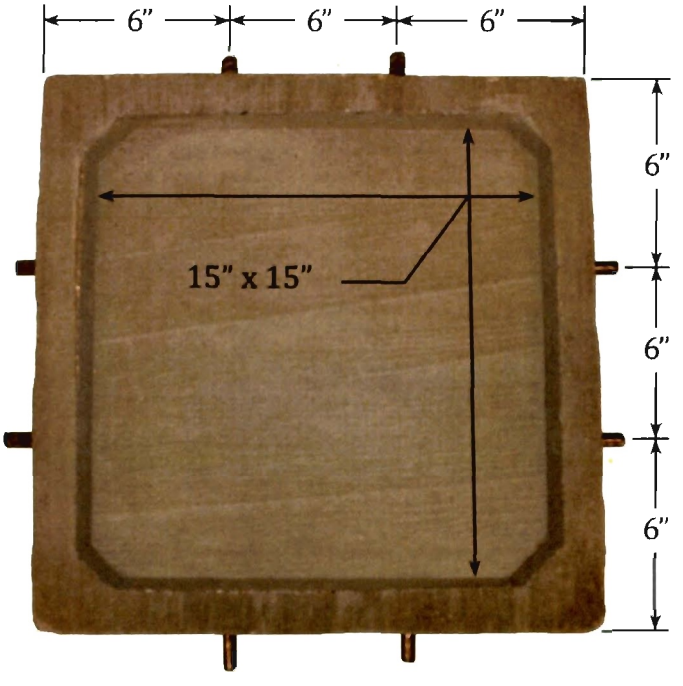

Figure 5.8: Typical 4 bar reinforced ponding specimen.

Four, 24-in.-long (533 mm), segments of deformed, No. 4 (No. 13), Grade 60 rebar were embedded within each of the sets for the 2 bar arrangement. The two bars in each of those sets were given 1 in. (26 mm) of cover with respect to the surface of the reservoir. Due to the reinforcement being placed at 1 in. (26 mm) below the reservoir surface, it was decided to test these specimens with 2 bars for 30 weeks to allow more time for the ingress of potential chlorides. Four, 24-in.-long (533 mm), segments of deformed No. 4 (No. 13), Grade 60 rebar were embedded within each of the sets for the 4

bar arrangements. Two of the four bars were positioned in the longitudinal direction and were given 0.5 in. (13 mm) of cover with respect to the surface of the reservoir. The remaining two bars were positioned directly beneath and in contact with the two longitudinal bars, but in the transverse direction. It was decided to test the specimens with 4 bars for 24 weeks since the reinforcement was placed closer to the reservoir surface than that of the 2 bar specimens and was expected to have experienced more exposure to penetrating chlorides that cause the development of corrosion. In an effort to prevent any rotation and/or movement of the bars during casting, plastic zip ties were used to connect the bars running perpendicular to one another. The bars were spaced in plan as shown in Figure 5.9.

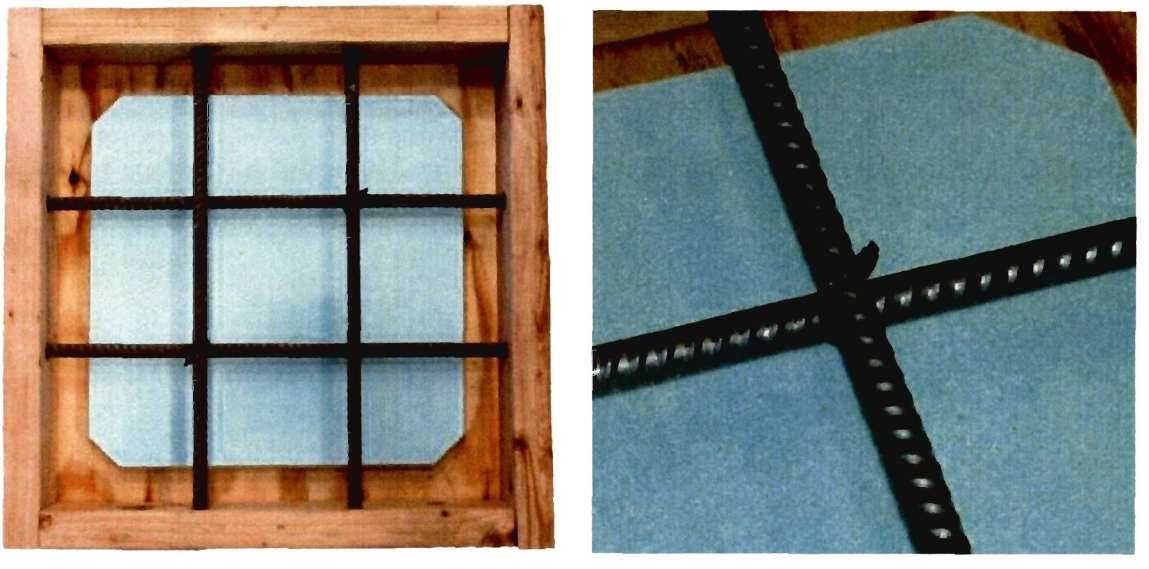

(a) (b)

Figure 5.9: Specimen formwork. (a) Rebar positioned within a form prior to casting. (b) Two perpendicular bars connected to one another using a plastic zip tie.

The forms used to cast the specimens were constructed of lumber and 1 in. thick (25 mm) polyisocyanurate foam. The walls of each form were made of four pieces of 1½ in. x 3½ in. (38 mm x 89 mm) lumber. Two ⅝ in.-diameter (16 mm) holes were drilled through each of the walls at locations that conformed to the rebar locations. A 21 in. x 21 in. x ¾ in. (533 mm x 533 mm x 19 mm) section of plywood was used as the bottom of each form. Centrally located on the top of the plywood was a 15 in. x 15 in. x 1 in. (381 mm x 381 mm x 25 mm) section of polyisocyanurate foam. The foam was secured to the plywood using Polyurethane Premium Construction Adhesive manufactured by Henkel Corporation. Prior to using the forms, the interior surface of each form was coated with a layer of release agent that was manufactured by Dayton Superior. A typical form is shown in Figure 5.9. A drawing of a typical form may be found within Appendix C.

During the weeks of testing, specimens were stored within a room that had an average ambient temperature of 68°F (20°C) and a relative humidity of 40 to 60 percent. Specimens were placed upon shelves in an elevated position that measured approximately 1 in. (25 mm) above the underlying shelf. The wet phase of a wet/dry cycle lasted for a total of two weeks and consisted of placing 0.53 gallons (2 liters) of saltwater within a specimen's reservoir. The saltwater remained within a specimen's reservoir during the entire two weeks and consisted of distilled water with 5 percent ACS grade sodium chloride (NaCl) by weight. To prevent any evaporation of the saltwater, each specimen was covered with plastic sheeting that was held down with an elastic band. An image of a typical specimen during the wet phase of testing is shown in Figure 5.10.

The dry phase of a wet/dry cycle began when the saltwater contained within the specimen's reservoir was removed with the use of a vacuum. Removing the saltwater from a specimen involved positioning the hose of the vacuum along the front right corner of the specimen's reservoir and slowly lowering it into the saltwater. The hose remained within the front right corner of the specimen's reservoir until the majority of the saltwater was removed. The hose was then removed from the specimen's reservoir and the specimen was then permitted to air dry, as shown in Figure 5.10 (b) above, for a period of one week.

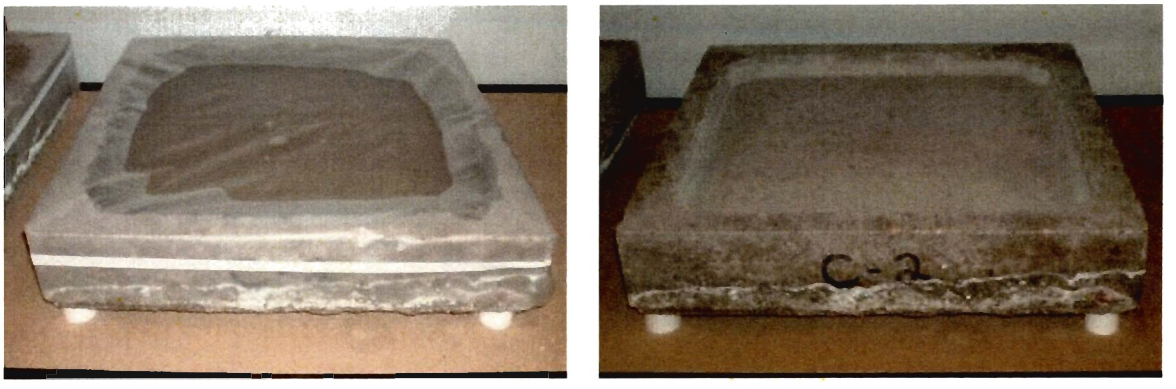

(a) (b)

Figure 5.10: Typical specimen during phases of testing. (a) The wet phase of testing, (b) The dry phase of testing.

The wet/dry cycling of the specimens began directly after collecting the baseline resistivity measurements for each specimen. Baseline readings were conducted within the first week after a group of specimens had reached an age of 28 days. Once the baseline measurement had been recorded, the first wet/dry cycle began. Concrete resistivity readings were then performed after every two consecutive wet/dry cycles (6 weeks).

The resistivity of each specimen was measured every six weeks with the use of a Canin$^+$, a corrosion analyzing instrument manufactured by Proceq. Canin$^+$ incorporated the use of a Wenner Probe, also known as a four probe resistivity meter, which had a fixed electrode spacing of 2 in. (51 mm) and a nominal alternating current (AC) output of 180 μA at a frequency of 72 Hz. The equipment had an impedance of 10 MΩ and an operating range of 0 to 99 kΩcm with a 1 kΩcm resolution. The equipment was portable and required six AA batteries.

Resistivity measurements began immediately after a wet phase of testing had been completed. Once the majority of the saltwater had been removed from the specimen, the remaining surface water was given time to evaporate. After approximately 30 minutes, the specimen began to reach a saturated-surface-dry (SSD) condition. The SSD condition was when the entire surface of a specimen's reservoir was visibly saturated, but did not

possess any available saltwater. Paper towels were used to absorb any excess amounts of saltwater that may have accumulated within an area along the surface of a specimen's reservoir. However, this was only carried out when other areas along the surface the specimen's reservoir began to dry out. After removing the excess water, a squirt bottle, containing distilled water, was then used to re-saturate the dry areas along the specimen's surface. Once re-saturated, a template, made from ¼-in.-thick (6 mm) plexiglass, was then used to cover the surface of the specimen's reservoir. The template contained six set of four holes that were evenly dispersed throughout its surface. A schematic layout of these holes may be seen in Figure 5.11. The holes were of the same diameter and were slightly larger than that of the Wenner Probe's four electrodes.

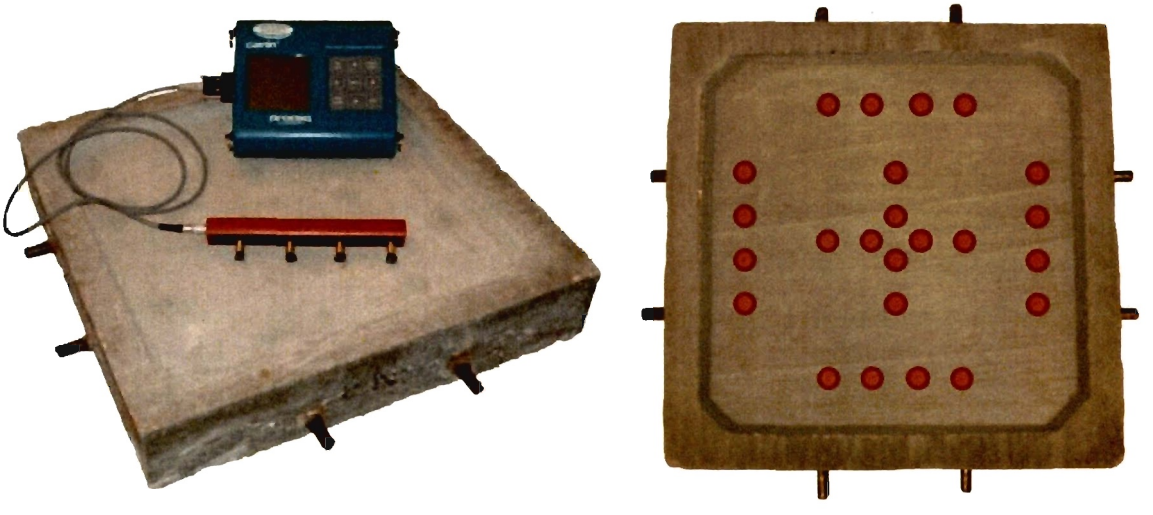

(a) (b)

Figure 5.11: Concrete resistivity equipment. (a) The Canin+ equipment alongside a specimen and the Wenner Probe. (b) Locations along a specimen where resistivity measurements were taken.

Preparation of the Wenner Probe consisted of removing the four sponges, partially inserted within the probe's electrodes, and letting them soak within distilled water. The sponges remained within the distilled water until the surface of the first specimen had reached the SSD condition. After the template was properly position within the specimen's reservoir, the sponges were then reinserted into the Wenner Probe's four electrodes. The Wenner Probe was then attached to the Canin$^+$ and the resistivity of the specimen was measured.

A specimen's resistivity was measured at the six locations shown in Figure 5.11(b). While conducting the measurements, any accumulation of water beneath the template was removed using paper towels. A measurement was deemed complete the moment the Canin$^+$ continually reported a value to within 0.2 kΩcm. After completing the first three measurements along a specimen, the four sponges located at the ends of the Wenner Probe's four electrodes, were re-saturated with distilled water through a dipping process. Once the sponges had been re-saturated the three remaining measurements were then taken.

5.6.2. Results. The resistivity for each specimen group over the course of the 30 and 24 weeks of testing is shown in Figure 5.12 and 5.13, respectively. Each data point in the figure is an average value that represents the measured resistance of a specimen set during the 30 and 24 weeks of testing. Error bars, representing a 95 percent confidence interval for each data point, are also shown in Figures 5.12 and 5.13. A data point's confidence interval was developed using the standard error of a set's mean value (SEM) [ASTM G16, 1995]. A data set consisted of three individual sets of six resistivity values which were gathered from the three specimens contained within each specimen group. Therefore, a data point's SEM was equal to the standard deviation of these 18 resistivity values divided by the square root of 18. Some error bars within Figures 5.12 and 5.13 are difficult to distinguish for they were very small values. A table of the resistivity values pertaining to a specific specimen within a specimen group located in Appendix C.

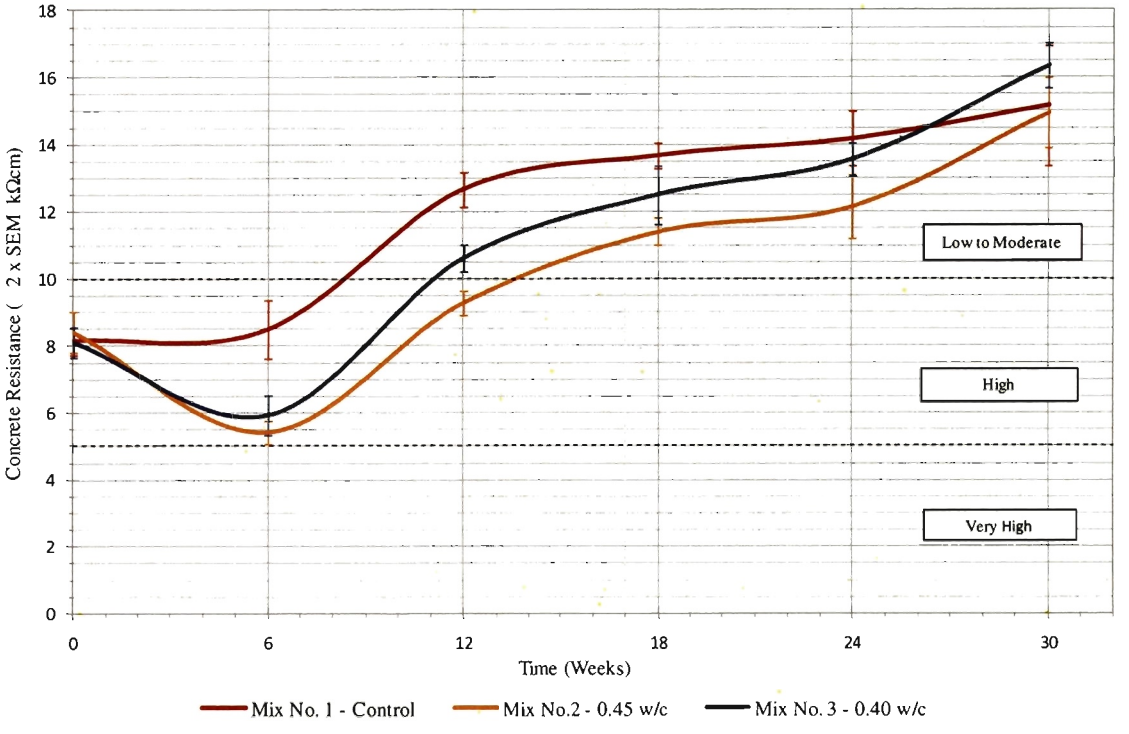

Figure 5.12: The trend in the average concrete resistance for each specimen type containing 2 bars during the 30 weeks of testing.

Overall, the trend in resistivity for all the concrete mixes increases over the period of testing. The resistivity trend over the period of testing is similar for Mix Nos. 2 and 3 of both plots. From about 6 to 12 weeks on, Mix No. 3 shows a slight increase in resistivity measurements over Mix No. 2 as shown in Figure 5.12. During the last 6 weeks of the wet/dry cycling, at about 26 weeks, Mix No. 1 begins to show a decrease in concrete resistivity as shown in Figure 5.12. The same trend is also apparent in Figure 5.13, namely that during the last 6 weeks of the wet/dry cycling, at about 21 weeks, Mix No. 1 begins to show a decrease in resistivity. However, at the end of testing at 30 weeks, Mix Nos. 2 and 3 show a continual increase in concrete resistivity in both Figures 5.12 and 5.13.

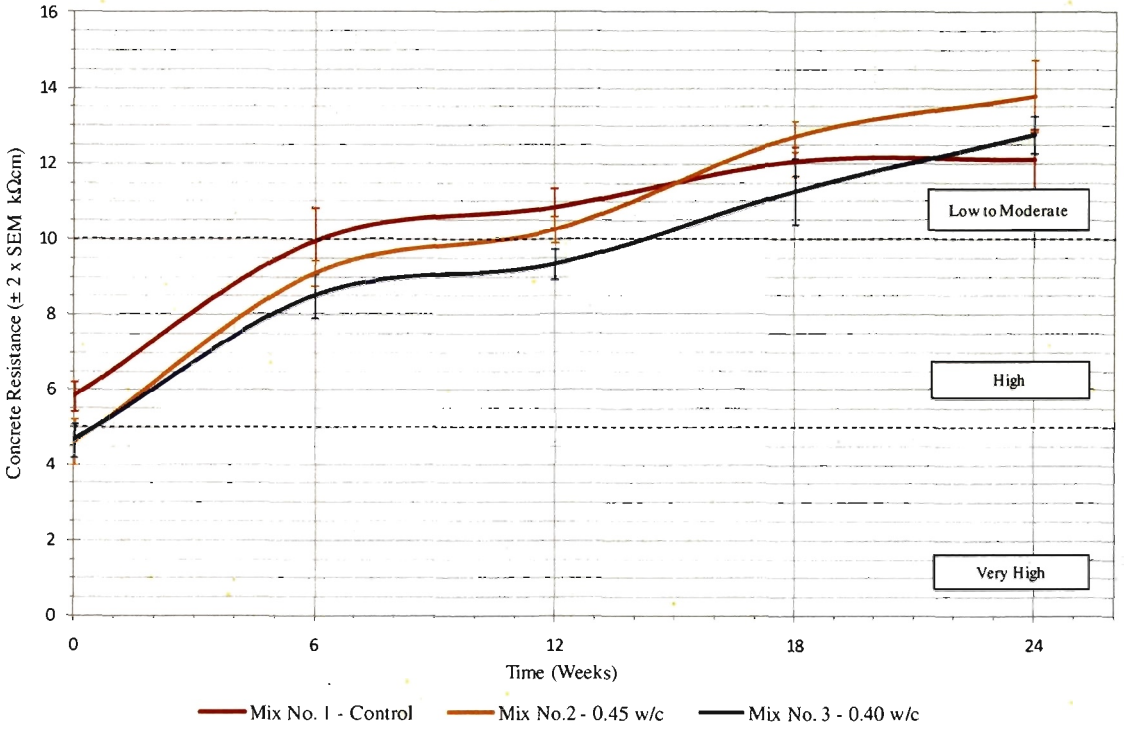

Figure 5.13: The trend in the average concrete resistance for each specimen type containing 4 bars during the 24 weeks of testing.

Using Table 5.6 and the overall resistance values reported within Figures 5.12 and 5.13, the corrosion rate of the reinforcing bars contained within each specimen group was generalized assuming that the bars were depassivated. At nearly 12 weeks, both plots reported resistivity measurements that correlate to a rate of corrosion of "low to moderate." Both plots show reported resistivity measurements that correlate to a rate of corrosion of "high" from the beginning of testing up to 12 weeks.

5.6.3. Conclusions. The resistivity measurements in Figures 5.12 and 5.13 show continual increase in resistivity of the concrete throughout the testing period of 30 and 24 weeks. Typically, for conventional reinforced concrete, it may be expected that Mix No. 1 would experience a maintained resistance or a decrease in resistance being exposed to a chloride environment for an extended period of time. Rather, Mix No. 1 indicated an

increase in resistivity to applied electrical current at early testing weeks, but began to show a gradual decrease in resistivity near the end of the testing period.

Table 5.6: Correlation between concrete resistivity and the rate of corrosion for a depassivated steel bar embedded within the concrete [Broomfield, 2007].

Concrete Resistivity	*Rate of Corrosion*
> 20 kΩcm	Low
10-20 kΩcm	Low to Moderate
5-10 kΩcm	High
< 5 kΩcm	Very High

At current allowable replacement percentages, fly ash is well-known for enhancing the durability of concrete due to the refined microstructure developed during hydration. This would then suggest that Mix Nos. 2 and 3 may experience increasing resistivity measurements throughout the testing period. Figures 5.12 and 5.13 show an increase in resistivity measurements throughout testing. This reported trend also coincides with the longer hydration period of fly ash compared to conventional concrete.

5.7. CORROSION POTENTIAL

5.7.1. Preparation and Testing. The construction and preparation for the specimens used during the concrete resistivity testing may be referenced in Section 5.6. An explanation of the wet/dry cycling that all specimens experienced may also be found in Section 5.6.

The wet/dry cycling of the specimens began directly after collecting the baseline corrosion potential measurements for each specimen. Baseline readings were conducted within the first week after a group of specimens had reached an age of 28 days. Once the

baseline measurement had been recorded the first wet/dry cycle began. Concrete corrosion potential readings were then performed after every two consecutive wet/dry cycles (6 weeks). The corrosion potential of the rebar embedded within a specimen was measured immediately after the specimen's resistivity readings were recorded. Using the Canin+ equipment, which had an operating range of ±999 mV and incorporated a copper/copper sulfate half-cell, the corrosion potential at three locations along the length of each embedded bar was measured. These locations were spaced 6 in. (152 mm) on center and were offset a distance 3 in. (76 mm) from a specimen's side. A schematic layout of the locations in which potential readings were taken along the surface of a specimen is shown in Figure 5.14.

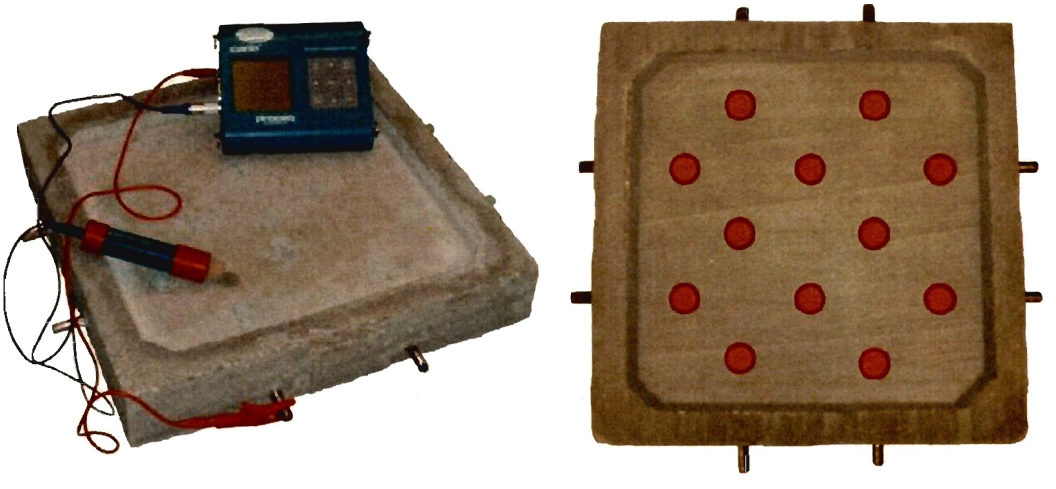

(a) (b)

Figure 5.14: Corrosion potential equipment and locations. (a) The Canin+ equipment alongside a specimen and the copper/copper sulfate half-cell. (b) Locations along a specimen where corrosion potential measurements were taken.

Prior to conducting the baseline corrosion potential measurements of the specimens, the half-cell was prepared in accordance to the operating manual. The half-

cell's cap, which contained a wooden plug underneath a sponge, was removed and placed within distilled water for approximately one hour. While soaking the wooden plug, the copper sulfate solution was prepared. The solution required a 10 to 4 ratio (by weight) of distilled water to copper sulfate crystals, plus an additional 0.5 teaspoon of copper sulfate crystals. Following the 10 to 4 ratio, the solution was prepared using 1.16 oz (33.0 g) of distilled water and 0.47 oz (13.2 g) of copper sulfate crystals. The solution was then transferred to the half-cell where an additional 0.14 oz (4.0 g) of copper sulfate crystals were added to the solution. The half-cell was then closed using the cap containing the saturated wooden plug. During the weeks when the half-cell was not in use, the end of the cell containing the wooden plug was capped to prevent the plug from drying out.

Before measuring the corrosion potential of an embedded bar contained within a specimen, the exposed steel along one end of the bar was cleaned. Cleaning of the steel was considered complete the moment a bright metal to bright metal connection between the bar and the voltmeter (or Canin^{+}) was achieved. The connection between the positive terminal of the voltmeter and the bar was made through the use of an alligator clip, as shown in Figure 5.14. After securely connecting the voltmeter to the bar, the half-cell was then connected to the voltmeter's negative terminal. The sponge attached to the end of the half-cell was then dipped into distilled water until it became fully saturated. Once the sponge was saturated, the three points, as can be seen in Figure 5.14, corresponding to the bar that was currently connected to the voltmeter were located with the use of a ruler. Measurements were then carried out by gently placing the half-cell upon each of the three locations. The recorded values were based off of the Canin^{+}'s ability to automatically acquire a value once a reading had become stable. After the three values were recorded, the sponge was then re-saturated and the corrosion potential values for the three remaining bars embedded within the specimen were obtained using the same procedure.

5.7.2. Results. Corrosion potential measurements for the six groups of reinforced specimens are shown in Figures 5.15 and 5.16. Each data point within the plot represents an average potential value for the three specimens contained within each group. Error bars, representing a 95 percent confidence interval for each data point, are also shown in Figures 5.15 and 5.16. A data point's confidence interval was developed using the standard error of a data set's mean value (SEM). Data sets for the specimens

containing 2 bars consisted of three individual sets of 6 potential measurements. Likewise for specimens containing 4 bars, although, individual sets consisted of 12 potential measurements. Therefore, a data point's SEM for specimens containing 2 bars was equal to the standard deviation of these 18 potential measurements divided by the square root of 18 and for specimens containing 4 bars was equal to the standard deviation of these 36 potential measurements divided by the square root of 36. The values calculated that represent the error bars for the following Figures 5.15 and 5.16 were small values and may be difficult to recognize. A table of potential measurements pertaining to a specific specimen within a specimen group may be found in Appendix C.

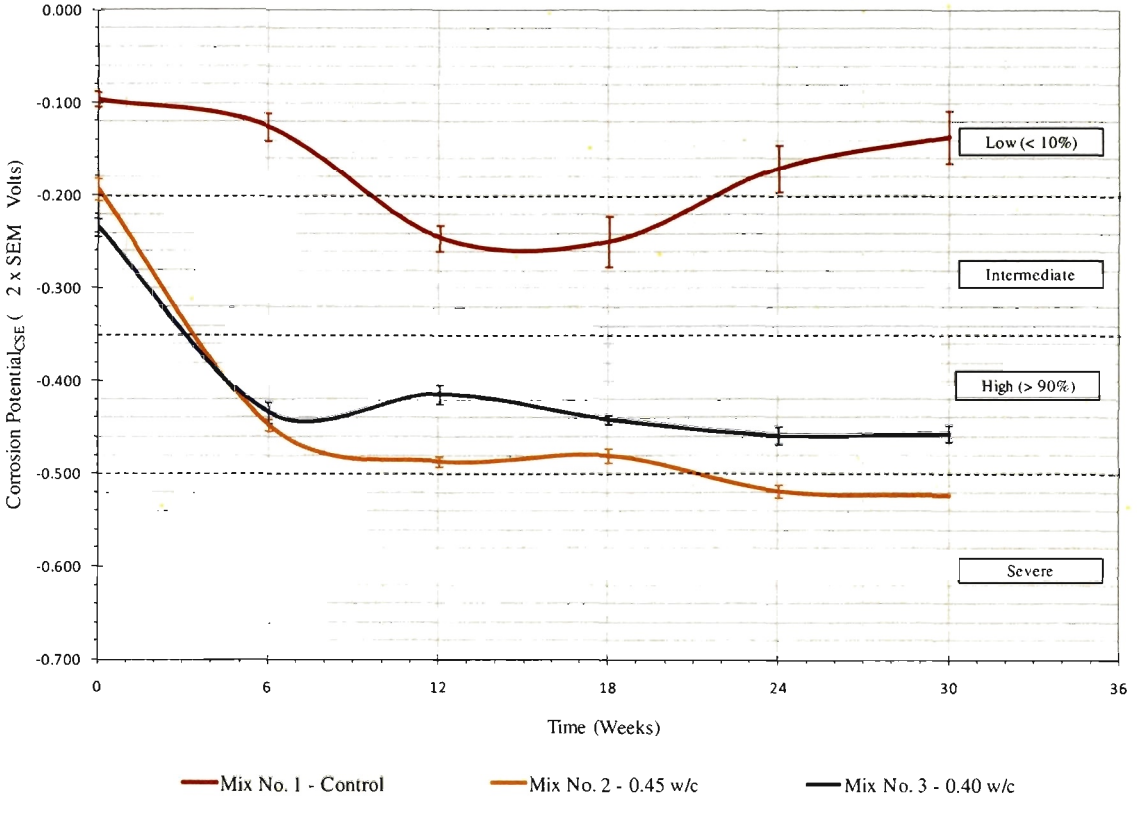

Figure 5.15: The trend of the average corrosion potential of each specimen containing 2 bars during the 30 weeks of testing.

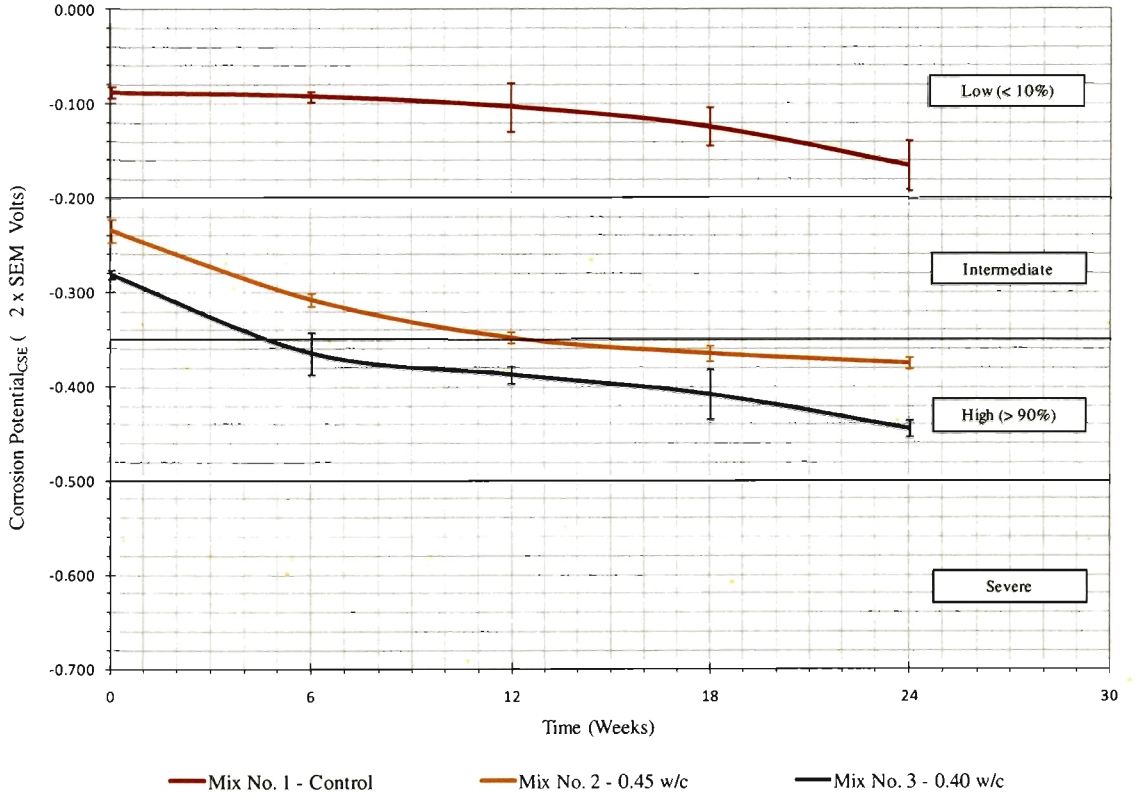

Figure 5:16: The trend of the average corrosion potential of each specimen containing 4 bars during the 24 weeks of testing.

As shown in Figure 5.15, Mix Nos. 2 and 3 containing 2 bars follow a similar trend in corrosion resistance, which decreases over the 30 weeks of testing. However, the trend in corrosion resistance of Mix No. 1 shows more positive half-cell potential measurements. Thus, Mix No. 1 would appear to have a higher corrosion resistance than Mix Nos. 2 and 3. The corrosion resistance of the specimens containing 4 bars is shown in Figure 5.16. The same trend of decreasing corrosion resistance is observed for Mix Nos. 2 and 3. Again, a more positive half-cell measurement, although decreasing, is reported for Mix No. 1 over the 24 week period of testing. According to Figures 5.15 and 5.16, Mix Nos. 2 and 3 containing 2 bars show a more negative corrosion potential than Mix Nos. 2 and 3 containing 4 bars.

Using Table 5.7 and the potential values shown in Figures 5.15 and 5.16, the probability of the bars corroding within each specimen group was determined at the end of the testing period. Of the six specimen groups, Mix Nos. 2 and 3 containing 2 and 4 bars reported final potential values of less than -350 mV. This indicted a "high (> 90%)" chance that each of the three specimens included within the four groups contained reinforcement that had begun to corrode. Mix No. 2 containing 2 bars reported a final potential of less than -500 mV, which indicated a "severe" chance that the rebar had begun to corrode. The two remaining groups of Mix No. 1 containing 2 and 4 bars had final potential values of -130 mV and -190 mV, respectively. This correlated to a "low (< 10%)" chance that a specimen belonging to either of those two groups contained corroding reinforcement.

Table 5.7: Correlation between the corrosion potential of a steel bar embedded within concrete and risk of corrosion [Broomfield, 2007].

Potential (CSE)	*Corrosion Risk*
> -200 mV	Low (< 10%)
-200 to -350 mV	Intermediate
-350 to -500 mV	High (> 90%)
< -500 mV	Severe

Determining the corrosion risk is not solely a function of the corrosion condition, but other factors as well. Potential measurements can be misleading by displaying very negative potential values. This may occur in saturated conditions where there is no oxygen to form a passive layer, however, with not oxygen, no corrosion can develop. Readings ranging from -350 mV to -500 mV simply indicates the steel is usually corroding actively. Values greater than -350 mV signify failing in the passive layer and

increasing amounts of steel are dissolving. Due to the nature of the testing with the measurements being linked by empirical comparisons and the probability of corrosion, no comparison between measurements and a percent area of corrosion to total exposed area can be made.

5.7.3. Conclusions. Figures 5.15 and 5.16 indicate that Mix No. 1 has nearly constant potential measurements throughout the testing period. The results conclude that the reinforcement contained within specimens of Mix No. 1 have a "low" probability of corrosion. However, the converse is noticed for Mix Nos. 2 and 3. Mix Nos. 2 and 3, containing 2 and 4 bars, both indicate similar results. The results lead to the conclusion that the reinforcement contained within specimens of Mix Nos. 2 and 3 have a "high" to "sever" chance of corrosion. Section 5.8 further discusses the correlation between the graphical representations of the probability of corrosion and the subsequent forensic evaluation.

5.8. FORENSIC EVALUATION

Upon completion of the 30 and 24-week-long ponding tests, a forensic evaluation was conducted on each group of specimens. The forensic evaluation involved a visual examination of the reinforcing bars embedded within a specimen after they were carefully removed from the concrete. Prior to the removal of the reinforcement, cores were taken from a portion of the selected specimens and the chloride profiles were developed.

5.8.1. Chloride Penetration Evaluation. The specimens containing reinforcement underwent a chloride penetration evaluation as well. Cores were taken from the center of each specimen and tested in the same manner as described in Section 5.4.1. Chloride penetration testing was performed on these specimens to determine if the concentration of chlorides at the depths in which the steel reinforcement was placed within the specimen were high enough to promote the development of corrosion. The chloride concentration results were then compared to the concrete resistivity and potential test results to verify the accuracy of those test methods on HVFA concrete.

As expected, a large concentration of water soluble chlorides was discovered along the surface of each specimen that was tested. All the cores taken from each mix

showed a significant decrease in chloride concentration from 0.25 in (6 mm) to 1.5 in. (38 mm). All three mixes containing 2 bars have chloride concentrations indicating a "high" risk for corrosion at 0.25 in. (13 mm) and a "moderate" risk for corrosion at 1 in. (26 mm). All three mixes containing 4 bars have chloride concentrations indicating a "moderate" risk for corrosion at 0.5 in. (13 mm) and a "low" risk for corrosion at 1 in. (26 mm).

5.8.2. Scaling Observations. As part of the forensic evaluation, observations were also made on the ponding specimens regarding efflorescence. Efflorescence is developed from the reaction of calcium carbonate ($Ca(OH)_2$) and carbon dioxide (CO_2), which leaves a white salt deposit on the surface of the concrete. This leaching of lime compounds is more likely to occur in concrete that is porous near the surface or when the concrete is exposed to a cycle of cool, wet weather followed by dry and hot weather. Gypsum and alkalis in the aggregate may have a similar effect of leading to a white deposit on the surface of the concrete.

The HFVA specimens containing 2 and 4 bars with *w/*cm of 0.45 and 0.40 both exhibited signs of white "lime scale" deposits at 4 to 6 weeks of the first 6 week "wet" cycle. The conventional concrete containing 2 and 4 bars with *w/cm* of 0.45 exhibited signs at 10 to 12 weeks of testing, but the white deposit was not extensive as the HVFA specimens. No surface delamination was observed on the specimens. Figures 5.17 through 5.20 show the visible white deposit on the specimens.

Figure 5.17: Mix No. 3 ponding specimen 1 with visible "lime scale" deposit.

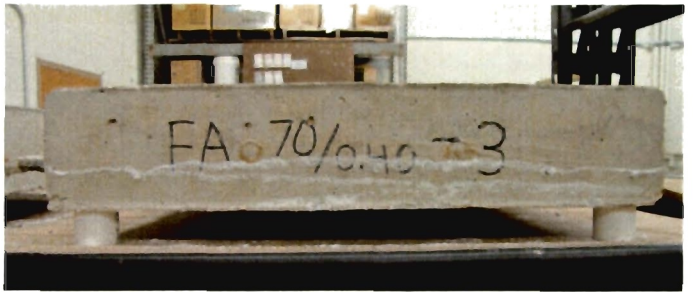

Figure 5.18: Mix No. 3 ponding specimen 3 with visible "lime scale" deposit.

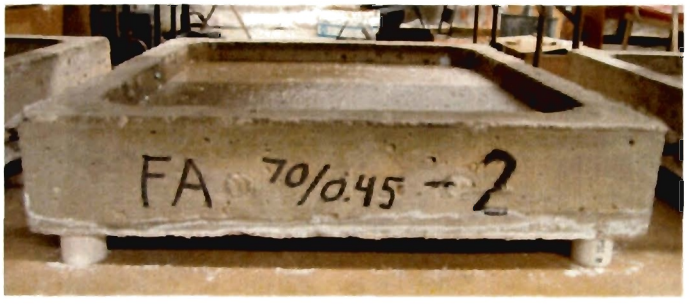

Figure 5.19: Mix No. 2 ponding specimen 2 with visible "lime scale" deposit.

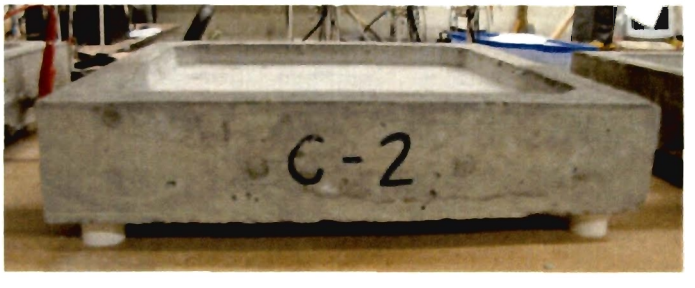

Figure 5.20: Mix No. 1 ponding specimen 2 with little to no "lime scale" deposit.

5.8.3. Removal of Reinforcement. Removal of reinforcing bars from a specimen was achieved by using an air chisel. The ponding dam that retained the solution was removed first and then portions of the concrete specimen were gradually removed. The air chisel was used at two angles to remove the concrete; 90° position and 45° position as shown in Figure 5.21. Any loose material along the length of each of the four reinforcing bars was removed by hand. Afterwards, each bar was visually examined and photographed.

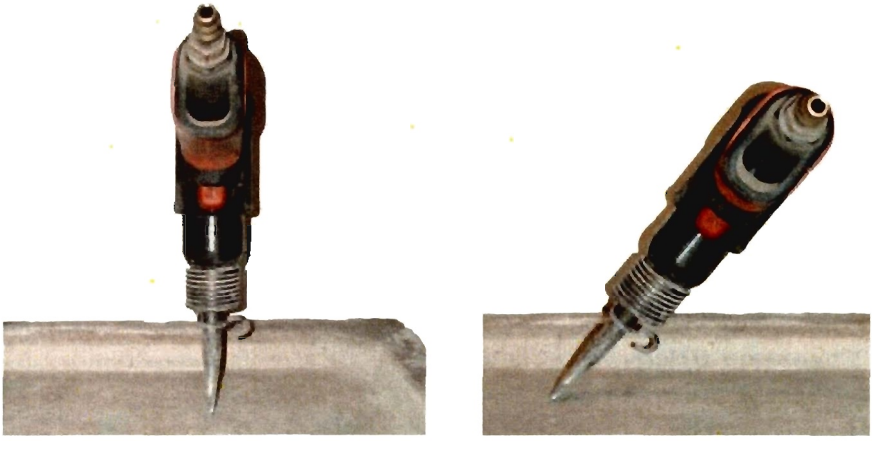

(a) (b)

Figure 5.21: The air chisel in different positions (a) the 90° position; (b) the 45° position.

5.8.4. Reinforcement Examination. The reinforcement was removed from two specimens of each concrete mix. Over all, the corrosion observed on the embedded reinforcement was very minimal. As shown in Figures 5.22 through 5.27 listed below, however, some concentrated areas of corrosion began to develop.

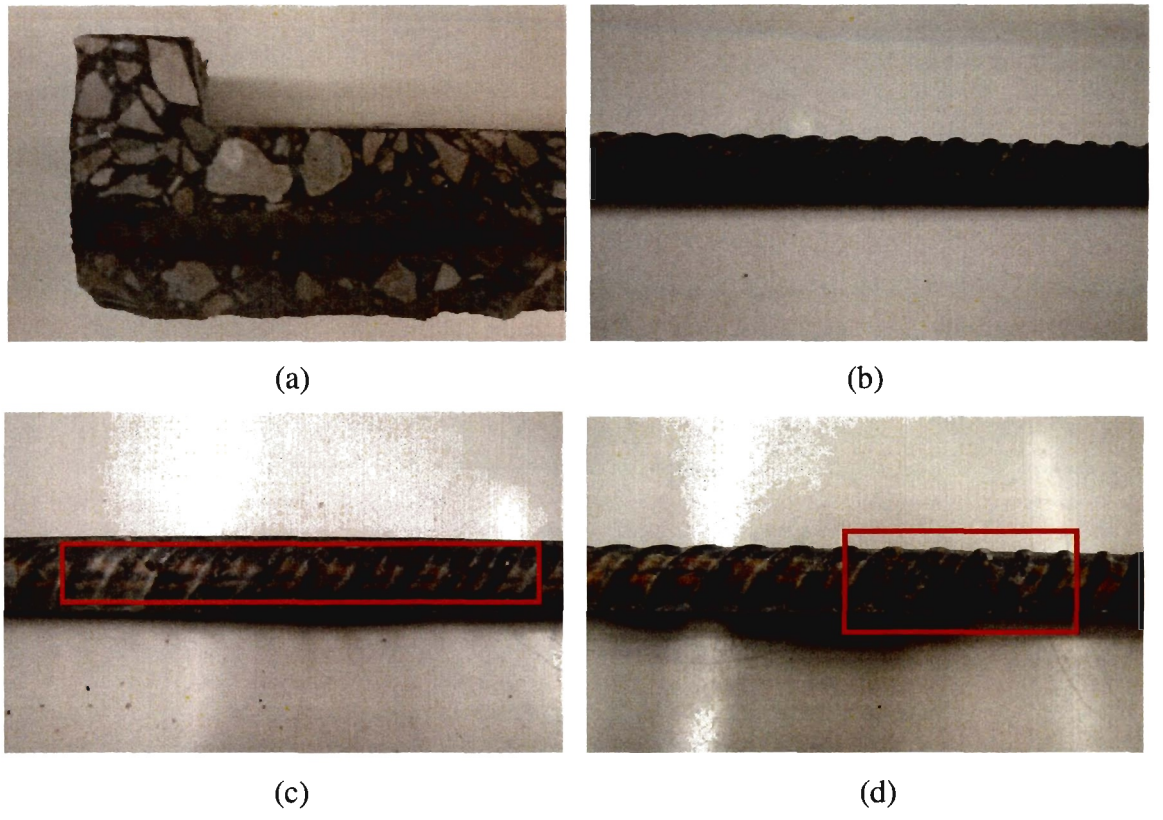

(a) (b)

(c) (d)

Figure 5.22: Reinforcment examination of Mix No. 1 containing 2 bars. Reinforcement is at 1 in. (25 mm) from reservoir surface. (a) Cross-section of ponding specimen. (b) Typical steel reinforcement showing no signs of corrosion. (c) Reinforcement showing early signs of corrosion. (d) Corrosion developed on reinforcement.

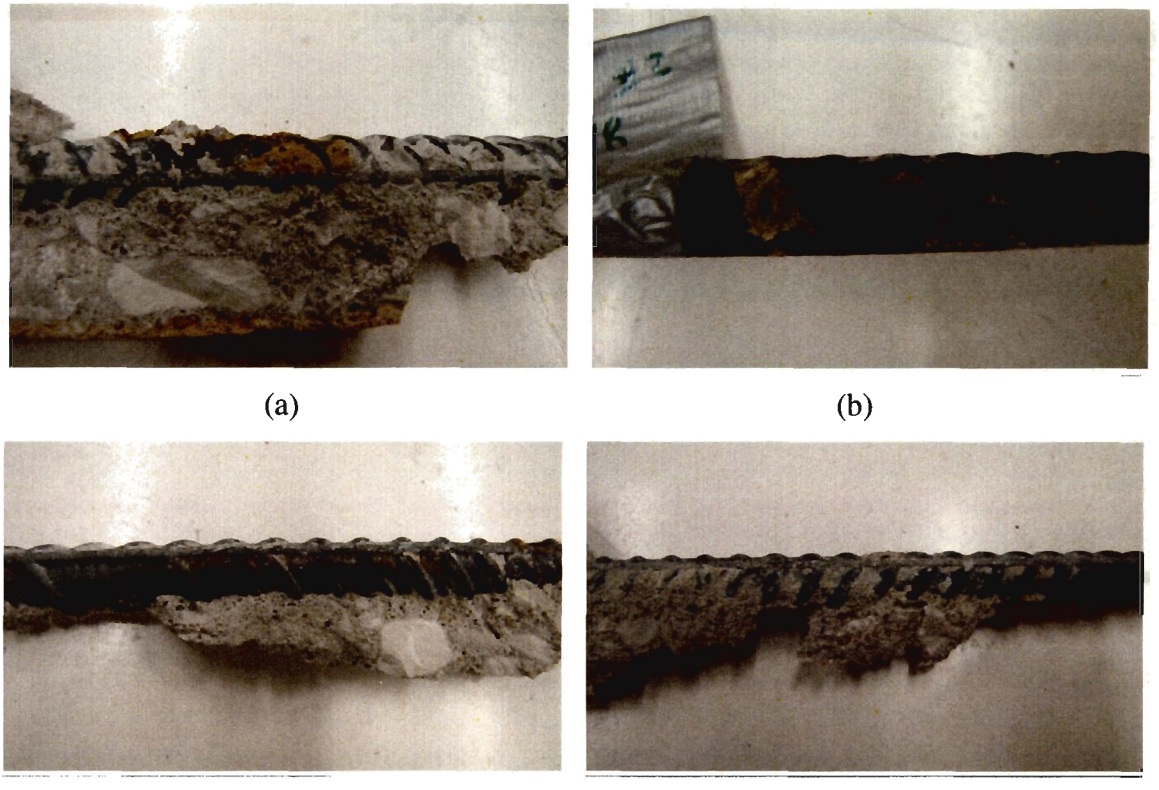

(a) (b)

(c) (d)

Figure 5.23: Reinforcement examination of Mix No. 2 containing 2 bars. Reinforcement is at 1 in. (25 mm) from reservoir surface. (a) Corrosion developing on reinforcement. (b) Corrosion spot on reinforcement. (c) and (d) No signs of corrosion on reinforcement.

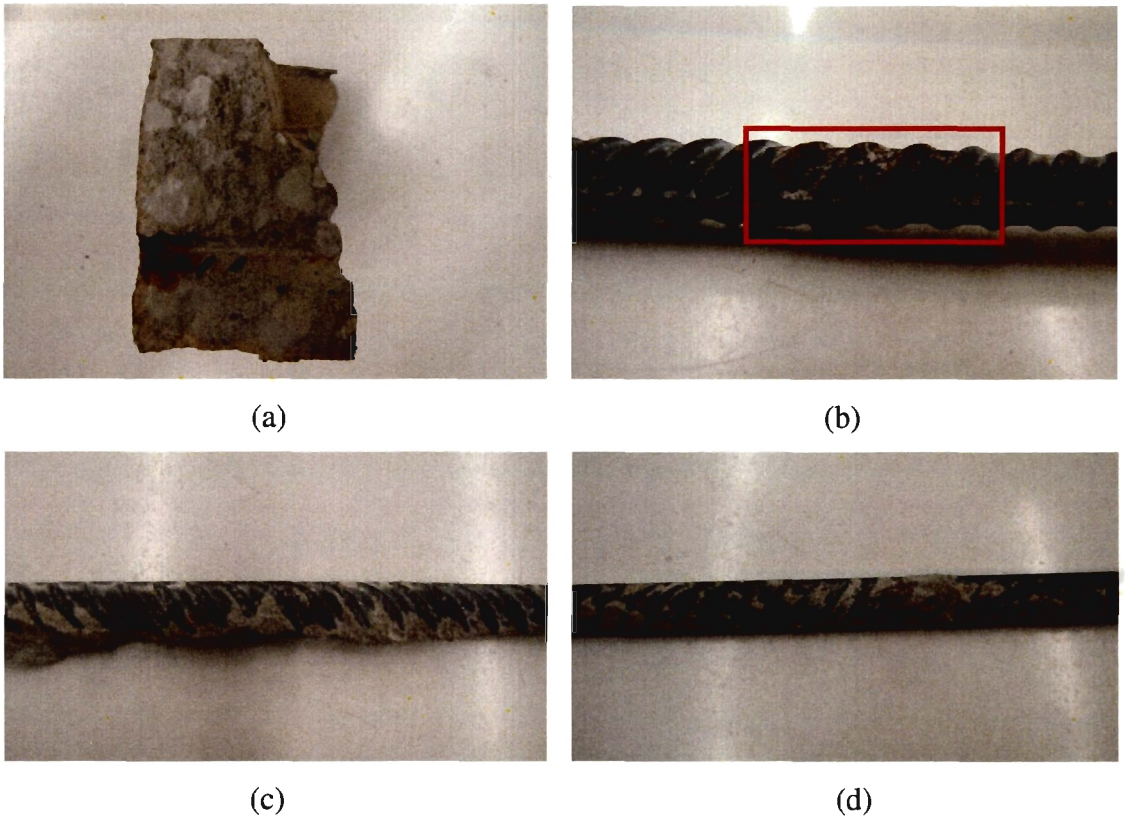

Figure 5.24: Reinforcement examination of Mix No. 3 contaning 2 bars. Reinforcement is at 1 in. (25 mm) from reservoir surface. (a) Cross-section of ponding specimen at reservoir edge. (b) Spot of corrosion 1 in. (25 mm) in length. (c) and (d) No signs of corrosion on reinforcement.

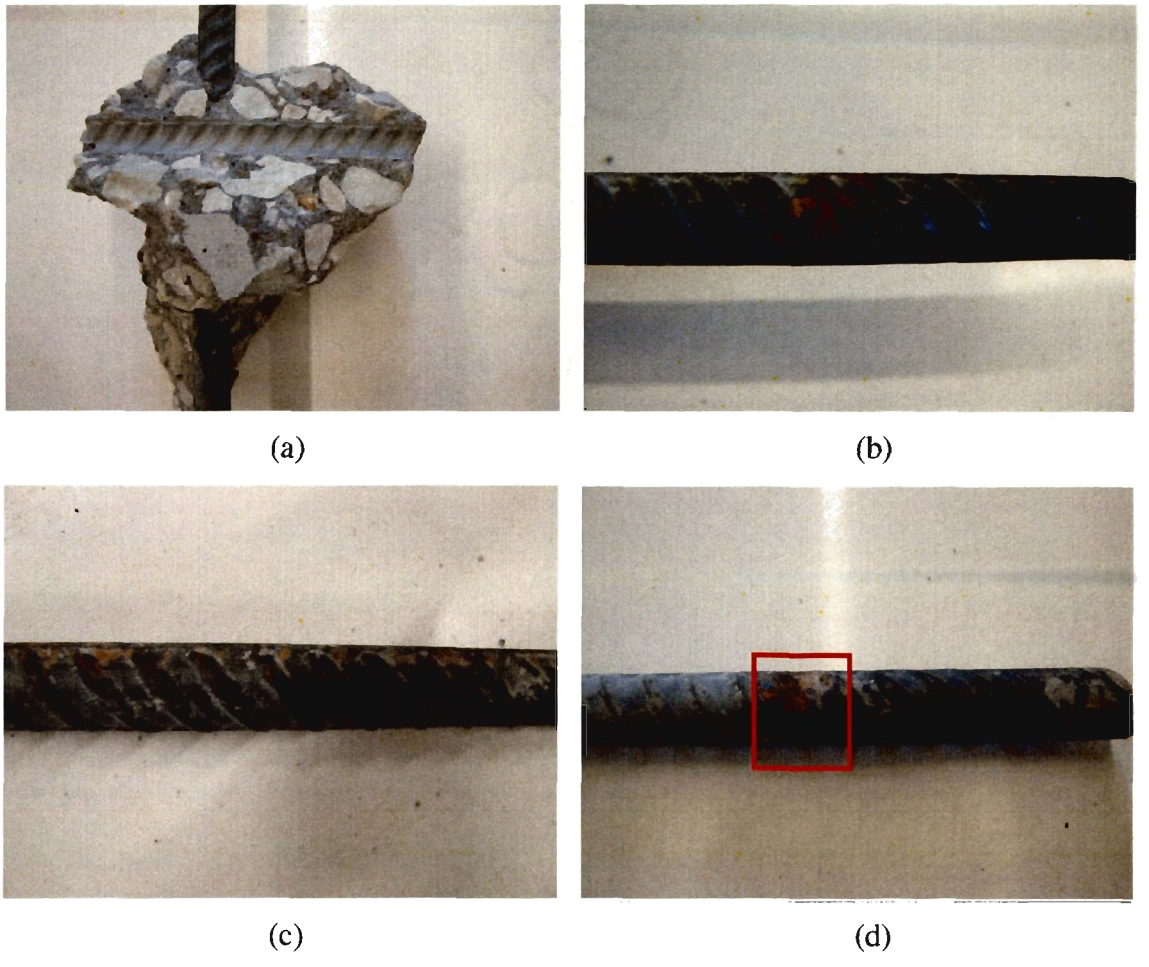

Figure 5.25: Reinforcement examination of Mix No. 1 containing 4 bars. (a) Vertical rebar embedded in concrete with transverse rebar removed showing no signs of corrosion on the concrete. (b) Indication of corrosion formation on rebar at ½ in. (12.5 mm) from reservoir surface. (c) Minimal signs of corrosion on rebar at ½ in. (12.5 mm) from reservoir surface. (d) Little to no rust formation on rebar at 1 in. (25 mm) from reservoir surface.

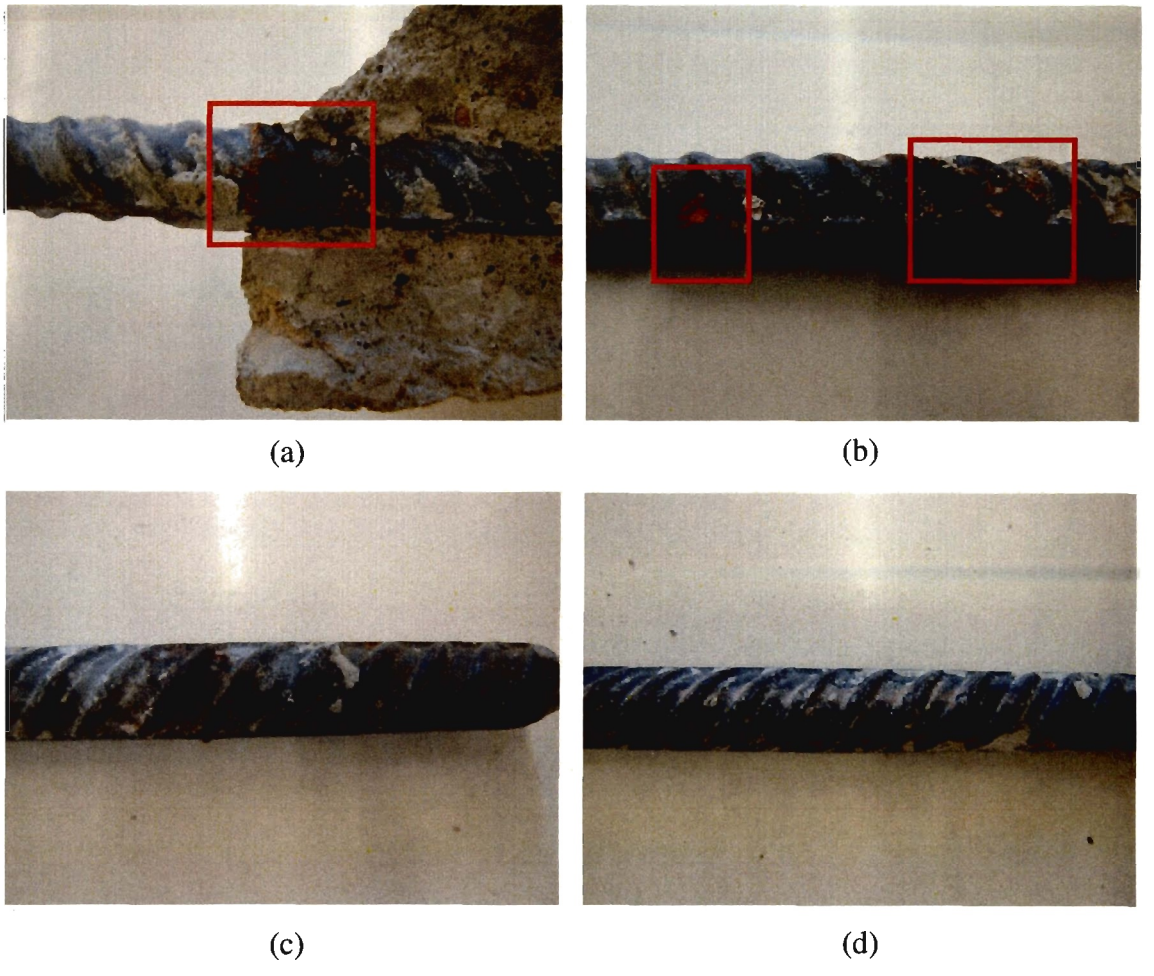

Figure 5.26: Reinforcement examination of Mix No. 2 containing 4 bars. (a) Rebar embedded in concrete showing corrosion development near edge of specimen. (b) Spots of corrosion developed on rebar at ½ in. (12.5 mm) from reservoir surface. (c) and (d) Minimal to no signs of corrosion at 1 in. (25mm) from reservoir surface.

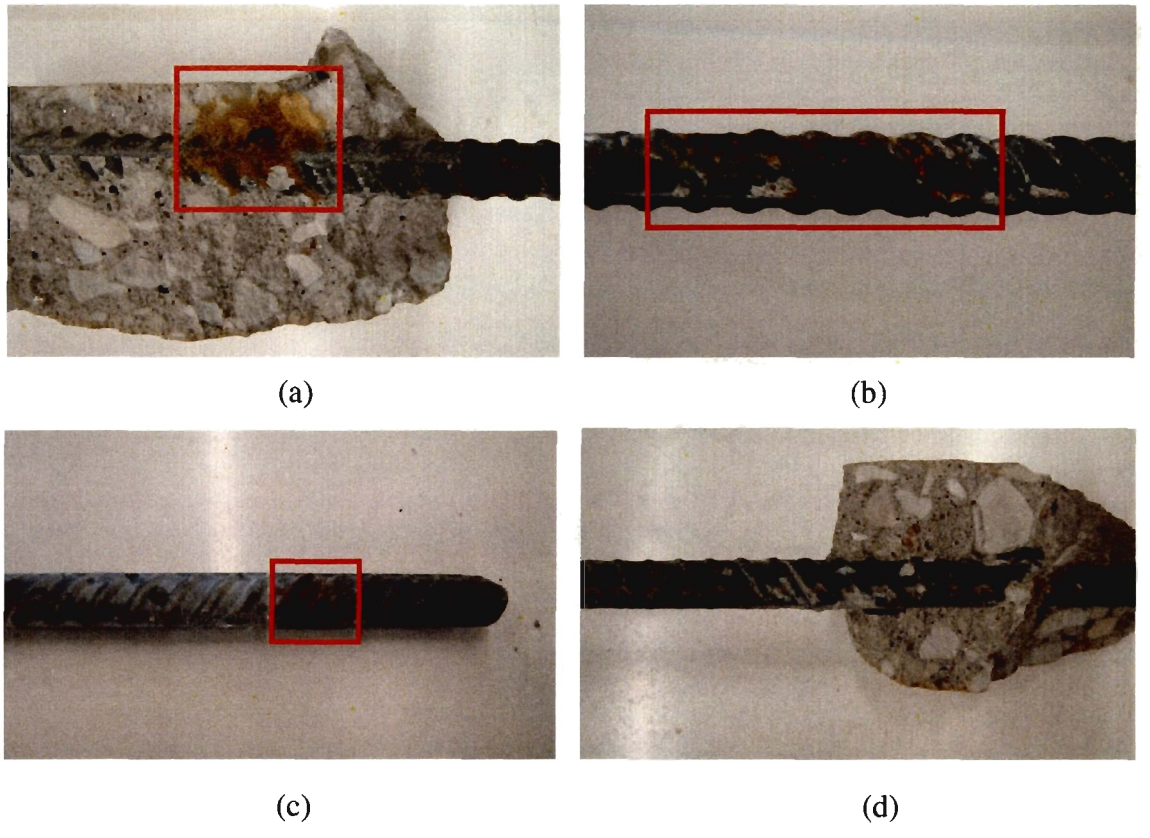

Figure 5.27: Reinforcement examination of Mix No. 3 containing 4 bars. (a) Reinforcement embedded in concrete showing a concentrated area of corrosion development. (b) Concentrated area of corrosion 1.5 in. (19 mm) in length at ½ in. (12.5 mm) from reservoir surface. (c) Minimal sign of corrosion development at 1 in. (25 mm) from reservoir surface.

5.8.5. Conclusions. The results shown of the chloride concentration testing lead to the conclusion that all the chloride profiles are consistent with the chloride penetration within the specimens; the highest concentration at the surface and decreasing in chloride concentration with depth. Due to the extended testing period of the specimens containing 2 bars, more chlorides were able to penetrate the specimens, increasing the risk for corrosion to develop on the embedded reinforcement. However, the forensic evaluation of the reinforcement within those specimens showed minimal signs of developed corrosion. The specimens containing 4 bars showed results of less chloride penetration, reducing the potential risk for the development of corrosion. Although, the risk for

corrosion was reported to be "moderate," again, the forensic evaluation of the reinforcement within those specimens showed minimal signs of developed corrosion. From these results, the conclusion can be drawn that while the chloride penetration testing reveals chloride levels within the concrete may promote corrosion, there is great variability in the fact that corrosion may not always develop at the risk correlated with the chloride concentrations.

5.9. CONCLUSIONS

All the results contained within Section 5 regarding the many durability tests performed are all valuable in determining the durability performance of HVFA concrete. Common relationships between the tests are recognized and summarized within this section to produce conclusions on the durability performance of the HVFA concrete tested.

The chloride permeability test shows similar results to that of the chloride profiles developed from ponding specimens. Mix No. 1 resulted in the highest permeability rating of the three concrete mixes evaluated for both chloride tests. The chloride permeability test results of Mix Nos. 2 and 3 coincide with the results found from the developed chloride profiles. Both HVFA concrete mixes show lower penetration concentrations of chlorides compared to that of Mix No. 1.

The freeze-thaw test revealed that Mix No. 3 is comparable to Mix No. 1 in terms of reported durability factors. The increased durability factors of Mix No. 3 over Mix No. 2 are likely attributed to the decreased *w/cm* from 0.45 to 0.40. The reduction in *w/cm* decreases the amount of free voids within the pore structure of the concrete. Mix No. 2, containing 70 percent fly ash at the same *w/cm* as Mix No. 1, did not perform as well as Mix Nos. 1 and 3, although it still indicated "good" resistance to freeze-thaw damage. In general, the test results indicated that the HVFA concrete was able to develop an adequate air-void system to resist freeze-thaw damage.

Forensic evaluation of the specimens revealed variation in the condition reported for the concrete resistivity and potential measurements. The resistivity results indicated a "low" to "moderate" rate of corrosion. This coincided with the forensic evaluation of the

removed embedded reinforcement. The resistivity test is concluded to be applicable for estimating the rate of corrosion on HVFA concrete.

The potential measurements, however, indicated a very different result when compared to the forensic evaluation. Mix Nos. 2 and 3 indicated a "high" chance of corrosion. The forensic investigation of the reinforcement from those concrete mixes showed otherwise. There was minimal to no corrosion development as shown in Figures 5.22 through 5.27. Based on the forensic investigation, it may be concluded that the probability of corrosion results from the concrete potential testing does not coincide with the actual situation within the specimens. The probability of corrosion rating for Mix No. 1 corresponds to the forensic evaluation of the removed embedded reinforcement. Therefore, the corrosion potential test may not be applicable to concrete containing high volumes of fly ash, or, on the other hand, the test values must be recalibrated for this type of specialty concrete.

6. FINDINGS, CONCLUSIONS, & RECOMMENDATIONS

6.1. FINDINGS

6.1.1. Mix Design. The test results, as shown in Figure 3.9, suggest that the highest strength HVFA concrete mixes are the 50 and 60 percent fly ash proportions with nearly identical results. The 70 percent fly ash mix, however, yielded a reasonable 3-day compressive strength of nearly 2,000 psi (13.8 MPa) and a 28-day strength of nearly 4,500 psi (31 MPa). Since both of these values are acceptable when designing concrete for construction, the final HVFA concrete mix chosen for this study was the 70 percent fly ash mix with 4 percent gypsum and 10 percent calcium hydroxide.

6.1.2. Hardened Concrete Property Tests. Obtaining comparable compressive strengths at 28 days with HVFA concrete versus conventional concrete was a goal in this study. Figure 4.2 illustrates that when the *w/cm* is decreased to 0.30, HVFA concrete does exhibit identical 28-day compressive strength values with a conventional concrete at a *w/cm* of 0.45. Also, at a *w/cm* of 0.30 in a HVFA concrete, the compressive strength exceeded that of the conventional concrete at 56 days. If the *w/cm* were increased slightly to 0.35, the HVFA concrete still exhibits a comparable compressive strength to that of conventional concrete with a *w/cm* of 0.45 at 56 days.

Early strength gain is important in construction, particularly for form removal. Figure 4.2 also shows that HVFA concrete having a *w/cm* consistent to a typical w/cm used in conventional concrete produces lower strengths not always suitable for normal construction practices. However, decreasing the HVFA concrete *w/cm* increases even early strength gain. HVFA concrete at 0.45 and 0.40 *w/cm* results in 1 day compressive strengths of less than 1,000 psi (6.9 MPa). Mix Design No. 1 reported a 1-day compressive strength of 2,574 psi (17.7 MPa). Although decreasing the *w/cm* to 0.35 and 0.30 does improve the 1 day compressive strengths, Mix Nos. 4 and 5 resulted in compressive strengths nearly 1,000 psi (6.9 MPa) less than that of Mix No. 1, but these strengths are likely sufficient for normal concrete construction practices.

When considering the differences in each mix design, the *w/cm* is the major factor. Each mix design was produced to investigate the effect decreasing the *w/cm* would have on the compressive strength. The behavior of the compressive strengths for

the mix designs analyzed coincides with results for traditional mix designs with decreasing *w/cm*. Even with a mix consisting of 70 percent fly ash and 30 percent portland cement, it is still shown that decreasing the *w/cm* increases the compressive strength at all ages. Low early strength development is expected in HVFA concrete and the data concludes this very well. Lowering the *w/cm* in conventional concrete will also produce increased compressive strengths, but workability becomes difficult without admixtures. The advantage to using HVFA concrete is that the *w/cm* can be reduced to produce compressive strengths comparable to conventional concrete while maintaining workability.

The flexural strength test was performed to assist in determining the tensile strength for Mix No. 3, the production HVFA concrete mix for the full scale specimen testing. Due to the failures occurring within the middle one-third region of the beams, the MOR can be expressed by PL/bd^2. This equation is based on the elastic beam theory which implies the tensile stress is proportional to the distance from the neutral axis. However, this is merely an estimate since the stresses induced under load generate a parabolic relationship. Thus, the MOR overestimates the tensile strength and it is suggested that the correct value of tensile strength is about ¾ of the theoretical modulus of rupture. Even for a conventional concrete, inconsistencies occur in determining the modulus of rupture.

The variability of the MOR test is significant and strongly affected by the moisture conditions of the specimen. Additional possibilities as to the reasons why the MOR test gives a higher value of strength than a direct tension test include: accidental eccentricity in a direct tensile test, which lowers the apparent strength of the concrete: the loading arrangement in a direct tensile test where the entire volume of the specimen is subjected to the maximum stress, increasing the potential for a weak element, and crack propagation blocked by less-stressed material closer to the neutral axis for the MOR test.

ACI 318 Building Code [2008] uses the expression $7.5\sqrt{f'_c}$, where f'_c equals the average 28-day compressive strength, as the calculated MOR for building design. This expression is used for mix designs generally consisting of between 70 and 100 percent portland cement. Since Mix No. 3 is comprised of 70 percent fly ash, the applicability of using this equation in calculating the tensile strength for mixes with this magnitude of fly

ash was evaluated. In using this particular approach, though, there is still some variability in calculating the MOR, even for 100 percent portland cement concrete mixes, with the actual coefficient ranging anywhere from 6 to 12. This equation showed that with the tested average stress value of 445 psi (3.0 MPa), the coefficient calculates to be 6.89. This value is well within the given range used for portland cement concrete mixes.

Significant variability of results from tensile testing is commonly recognized. Also, it is recognized that the MOR test rather overestimates the tensile strength of concrete, while the splitting tensile strength test determines tensile strengths closer to the direct tensile strength of concrete, only being 5 to 12 percent higher [Neville, 1997]. Mix No. 1 reported a tensile strength of $6.36\sqrt{f'_c}$ and Mix Nos. 2 and 3 reported tensile strengths of 6.83 and $6.86\sqrt{f'_c}$, respectively.

Like compressive strength, the modulus of elasticity is significantly affected by the modulus of the aggregate used in the concrete. Therefore, the modulus of elasticity is sensitive and measured values can be higher or lower than the specified calculated modulus of elasticity in accordance with ACI 318 [2008]. The measured values typically range from 80 to 120 percent of the specified calculated value according to ACI 318-08 [2008]. Taking this into consideration, the average tested modulus of elasticity for Mix No. 2 falls within this range at 115 percent of the specified calculated modulus of elasticity. Mix No. 3 is slightly outside of this range at 130 percent. As for Mix No. 1, it lies significantly outside of this typical range at 150 percent of the specified calculated modulus of elasticity.

The HVFA concrete mixes exhibited much lower shrinkage strains than the 100 percent portland cement concrete mix. The results of this test conclude that the addition of fly ash in the concrete has a significant effect on the shrinkage strain experienced by each specimen. Section 2.4.2 discusses that the addition of fly ash increases the volume of paste and may increase shrinkage provided the *w/cm* remains unchanged. This study examined two *w/cm* for the HVFA concrete of 0.45 and 0.40. It is to be expected that decreasing the *w/cm* from 0.45 to 0.40 in the HFVA concrete mix would reduce the shrinkage. The results of the data not coinciding with this may be attributed to the humidity conditions at which the specimens of Mix No. 3 were stored, which were indoor ambient conditions but not within a controlled environmental chamber. Nonetheless, the

HVFA concrete specimens experienced noticeably less shrinkage than the 100 percent portland cement concrete with a *w/cm* of 0.45.

The standard error plots shown in Figure 4.10 indicate that each mix design has statistically different shrinkage strains from one another over the period of testing. If the results from any one mix were to fall within the standard error variation of any other concrete mix tested, this would indicate those mixes would not be statistically different. However, none of the concrete mixes exhibited this result. Tables pertaining to standard error values for a specific specimen may be found in Appendix B.

Figures 4.11 through 4.13 shows the average shrinkage of each mix and the shrinkage prediction models used for comparison. The results for Mix No. 1 indicate that the B3 Model could be used to predict an estimation of the shrinkage experienced within the concrete. As for Mix Nos. 2 and 3, the models noticeably overestimate the shrinkage. The models tended to over predict the shrinkage for Mix No. 2 more than for Mix No. 3. If any of the shrinkage prediction plots were within the standard error bar ranges of either concrete mix, then it could be concluded the model's prediction of shrinkage would not be statistically different than the reported measured shrinkage values. Previously discussed in Section 4.7.2 is the fact that these models are based on conventional concrete mixes. The models overestimating the shrinkage for Mix Nos. 2 and 3 may be attributed to this fact, indicating that a HVFA concrete mixes may use more of the available water for hydration and leave less available for shrinkage.

6.1.3. Durability Tests. All the results contained within Section 5 regarding the many durability tests performed are all valuable in determining the durability performance of HVFA concrete. Common relationships between the tests are recognized and summarized within this section to produce conclusions on the durability performance of the HVFA concrete tested.

The chloride permeability test shows similar results to that of the chloride profiles developed from ponding specimens. Mix No. 1 resulted in the highest permeability rating of the three concrete mixes evaluated for both chloride tests. The chloride permeability test results of Mix Nos. 2 and 3 coincide with the results found from the developed chloride profiles. Both HVFA concrete mixes show lower penetration concentrations of chlorides compared to that of Mix No. 1.

The freeze-thaw test revealed that Mix No. 3 is comparable to Mix No. 1 in terms of reported durability factors. The increased durability factors of Mix No. 3 over Mix No. 2 are likely attributed to the decreased *w/cm* from 0.45 to 0.40. The reduction in *w/cm* decreases the amount of free voids within the pore structure of the concrete. Mix No. 2, containing 70 percent fly ash at the same *w/cm* as Mix No. 1, did not perform as well as Mix Nos. 1 and 3, although it still indicated "good" resistance to freeze-thaw damage. In general, the test results indicated that the HVFA concrete was able to develop an adequate air-void system to resist freeze-thaw damage.

Forensic evaluation of the specimens revealed variation in the condition reported for the concrete resistivity and potential measurements. The resistivity results indicated a "low" to "moderate" rate of corrosion. This coincided with the forensic evaluation of the removed embedded reinforcement.

The potential measurements, however, indicated a very different result when compared to the forensic evaluation. Mix Nos. 2 and 3 indicated a "high" chance of corrosion. The forensic investigation of the reinforcement from those concrete mixes showed otherwise. There was minimal to no corrosion development as shown in Figures 5.22 through 5.27.

6.2. CONCLUSIONS

Based on the previously stated findings, the following conclusions can be drawn in reference to the evaluation and prediction of the performance of HVFA concrete:

1. Decreasing the *w/cm* to 0.30 of HVFA concrete will produce comparable compressive strength at 28 days to that of a conventional concrete.
2. HVFA concrete will increase in compressive strength as the *w/cm* is decreased.
3. The MOR test overestimates the tensile strength of HVFA concrete.
4. The ACI 318 [2008] equation for the MOR is applicable to HVFA concrete.
5. The splitting tensile strength test produced similar tensile strength values among the HVFA concretes, excluding the compressive strength variation.
6. The splitting tensile strength test may be used to define tensile strength for HVFA concrete.

7. The ACI 318 [2008] equation for modulus of elasticity is as applicable to HVFA concrete as it is to conventional concrete.
8. The HVFA concrete mixes exhibited lower concrete shrinkage strains than portland cement concrete.
9. The HVFA concrete mixes exhibited lower chloride permeability according to the chloride permeability tests by the electrical and ponding methods.
10. Reducing the *w/cm* from 0.45 to 0.40 in the HVFA concrete increases the freeze-thaw resistance.
11. The resistivity of HVFA concrete increases with time.
12. The corrosion potential test does not correlate well between the measurements and actual reinforcement corrosion; therefore, this test may not be used or shall be calibrated for use on HVFA concrete.
13. The chloride permeability testing performed on the specimens containing reinforcement indicated there was potential for corrosion development; however, the level of probable corrosion did not correlate with the forensic evaluation of the reinforcement.

6.3. RECOMMENDATIONS

Based on the findings and conclusions stated in the previous sections, the following recommendations were derived in regard to the use of HVFA concrete:

1. The HVFA concrete mixes studied may be used in construction where a standard 4,000 psi (27.5 MPa) concrete mix design is required.
2. Excluding the half-cell potential method, existing relationships for hardened material properties and durability for conventional concretes are applicable to the HVFA concrete mixes studied.
3. Additional testing is required on the applicability of half-cell potential for evaluating corrosion in the HVFA concrete mixes studied.
4. The HVFA concrete mixes studied offers a sustainable alternative to conventional concrete in terms of carbon dioxide emissions and embodied energy.

APPENDIX A
HARDENED PROPERTY TESTS

Table A – 1: Average compressive strengths for Mix No. 1.

MIX No. 1 - CONTROL (100% PC)	
Time (Days)	*Strength (psi)*
0	0
1	2574
3	3764
7	4602
28	5610
56	6218

Table A – 2: Average compressive strengths for Mix No. 2.

MIX No. 2 - 70 % FA (w/cm = 0.45)	
Time (Days)	*Strength (psi)*
0	0
1	598
3	1171
7	1821
28	2720
56	3842

Table A – 3: Average compressive strengths for Mix No. 3.

MIX No. 3 - 70 % FA (w/cm = 0.40)	
Time (Days)	*Strength (psi)*
0	0
1	786
3	1631
7	2354
28	4176
56	4477

Table A – 4: Average compressive strengths for Mix No. 4.

MIX No. 4 - 70 % FA (w/cm = 0.35)	
Time (Days)	*Strength (psi)*
0	0
1	1350
3	2592
7	3649
28	5162
56	6011

Table A – 5: Average compressive strengths for Mix No. 5.

MIX No. 5 - 70 % FA (w/cm = 0.30)	
Time (Days)	*Strength (psi)*
0	0
1	1690
3	3104
7	3732
28	5546
56	6883

MISSOURI S&T University of Science & Technology

Flexural Strength: Modulus of Rupture

Standard: ASTM C 78

Specimen	
Sample Type	6" x 6" x 24" Concrete Beam
Load Type	Third Point
Load Rate	30 lb/sec
Geometry	Beam 3rd
Width	6.0"
Depth	6.0"
Span Length	18.0"
Area	12.0 in^2

MIX No. 3 - 70 % FA (W/C = 0.40)		
Specimen	*Load (lb)*	*Stress (psi)*
# 1	4261	439
# 2	4395	400
# 3	3899	497

Compressive Strength	4176	psi
Average Stress	445	psi
Modulus of Rupture = $7.5\sqrt{f'c}$	485	psi
Coefficient	6.88	(Standard coefficient range of 6 to 12)

Figure A – 6: Flexural strength test data.

MISSOURI S&T University of Science & Technology

Splitting Tensile Strength Test

Standard: ASTM C 496

Specimen

Diameter 6"

Length 12"

Loading Rate 283 lbf

$$T = \frac{2*P}{\prod*L*D}$$

T: splitting tensile strength (psi)

P: maximum aplied load indicated (lbf)

L: length (in)

D: diamter (in)

MIX No. 1 - CONTROL (100% PC)		
Specimen	D_{AVG} *(in)*	*Max Load (lbf)*
# 1	6.012	61680
# 2	6.000	61050
# 3	6.039	38955

Average Max Load	53895	lbf
Average Compressive Strength	5610	psi
Average Tensile Strength	477	psi
Tensile Coefficient	6.36	
Calculated Tensile Strength	719.56	psi

MIX No. 2 - 70 % FA (W/C = 0.45)		
Specimen	D_{AVG} *(in)*	*Max Load (lbf)*
# 1	6.041	43980
# 2	5.697	36255
# 3	6.024	40605

Average Max Load	40280	lbf
Average Compressive Strength	2720	psi
Average Tensile Strength	356	psi
Tensile Coefficient	6.83	
Calculated Tensile Strength	772.33	psi

MIX No. 3 - 70 % FA (W/C = 0.40)		
Specimen	D_{AVG} *(in)*	*Max Load (lbf)*
# 1	5.720	56979
# 2	6.025	56472
# 3	5.725	36797

Average Max Load	50083	lbf
Average Compressive Strength	4176	psi
Average Tensile Strength	445	psi
Tensile Coefficient	6.89	
Calculated Tensile Strength	775.01	psi

Figure A – 7: Splitting tensile strength test data.

MISSOURI S&T University of Science & Technology

Modulus of Elasticity

Standard: ASTM C 469

Specimen

Load Rate	1000 lb/sec
Laod Type	Cyclic
Geometry	Cylinder
Diameter	6.00"
Length	12.0"
Cylinder Correction Factor	1.0
Gage Length	8.0 in
Area	28.27 in^2

MIX No. 1 - CONTROL (100% PC)		
Specimen	*Load (lbf)*	*C 496 (psi)*
# 1	38947	5,800,000
# 2	*38951*	5,900,000
# 3	38913	5,700,000

Compressive Strength	5610	psi
Average Max Load	38,930	lbf
Average C 496	5,800,000	psi
57000√f'c Calculated Value	4,300,000	psi

MIX No. 2 - 70 % FA (W/C = 0.45)		
Specimen	*Load (lbf)*	*C 496 (psi)*
# 1	17082	3,500,000
# 2	17073	3,300,000
# 3	17075	3,500,000

Compressive Strength	2720	psi
Average Max Load	17,079	lbf
Average C 496	3,433,333	psi
57000√f'c Calculated Value	2,900,000	psi

MIX No. 3 - 70 % FA (W/C = 0.40)		
Specimen	*Load (lbf)*	*C 496 (psi)*
# 1	19246	4,680,000
# 2	19224	4,745,000
# 3	19204	4,940,000

Compressive Strength	4176	psi
Average Max Load	19,225	lbf
Average C 496	4,788,333	psi
57000√f'c Calculated Value	3,680,000	psi

Figure A – 8: Modulus of elasticity test data.

APPENDIX B
SHRINKAGE ANALYSIS

MIX 1 - 70% FA w/c = 0.45

Cast Date: 4/30/2010 Time of Cast: 2:30 100% PC w/c = 0.40

		Age of Mix:	0	1	2	3	4	5	6
		Days after opening:	-1	0	1	2	3	4	5
Material	Specimen	Number	4/30/2010 12:00 AM	5/1/2010 12:00 AM	5/2/2010 12:00 AM	5/3/2010 12:00 AM	5/4/2010 12:00 AM	5/5/2010 12:00 AM	5/6/2010 12:00 AM
	Refer Bar		715	715	715	716	716	715	714
NC	1	1--1	0	-62.72	-125.44	-196.00	-250.88	-297.92	-297.92
NC	1	1--2	0	-78.40	-156.80	-243.04	-274.40	-297.92	-360.64
NC	1	1--3	0	-54.88	-109.76	-172.48	-203.84	-227.36	-243.04
NC	1	2--1							
NC	1	2--2							
NC	1	2--3							
NC	1	3--1	0	-54.88	-109.76	-172.48	-235.20	-290.08	-258.72
NC	1	3--2	0	-54.88	-109.76	-172.48	-227.36	-274.40	-266.56
NC	1	3--3	0	0.00	0.00	0.00	0.00	0.00	0.00
	Average		0	-50.96	-101.92	-159.41	-198.61	-231.28	-237.81
NC	2	1--1	0	-54.88	-109.76	-172.48	-203.84	-227.36	-258.72
NC	2	1--2	0	-62.72	-125.44	-196.00	-235.20	-266.56	-274.40
NC	2	1--3	0	-54.88	-109.76	-172.48	-196.00	-211.68	-258.72
NC	2	2--1	0	-39.20	-78.40	-125.44	-125.44	-117.60	-133.28
NC	2	2--2	0	-15.68	-31.36	-54.88	-78.40	-94.08	-125.44
NC	2	2--3	0	-141.12	-282.24	-431.20	-493.92	-548.80	-556.64
NC	2	3--1							
NC	2	3--2	0	-86.24	-172.48	-266.56	-313.60	-352.80	-439.04
NC	2	3--3							
	Average		0	-64.96	-129.92	-202.72	-235.20	-259.84	-292.32
NC	3	1--1	0	-54.88	-109.76	-117.60	-141.12	-156.80	-196.00
NC	3	1--2	0	-7.84	-15.68	-31.36	-70.56	-101.92	-117.60
NC	3	1--3	0	-39.20	-78.40	-125.44	-148.96	-164.64	-196.00
NC	3	2--1	0	-47.04	-94.08	-148.96	-188.16	-219.52	-250.88
NC	3	2--2	0	-47.04	-94.08	-148.96	-172.48	-188.16	-211.68
NC	3	2--3	0	-78.40	-156.80	-243.04	-227.36	-203.84	-258.72
NC	3	3--1	0	-54.88	-109.76	-172.48	-227.36	-274.40	-258.72
NC	3	3--2	0	-54.88	-109.76	-172.48	-227.36	-274.40	-274.40
NC	3	3--3	0	-47.04	-94.08	-148.96	-188.16	-219.52	-227.36
	Average		0	-47.91	-95.82	-145.48	-176.84	-200.36	-221.26
NC	4	1--1	0	-23.52	-47.04	-78.40	-86.24	-86.24	-109.76
NC	4	1--2	0	-15.68	-31.36	-54.88	-78.40	-94.08	-94.08
NC	4	1--3	0	-47.04	-94.08	-148.96	-148.96	-141.12	-172.48
NC	4	2--1	0	-15.68	-31.36	-54.88	-117.60	-172.48	-133.28
NC	4	2--2	0	-23.52	-47.04	-78.40	-133.28	-180.32	-180.32
NC	4	2--3	0	-62.72	-125.44	-148.96	-172.48	-188.16	-297.92
NC	4	3--1	0	-31.36	-62.72	-101.92	-117.60	-125.44	-125.44
NC	4	3--2	0	-62.72	-125.44	-196.00	-243.04	-282.24	-282.24
NC	4	3--3	0	-62.72	-125.44	-196.00	-235.20	-266.56	-274.40
	Average		0	-38.33	-76.66	-117.60	-148.09	-170.74	-185.55
verage Raw Shrinkage of Mix No.			0	50.54	101.08	156.30	189.68	215.55	234.24
Standard Deviation			0	11.02	22.03	35.49	36.73	38.51	44.44
Standard Error			0	5.51	11.02	17.75	18.36	19.25	22.22
ACI 209 R-92 Model			0	11.60	25.95	50.57	73.97	96.24	117.45
B3 Model			0	26.60	58.80	85.30	105.87	123.29	138.62
		τsh =	0	0.00	116.63	110.33	106.81	104.38	102.54
		Ecm607/Ecm	0	0.00	0.98	0.98	0.98	0.98	0.98
		εsh∞	0	0.00	812.21	812.95	813.32	813.55	813.68
		S(t,tc) =	0	0.00	0.09	0.13	0.17	0.19	0.22
CEB MC90 Model			0	31.80	53.81	75.67	92.16	105.84	117.69
		βs(t-tc) =	0	0.00	0.11	0.15	0.18	0.21	0.23

Figure B – 1: Example of recorded shrinkage measurements during testing for Mix No. 1.

MIX 2 - 70% FA w/c = 0.45

Cast Date: 11/4/2010 Time of Cast: 10:30 70% FA w/c = 0.45

		Humidity:	0	24	22	22	25	23	42
		Age of Mix:	0	1	2	3	4	5	6
		Days after opening:	-1	0	1	2	3	4	5
Material	Specimen	Number	11/4/2010 12:00 AM	11/5/2010 12:15 PM	11/6/2010 4:00 AM	11/7/2010 7:00 PM	11/8/2010 10:00 AM	11/9/2010 3:00 AM	11/10/2010 11:30 AM
Refer Bar				715	714	715	713	714	714
70/0.45	1	1--1	0	-15.68	-23.52	-54.88	-101.92	-94.08	-94.08
70/0.45	1	1--2	0	-31.36	-54.88	-86.24	-94.08	-133.28	-148.96
70/0.45	1	1--3	0	-78.40	-148.96	-180.32	-148.96	-172.48	-211.68
70/0.45	1	2--1	0	0.00	7.84	-23.52	-23.52	-39.20	-70.56
70/0.45	1	2--2	0	-31.36	-54.88	-86.24	-94.08	-117.60	-117.60
70/0.45	1	2--3	0	-39.20	-70.56	-117.60	-109.76	-133.28	-156.80
70/0.45	1	3--1	0	-54.88	-101.92	-148.96	-141.12	-180.32	-188.16
70/0.45	1	3--2	0	-47.04	-86.24	-133.28	-156.80	-188.16	-203.84
70/0.45	1	3--3	0	-54.88	-101.92	-148.96	-125.44	-172.48	-188.16
Average			0	-39.20	-70.56	-108.89	-110.63	-136.76	-153.32
70/0.45	2	1--1	0	-15.68	-39.20	-78.40	-54.88	-70.56	-62.72
70/0.45	2	1--2	0	-31.36	-70.56	-94.08	-109.76	-101.92	-101.92
70/0.45	2	1--3	0	-39.20	-86.24	-78.40	-78.40	-141.12	-172.48
70/0.45	2	2--1	0	23.52	39.20	-15.68	-15.68	-31.36	-54.88
70/0.45	2	2--2	0	0.00	-7.84	360.64	-47.04	-78.40	-86.24
70/0.45	2	2--3	0	-15.68	-39.20	-101.92	-70.56	-78.40	-94.08
70/0.45	2	3--1	0	-7.84	-23.52	-54.88	-39.20	-54.88	-70.56
70/0.45	2	3--2	0	-47.04	-101.92	-148.96	-133.28	-164.64	-172.48
70/0.45	2	3--3	0	-7.84	-23.52	-62.72	-47.04	-62.72	-86.24
Average			0	-15.68	-39.20	-30.49	-66.20	-87.11	-100.18
70/0.45	3	1--1	0	-15.68	-39.20	-54.88	-70.56	-101.92	-117.60
70/0.45	3	1--2	0	-7.84	-23.52	-54.88	-54.88	-86.24	-101.92
70/0.45	3	1--3	0	15.68	23.52	-23.52	-39.20	-31.36	-54.88
70/0.45	3	2--1	0	7.84	7.84	-54.88	-39.20	-54.88	-70.56
70/0.45	3	2--2	0	-15.68	-39.20	-62.72	-109.76	-94.08	-101.92
70/0.45	3	2--3	0	0.00	-7.84	-47.04	-54.88	-86.24	-125.44
70/0.45	3	3--1	0	-39.20	-86.24	-101.92	-94.08	-101.92	-133.28
70/0.45	3	3--2	0	-47.04	-101.92	-117.60	-133.28	-156.80	-156.80
70/0.45	3	3--3	0	-62.72	-133.28	-156.80	-156.80	-180.32	-188.16
Average			0	-18.29	-44.43	-74.92	-83.63	-99.31	-116.73
70/0.45	4	1--1	0	-47.04	-101.92	-101.92	-94.08	-117.60	-133.28
70/0.45	4	1--2	0	-47.04	-101.92	-141.12	-172.48	-188.16	-196.00
70/0.45	4	1--3	0	-39.20	-86.24	-125.44	-125.44	-148.96	-156.80
70/0.45	4	2--1	0	15.68	23.52	-7.84	-7.84	-15.68	-54.88
70/0.45	4	2--2	0	7.84	7.84	-31.36	-31.36	-39.20	-70.56
70/0.45	4	2--3	0	-47.04	-101.92	-117.60	-133.28	-141.12	-133.28
70/0.45	4	3--1	0	-39.20	-86.24	-109.76	-117.60	-133.28	-156.80
70/0.45	4	3--2	0	-23.52	-54.88	-86.24	-125.44	-133.28	-141.12
70/0.45	4	3--3	0	-54.88	-117.60	-156.80	-164.64	-172.48	-196.00
Average			0	-30.49	-68.82	-97.56	-108.02	-121.08	-137.64
verage Raw Shrinkage of Mix No.			0	25.92	55.75	77.96	92.12	111.07	126.96
Standard Deviation			0	10.96	16.25	34.66	21.13	22.16	23.31
Standard Error			0	5.48	8.13	17.33	10.56	11.08	11.66
ACI 209 R-92 Model			0	8.20	17.71	34.51	50.48	65.68	80.16
B3 Model			0	47.90	72.41	105.08	130.50	152.04	171.05
		τsh =	0	0.00	139.76	132.22	128.00	125.09	122.88
		Ecm607/Ecm	0	0.00	0.97	0.97	0.98	0.98	0.98
		εsh∞	0	0.00	916.70	917.43	917.81	918.04	918.20
		S(t,tc) =	0	0.00	0.08	0.12	0.15	0.18	0.20
CEB MC90 Model			0	43.10	66.68	93.77	114.21	131.16	145.84
		βs(t-tc) =	0	0.00	0.11	0.15	0.18	0.21	0.23

Figure B – 2: Example of recorded shrinkage measurements during testing for Mix No. 2.

MIX 3 - 70% FA w/c = 0.40

Cast Date: 6/2/2010 Time of Cast: 10:30 70% FA w/c = 0.40

		Humidity:	0	60	68	74	56	64	66	67
		Age of Mix:	0	1	2	3	4	5	6	7
		Days after opening:	-1	0	1	2	3	4	5	6
Material	Specimen	Number	6/2/2010 0	6/3/2010 0:00	6/4/2010 12:30	6/5/2010 4:30	6/6/2010 1:20	6/7/2010 4:15	6/8/2010 2:30	6/9/2010 12:00
Refer Bar			715	715	716	715	713	713	715	714
70/0.40	1	1--1	0	-109.76	-227.36	-329.28	-274.40	-290.08	-243.04	-235.20
70/0.40	1	1--2	0	0.00	-7.84	0.00	15.68	-15.68	-47.04	-47.04
70/0.40	1	1--3	0	-15.68	-39.20	-47.04	-62.72	-78.40	-125.44	-94.08
70/0.40	1	2--1	0	-62.72	-133.28	-188.16	-196.00	-211.68	-243.04	-235.20
70/0.40	1	2--2	0	-62.72	-133.28	-188.16	-1003.52	-1027.04	-1058.40	-1034.88
70/0.40	1	2--3	0	-54.88	-117.60	-164.64	-196.00	-203.84	-227.36	-211.68
70/0.40	1	3--1	0	-47.04	-101.92	-141.12	-203.84	-219.52	-243.04	-243.04
70/0.40	1	3--2	0	-39.20	-86.24	-117.60	-148.96	-164.64	-196.00	-188.16
70/0.40	1	3--3	0	-23.52	-54.88	-70.56	-101.92	-141.12	-156.80	-156.80
Average			0	-46.17	-100.18	-138.51	-241.30	-261.33	-282.24	-271.79
70/0.40	2	1--1	0	15.68	31.36	47.04	39.20	39.20	39.20	47.04
70/0.40	2	1--2								
70/0.40	2	1--3	0	-31.36	-62.72	-94.08	-109.76	-109.76	-109.76	-148.96
70/0.40	2	2--1	0	-47.04	-94.08	-141.12	-117.60	-125.44	-141.12	-141.12
70/0.40	2	2--2	0	-47.04	-94.08	-141.12	-125.44	-156.80	-180.32	-180.32
70/0.40	2	2--3	0	-31.36	-62.72	-94.08	-70.56	-78.40	-101.92	-109.76
70/0.40	2	3--1	0	-7.84	-15.68	-23.52	-54.88	-86.24	-109.76	-133.28
70/0.40	2	3--2	0	-31.36	-62.72	-94.08	-125.44	-172.48	-196.00	-196.00
70/0.40	2	3--3	0	-47.04	-94.08	-141.12	-172.48	-211.68	-227.36	-227.36
Average			0	-28.42	-56.84	-85.26	-92.12	-112.70	-128.38	-136.22
70/0.40	3	1--1	0	-23.52	-47.04	-54.88	-62.72	-94.08	-109.76	-125.44
70/0.40	3	1--2	0	23.52	47.04	86.24	54.88	70.56	62.72	70.56
70/0.40	3	1--3								
70/0.40	3	2--1	0	-47.04	-94.08	-125.44	-141.12	-141.12	-164.64	-164.64
70/0.40	3	2--2	0	-70.56	-141.12	-196.00	-227.36	-250.88	-266.56	-266.56
70/0.40	3	2--3	0	-62.72	-125.44	-172.48	-203.84	-211.68	-250.88	-243.04
70/0.40	3	3--1	0	-54.88	-109.76	-148.96	-180.32	-203.84	-211.68	-227.36
70/0.40	3	3--2	0	-62.72	-125.44	-172.48	-141.12	-250.88	-258.72	-258.72
70/0.40	3	3--3	0	-78.40	-156.80	-219.52	-258.72	-297.92	-305.76	-313.60
Average			0	-47.04	-94.08	-125.44	-145.04	-172.48	-188.16	-191.10
70/0.40	4	1--1	0	-31.36	-54.88	-86.24	-109.76	-117.60	-133.28	-188.16
70/0.40	4	1--2	0	-31.36	-54.88	-86.24	-109.76	-117.60	-133.28	-172.48
70/0.40	4	1--3	0	-31.36	-54.88	-86.24	-101.92	-101.92	-117.60	-125.44
70/0.40	4	2--1	0	31.36	70.56	101.92	86.24	70.56	47.04	23.52
70/0.40	4	2--2	0	-47.04	-86.24	-133.28	-141.12	-148.96	-180.32	-227.36
70/0.40	4	2--3	0	-39.20	-70.56	-109.76	-117.60	-141.12	-164.64	-164.64
70/0.40	4	3--1	0	-70.56	-133.28	-203.84	-235.20	-250.88	-266.56	-274.40
70/0.40	4	3--2	0	-78.40	-148.96	-227.36	-274.40	-282.24	-305.76	-305.76
70/0.40	4	3--3	0	-86.24	-164.64	-250.88	-282.24	-305.76	-329.28	-344.96
Average			0	-42.68	-77.53	-120.21	-142.86	-155.06	-175.96	-197.74
verage Raw Shrinkage of Mix No			0	41.08	82.16	117.36	155.33	175.39	193.69	199.21
Standard Deviation			0	8.65	19.40	22.74	62.31	62.55	64.42	55.69
Standard Error			0	4.32	9.70	11.37	31.15	31.28	32.21	27.84
ACI 209 R-92 Model			0	15.60	20.39	39.74	58.14	75.64	92.31	108.21
B3 Model			0	42.30	60.53	87.85	109.09	127.09	142.96	157.31
		τsh =	0	0.00	135.87	128.54	124.44	121.61	119.46	117.73
		Ecm607/Ecm	0	0.00	0.97	0.98	0.98	0.98	0.98	0.98
		εsh∞	0	0.00	902.24	902.96	903.35	903.58	903.73	903.83
		S(t,tc) =	0	0.00	0.09	0.12	0.15	0.18	0.20	0.22
CEB MC90 Model			0	36.70	65.23	91.74	111.73	128.31	142.68	155.46
		βs(t-tc) =	0	0.00	0.11	0.15	0.18	0.21	0.23	0.25

Figure B – 3: Example of recorded shrinkage measurements during testing for Mix No. 3.

APPENDIX C
DURABILITY TESTS

FORMWORK :

(PONDING SPECIMENS)

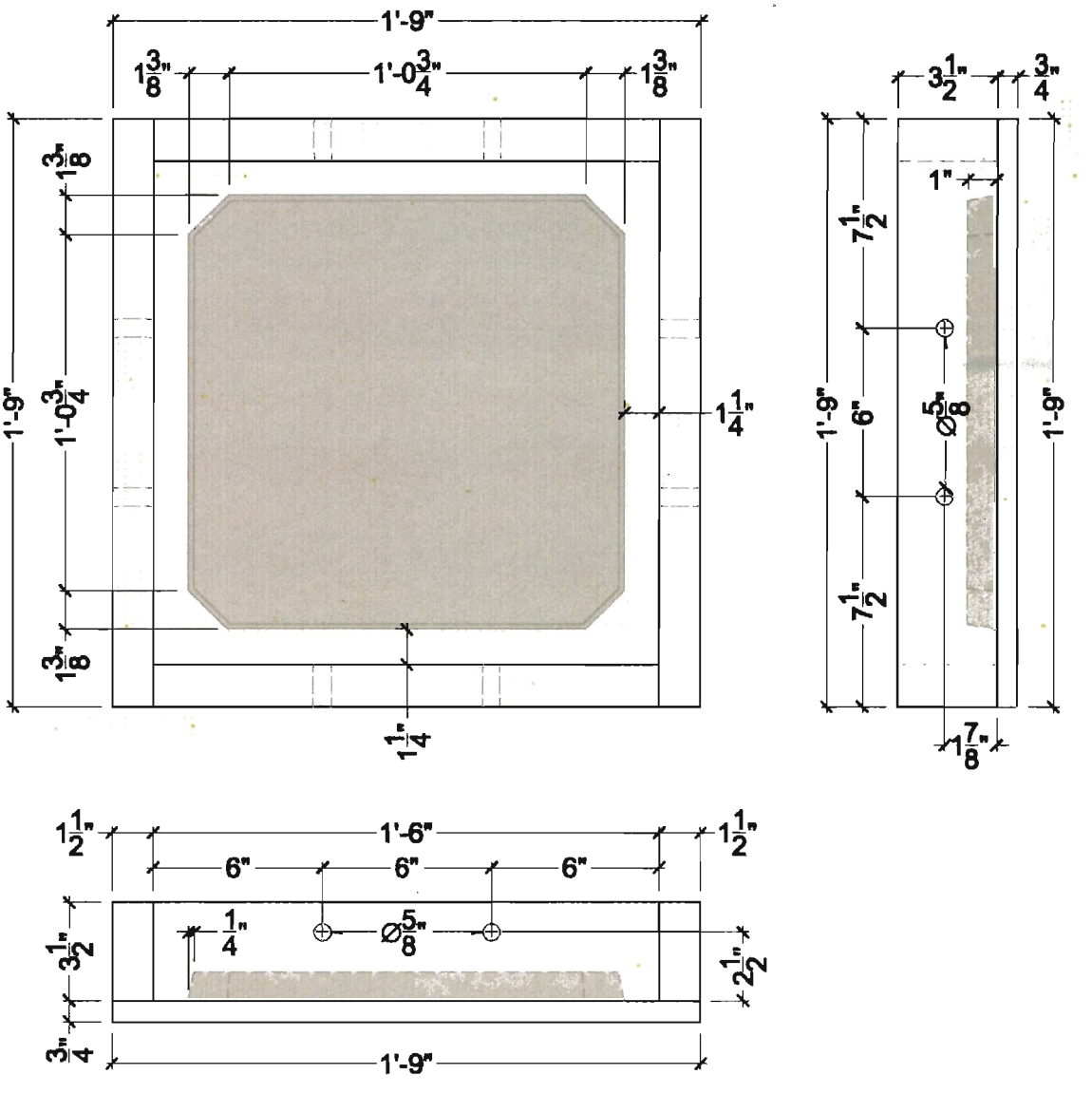

Figure C – 1: Typical ponding specimen form details and dimensions.

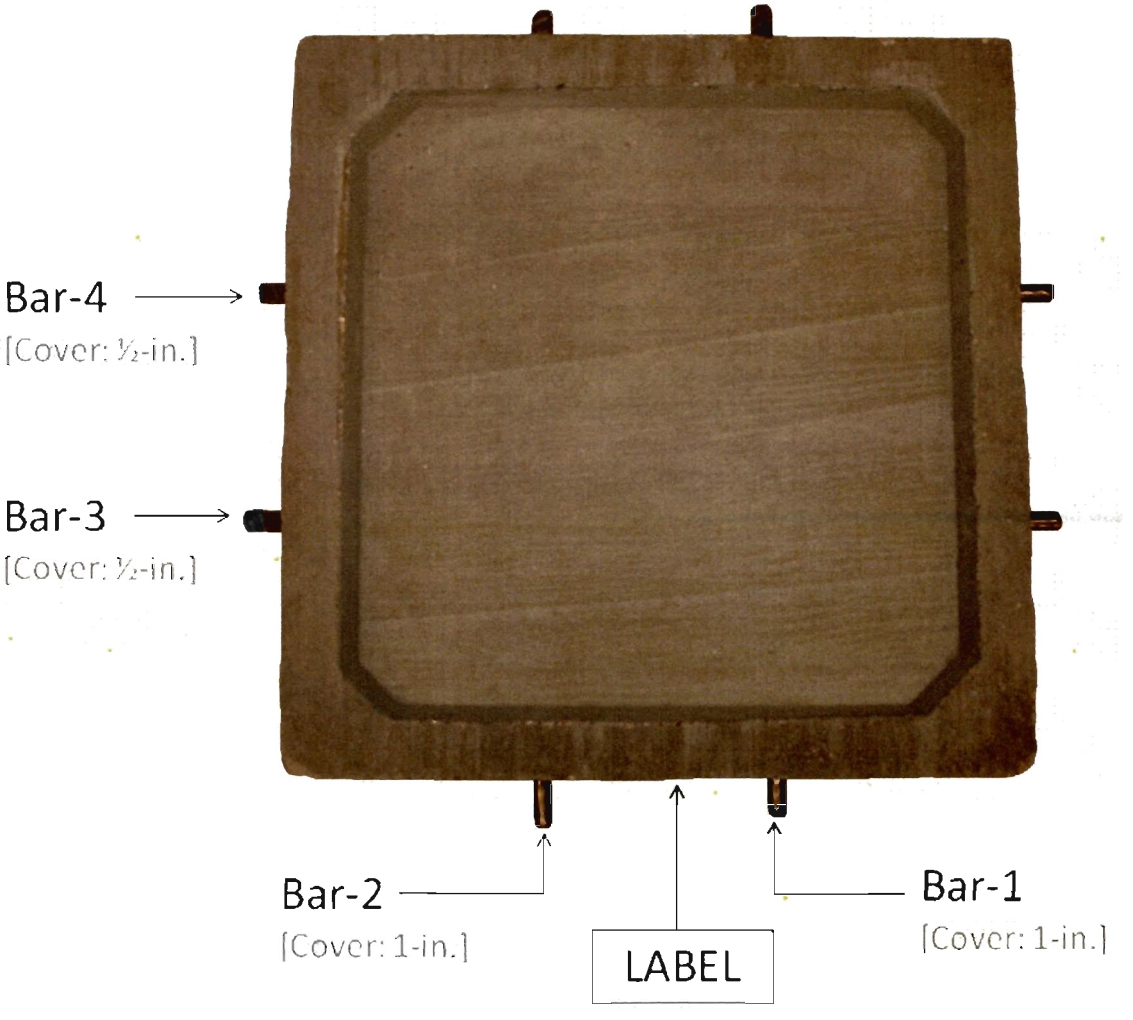

Figure C – 2: Labeling of bars embedded within a ponding specimen with respect to the specimen's label.

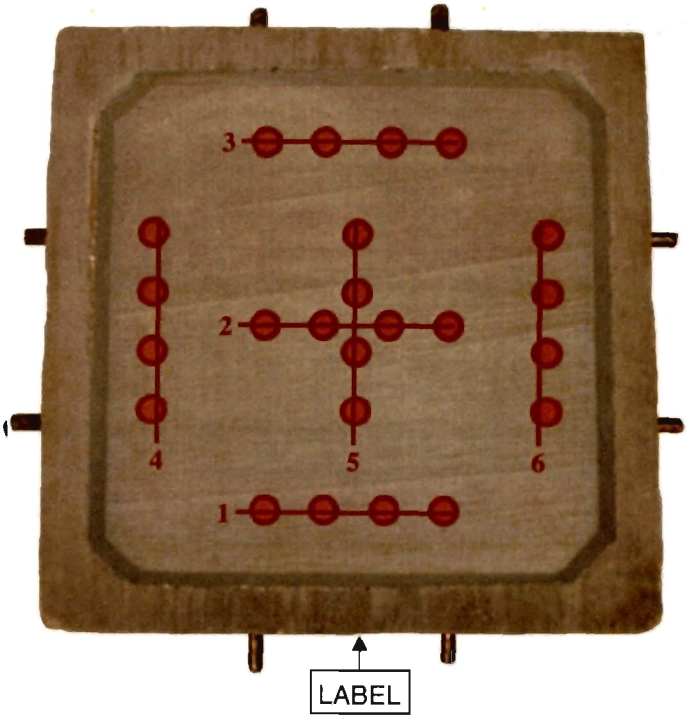

(a)

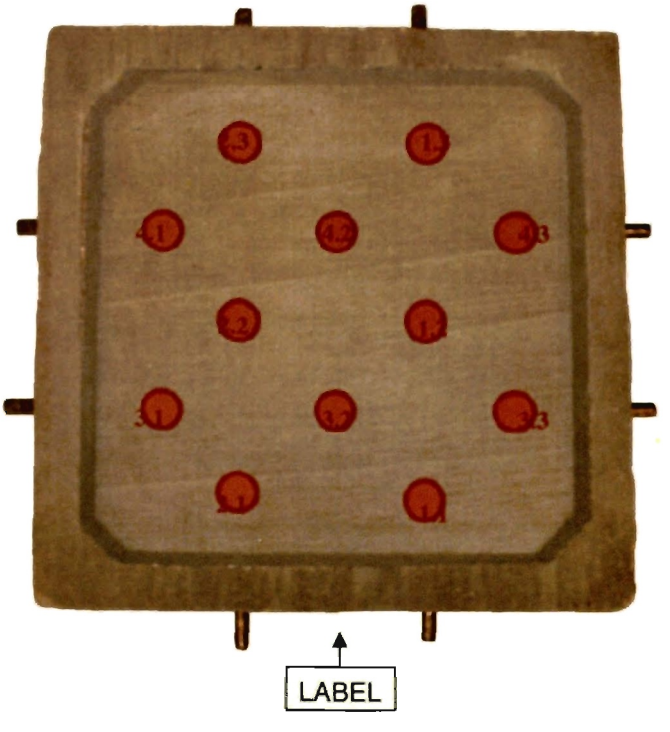

(b)

Figure C – 3: The locations of the (a) resistivity and (b) corrosion potential measurements with respect to a ponding specimen's label.

	2-BAR	*Resistivity Measurements (kΩcm) vs. Time (weeks):*					
	Location:	*0*	*6*	*12*	*18*	*24*	*30*
Specimen (Control): *C-1*	*1*	8.0	9.8	14.0	14.0	17.0	21.0
	2	7.4	6.6	12.0	13.0	13.0	16.0
	3	9.1	9.0	13.0	14.0	14.0	11.0
	4	8.2	4.6	11.0	12.0	9.5	19.0
	5	8.1	8.6	12.0	14.0	16.0	18.0
	6	7.4	9.0	12.0	14.0	15.0	17.0
C-2	*1*	9.9	9.7	12.0	15.0	16.0	13.0
	2	6.4	7.5	11.0	13.0	12.0	15.0
	3	9.2	8.1	13.0	14.0	15.0	16.0
	4	7.2	9.4	13.0	13.0	16.0	8.6
	5	8.0	10.0	13.0	14.0	15.0	8.7
	6	8.2	8.6	12.0	13.0	14.0	9.5
C-3	*1*	9.0	9.4	14.0	15.0	16.0	20.0
	2	7.2	7.7	12.0	13.0	14.0	16.0
	3	9.2	6.9	13.0	13.0	8.5	18.0
	4	8.2	9.4	14.0	14.0	15.0	21.0
	5	8.0	9.4	14.0	14.0	15.0	18.0
	6	8.0	9.1	13.0	14.0	14.0	7.0
C-1 Average:		8.0	7.9	12.3	13.5	14.1	17.0
C-2 Average:		8.2	8.9	12.3	13.7	14.7	11.8
C-3 Average:		8.3	8.7	13.3	13.8	13.8	16.7
Overall Average:		8.15	8.49	12.67	13.67	14.17	15.16
Standard Dev.:		0.87	1.39	0.97	0.77	2.24	4.48
SEM:		0.21	0.33	0.23	0.18	0.53	1.06
Maximum:		9.9	10.0	14.0	15.0	17.0	21.0
Minimum:		6.4	4.6	11.0	12.0	8.5	7.0

Figure C – 4: Recorded resistivity measurements throughout testing period for Mix No. 1 containing 2 bars.

Specimen (70% / 0.45):	2-BAR Location:	Resistivity Measurements (kΩcm) vs. Time (weeks): 0	6	12	18	24	30
FA-1	1	10.0	5.6	9.5	12.0	14.0	18.0
	2	8.5	5.0	8.5	11.0	11.0	16.0
	3	9.7	3.4	8.9	12.0	6.8	11.0
	4	9.8	5.1	9.6	11.0	13.0	17.0
	5	8.8	5.5	10.0	11.0	13.0	15.0
	6	8.8	5.6	9.3	11.0	13.0	16.0
FA-2	1	9.7	5.7	10.0	13.0	14.0	16.0
	2	7.1	5.1	8.6	11.0	12.0	16.0
	3	9.6	6.0	9.4	10.0	7.8	14.0
	4	7.9	5.3	9.6	12.0	13.0	15.0
	5	7.3	5.6	9.5	11.0	14.0	16.0
	6	7.9	5.6	9.6	11.0	13.0	15.0
FA-3	1	9.7	5.5	10.0	12.0	13.0	17.0
	2	6.1	4.7	8.8	10.0	11.0	15.0
	3	8.8	5.6	9.6	13.0	11.0	8.8
	4	8.6	7.2	6.8	12.0	13.0	16.0
	5	6.1	5.4	9.5	11.0	13.0	14.0
	6	7.0	5.7	9.7	11.0	13.0	13.0
FA-1 Average:		9.3	5.0	9.3	11.3	11.8	15.5
FA-2 Average:		8.3	5.6	9.5	11.3	12.3	15.3
FA-3 Average:		7.7	5.7	9.1	11.5	12.3	14.0
Overall Average:		8.41	5.42	9.27	11.39	12.14	14.93
Standard Dev.:		1.27	0.72	0.76	0.85	2.00	2.21
SEM:		0.30	0.17	0.18	0.20	0.47	0.52
Maximum:		10.0	7.2	10.0	13.0	14.0	18.0
Minimum:		6.1	3.4	6.8	10.0	6.8	8.8

Figure C – 5: Recorded resistivity measurements throughout testing period for Mix No. 2 containing 2 bars.

Specimen (70% / 0.40):		2-BAR	Resistivity Measurements (kΩcm) vs. Time (weeks):					
		Location:	0	6	12	18	24	30
	FA-1	1	8.2	7.7	12.0	14.0	15.0	19.0
		2	7.4	5.4	10.0	12.0	13.0	15.0
		3	9.8	3.6	10.0	13.0	14.0	18.0
		4	8.0	7.6	11.0	13.0	14.0	18.0
		5	8.2	6.8	11.0	12.0	13.0	18.0
		6	8.1	6.0	11.0	13.0	15.0	17.0
	FA-2	1	9.8	7.7	12.0	15.0	15.0	18.0
		2	8.2	3.5	10.0	12.0	13.0	16.0
		3	9.0	5.1	10.0	10.0	14.0	16.0
		4	8.2	6.8	11.0	12.0	14.0	16.0
		5	8.1	4.3	12.0	13.0	13.0	16.0
		6	8.1	5.9	11.0	18.0	11.0	17.0
	FA-3	1	9.0	5.6	10.0	11.0	13.0	15.0
		2	6.1	5.5	9.3	10.0	12.0	15.0
		3	8.2	6.3	11.0	12.0	14.0	14.0
		4	6.6	6.8	10.0	12.0	14.0	15.0
		5	7.2	6.0	10.0	11.0	14.0	16.0
		6	7.8	6.1	9.6	12.0	13.0	15.0
	FA-1 Average:		8.3	6.2	10.8	12.8	14.0	17.5
	FA-2 Average:		8.6	5.6	11.0	13.3	13.3	16.5
	FA-3 Average:		7.5	6.1	10.0	11.3	13.3	15.0
	Overall Average:		8.11	5.93	10.61	12.50	13.56	16.33
	Standard Dev.:		0.94	1.25	0.84	1.86	1.04	1.41
	SEM:		0.22	0.30	0.20	0.44	0.25	0.33
	Maximum:		9.8	7.7	12.0	18.0	15.0	19.0
	Minimum:		6.1	3.5	9.3	10.0	11.0	14.0

Figure C – 6: Recorded resistivity measurements throughout testing period for Mix No. 3 containing 2 bars.

Specimen (Control):		4-BAR Location:	Resistivity Measurements (kΩcm) vs. Time (weeks): 0	6	12	18	24
	C-1	1	5.1	9.0	10.0	11.0	12.0
		2	4.5	9.7	10.0	11.0	12.0
		3	5.0	9.6	10.0	12.0	12.0
		4	6.9	11.0	13.0	15.0	15.0
		5	6.8	11.0	12.0	13.0	13.0
		6	6.8	8.2	11.0	11.0	11.0
	C-2	1	6.5	11.0	12.0	14.0	14.0
		2	6.8	10.0	12.0	13.0	14.0
		3	7.5	11.0	11.0	13.0	10.0
		4	5.2	9.8	10.0	13.0	11.0
		5	5.1	9.8	10.0	11.0	9.4
		6	5.1	9.7	9.9	11.0	12.0
	C-3	1	6.9	11.0	12.0	14.0	15.0
		2	6.1	10.0	11.0	12.0	13.0
		3	6.8	11.0	11.0	11.0	15.0
		4	4.4	9.0	9.5	11.0	10.0
		5	4.3	8.5	10.0	10.0	11.0
		6	5.1	9.8	11.0	11.0	8.6
C-1 Average:			5.9	9.8	11.0	12.2	12.5
C-2 Average:			6.0	10.2	10.8	12.5	11.7
C-3 Average:			5.6	9.9	10.8	11.5	12.1
Overall Average:			5.83	9.95	10.86	12.06	12.11
Standard Dev.:			1.05	0.90	1.00	1.39	1.97
SEM:			0.25	0.21	0.24	0.33	0.46
Maximum:			7.5	11.0	13.0	15.0	15.0
Minimum:			4.3	8.2	9.5	10.0	8.6

Figure C – 7: Recorded resistivity measurements throughout testing period for Mix No. 1 containing 4 bars.

Specimen (70% / 0.45):		4-BAR Location:	Resistivity Measurements (kΩcm) vs. Time (weeks): 0	6	12	18	24
	FA-1	1	5.2	9.5	11.0	14.0	15.0
		2	5.0	9.6	12.0	15.0	12.0
		3	4.4	9.9	12.0	16.0	17.0
		4	4.4	9.4	11.0	14.0	15.0
		5	5.1	9.2	10.0	14.0	8.7
		6	5.9	10.0	9.5	12.0	16.0
	FA-2	1	6.7	6.9	6.9	11.0	11.0
		2	3.4	7.6	8.5	10.0	11.0
		3	2.5	7.0	8.5	11.0	12.0
		4	5.3	8.6	9.7	16.0	8.6
		5	5.2	8.5	10.0	13.0	14.0
		6	4.3	8.5	10.0	14.0	16.0
	FA-3	1	8.6	9.5	12.0	16.0	18.0
		2	4.1	11.0	12.0	15.0	17.0
		3	3.5	11.0	13.0	1.0	17.0
		4	3.2	10.0	9.5	12.0	14.0
		5	3.3	9.6	10.0	12.0	14.0
		6	2.8	8.2	9.4	13.0	12.0
	FA-1 Average:		5.0	9.6	10.9	14.2	14.0
	FA-2 Average:		4.6	7.9	8.9	12.5	12.1
	FA-3 Average:		4.3	9.9	11.0	11.5	15.3
	Overall Average:		4.61	9.11	10.28	12.72	13.79
	Standard Dev.:		1.50	1.18	1.55	3.44	2.86
	SEM:		0.35	0.28	0.36	0.81	0.68
	Maximum:		8.6	11.0	13.0	16.0	18.0
	Minimum:		2.5	6.9	6.9	1.0	8.6

Figure C – 8: Recorded resistivity measurements throughout testing period for Mix No. 2 containing 4 bars.

Specimen (70% / 0.40):	4-BAR Location:	Resistivity Measurements (kΩcm) vs. Time (weeks): 0	6	12	18	24
FA-1	1	5.0	8.5	10.0	12.0	14.0
	2	3.5	7.9	9.6	12.0	10.0
	3	3.5	8.4	9.4	12.0	17.0
	4	6.0	9.4	11.0	15.0	13.0
	5	3.3	8.5	10.0	13.0	15.0
	6	7.7	9.1	10.0	13.0	15.0
FA-2	1	4.4	8.1	8.5	9.6	8.6
	2	4.3	8.1	8.5	8.9	11.0
	3	3.4	8.0	8.5	9.3	11.0
	4	6.3	9.0	10.0	7.8	11.0
	5	5.0	9.0	9.6	12.0	12.0
	6	4.3	8.8	9.5	12.0	15.0
FA-3	1	5.1	8.5	9.5	11.0	15.0
	2	4.2	8.8	9.0	12.0	15.0
	3	5.1	9.0	10.0	13.0	15.0
	4	6.0	7.4	7.5	9.0	9.3
	5	3.0	8.1	8.6	10.0	11.0
	6	3.5	8.1	8.8	11.0	12.0
FA-1 Average:		4.8	8.6	10.0	12.8	14.0
FA-2 Average:		4.6	8.5	9.1	9.9	11.4
FA-3 Average:		4.5	8.3	8.9	11.0	12.9
Overall Average:		4.64	8.48	9.33	11.26	12.77
Standard Dev.:		1.26	0.52	0.83	1.84	2.43
SEM:		0.30	0.12	0.19	0.43	0.57
Maximum:		7.7	9.4	11.0	15.0	17.0
Minimum:		3.0	7.4	7.5	7.8	8.6

Figure C – 9: Recorded resistivity measurements throughout testing period for Mix No. 3 containing 4 bars.

Measurement of the acid soluble chloride content of hardened concrete by the RCT method 2 BAR CONTROL

Report #: _____ **Structure:** _____ **Project:** _____

Date of testing: _____ **Electrode #:** _____ **Person:** _____

Testing Lab: _____ **Address:** _____ **Phone:** _____

RCT

HARDENED CONCRETE

1.5 gram of concrete dust dissolved in a RCT-1023 vial with 10 milliliter of extraction liquid

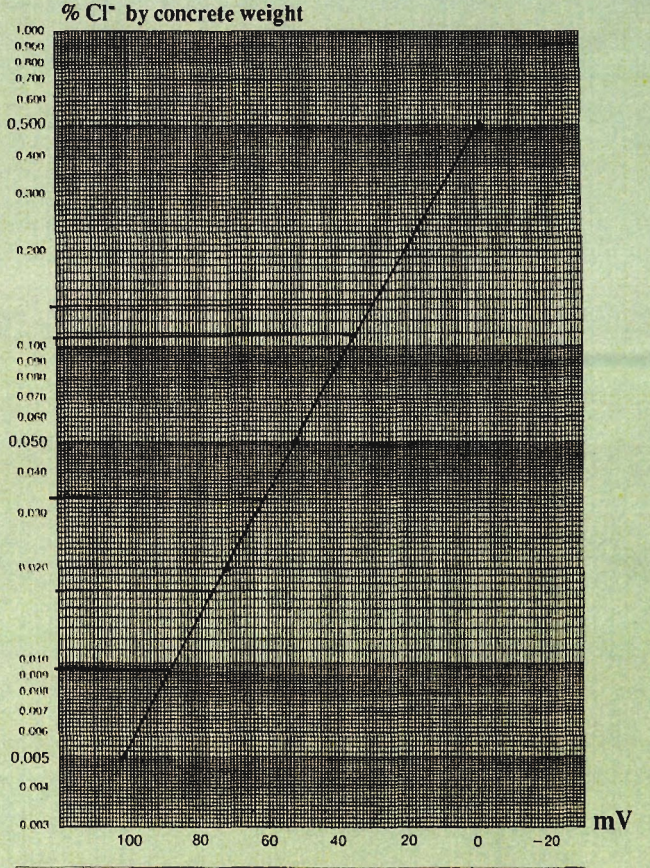

CALIBRATION:

Liquid	Clear	Purple	Green	Pink
% Cl	0.005	0.020	0.050	0.500
mV before	101.5	76.5	52.3	-4
mV after				

SAMPLE #	1		2		Remarks
	mV	% Cl	mV	% Cl	
0"	29.4	0.132			
1/4"	34.3	0.108			
3/4"	61.6	0.033			
1 1/2"	88.1	0.0099			
2"	75.5	0.017			

Figure C - 10: Typical data sheet used while conducting a chloride analysis upon a set of ponding specimens.

BIBLIOGRAPHY

AASHTO T 259 (2002). Resistance of Concrete to Chloride Ion Penetration. *American Association of State Highway and Transportation Officials,* Washington D.C.

ACI 211.1 (1991). Standard Practice for Selecting Proportions for Normal, Heavyweight, and Mass Concrete. *American Concrete Institute,* Farmington Hills, MI.

ASTM C 39 (2010). Standard Test Method for Compressive Strength of Cylindrical Concrete Specimens. *American Society of Testing and Materials,* West Conshohocken, PA.

ASTM C 78 (2010). Standard Test Method for Flexural Strength of Concrete (Using Simple Beam with Third-Point Loading) *American Society of Testing and Materials,* West Conshohocken, PA.

ASTM C 157 (2008). Standard Test Method for Length Change of Hardened Hydraulic-Cement Mortar and Concrete. *American Society of Testing and Materials,* West Conshohocken, PA.

ASTM C 469 (2002). Standard Test Method for Static Modulus of Elasticity and Poissons Ratio of Concrete in Compression. *American Society of Testing and Materials,* West Conshohocken, PA.

ASTM C 496 (2004). Standard Test Method for Splitting Tensile Strength of Cylindrical Concrete Specimens. *American Society of Testing and Materials,* West Conshohocken, PA.

ASTM C 566 (1997). Standard Test Method for Total Evaporable Moisture Content of Aggregate by Drying. *American Society of Testing and Materials,* West Conshohocken, PA.

ASTM C 617 (2010). Standard Practice for Capping Cylindrical Concrete Specimens. *American Society of Testing and Materials,* West Conshohocken, PA.

ASTM C 618 (2004). Standard Guide for Coal Fly Ash and Raw or Calcined Natural Pozzolan for Use in Concrete. *American Society of Testing and Materials,* West Conshohocken, PA.

ASTM C 876 (2009). Standard Test Method for Corrosion Potentials of Uncoated Reinforcing Steel in Concrete. *American Society of Testing and Materials,* West Conshohocken, PA.

ASTM C 1152 (2004). Standard Test Method for Acid-Soluble Chloride in Mortar and Concrete. *American Society of Testing and Materials*, West Conshohocken, PA.

ASTM C 1202 (2009). Standard Test Method for Water-Soluble Chloride in Mortar and Concrete. *American Society of Testing and Materials*, West Conshohocken, PA.

ASTM C 1543 (2010). Standard Test Method for Determining the Penetration of Chloride Ion into Concrete by Ponding. *American Society of Testing and Materials,* West Conshohocken, PA.

ASTM C 1802 (2008). Standard Test Method for Electrical Indication of Concrete's Ability to Resist Chloride Ion Penetration. *American Society of Testing and Materials*, West Conshohocken, PA.

ASTM G 16 (2010). Standard Guide for Applying Statistics to Analysis of Corrosion Data. *American Society of Testing and Materials*, West Conshohocken, PA.

A. M. Neville (1997). *Properties of Concrete.* John Wiley and Sons, Inc. (Fourth Edition).

Bargaheiser, Keith and Butalia, Tarunjit S. (2005). Prevention of Corrosion in Concrete Using Fly Ash Concrete Mixes. Department of Civil and Environmental Engineering and Geodetic Science. The Ohio State University, Columbus, OH.

Bentz, Dale P. and Ferraris, Chiara F. (2001). Rheology and Setting of High Volume Fly Ash Mixtures. *National Institute of Standards and Technology.* Gaithersburg, MD.

Bhardwaj, M.C., Batra, V.S., Sastry, V.V. (1980). "Effect of Admixtures (Calcium Chloride) on Pozzalana Concrete." *Indian Concrete Journal,* V. 54, No. 5, May, --. 134-138.

Broomfield, John P. (2007). *Corrosion of Steel in Concrete: Understanding, Investigation and Repair.* Taylor & Francis (Second Edition).

Cabrera, J. G., and Atis, C. D. (1999). "Design and Properties of High Volume Fly Ash High-Performance Concrete," *Proc., ACI Int. Conf. On High Performance Concrete and Performance and Quality Control Structures,* ACI SP-186, pp. 21-37.

Davis, R.E., Carlson, R. W., Kelly, J. W., and Davis H. E. (1937). "Properties of Cements and Concretes Containing Fly Ash," *ACI Journal, Proceedings May-June,* Vol. 33, No. 5, pp. 577-612.

Deshpande, Swapnil, Darwin, David, Browning, JoAnn, (2007). "Evaluating Free Shrinkage of Concrete for Conctrol of Cracking in Bridge Decks," *SM Report No. 89.* The University of Kansas Center for Research, Inc., Lawrence, KS.

Gu, P. and Beaudoin, J. (1998). Obtaining Effective Half-Cell Potential Measurements in Reinforced Concrete Structures. *Institute for Research in Construction, No. 18*, 1-4.

Hindy, E., Miao, B., Chaallal, O., and Aitein, P. (1994). "Drying Shrinkage of Ready-Mixed High-Performance Concrete," *ACI Structural Journal, May-Jun.*, Vol. 91, No. 3, pp. 300-305.

Hooton, Doug, R (2006). *Technical Questions - ACI Concrete Knowledge Center.* Retrieved from http://www.concrete.org/FAQ/afmviewfaq.asp?faqid=64.

Hopkins, D.S., Thomas, M.D.A., Oates, D.B., Girn, G., Munro, R. (2003). York University uses High-Volume Fly Ash Concrete for Green Building. Department of Civil Engineering, University of Toronto, Canada.

Huffman, Morris and ACI Committee 232. (2003). "Use of Fly Ahs in Concrete," *Report No. ACI 232.2R-03.* American Concrete Institute, Farmington Hills, MI.

Lane, R. O. (1983). "Effects of Fly Ash on freshly Mixed Concrete," *Concrete International,* V. 5, No. 10, October, pp. 50-52.

McDonald, David B. and ACI Committee 209. (2005). "Report on Factors Affecting Shrinkage and Creep of Hardened Concrete," *Report No. ACI 209.1R-05.* American Concrete Institute, Farmington Hills, MI.

Monfore, G.E. (1968). "The Electrical Resistivity of Concrete," *Journal of the PCA Research and Development Laboratories,* Vol. 10, No. 2, May, pages 35 to 48.

Neville A. M. (1997). *Properties of Concrete.* John Wiley and Sons, Inc. (Fourth Edition).

Office of Research, Development, and Technology, Office of Safety, RDT. (1997). "User Guidelines for Waste and Byproduct Materials in Pavement Construction," *Report No. FHWA-RD-97-148.* Federal Highway Administration, Cortest Columbus Technologies.

Philleo, R. E. (1991). "Concrete Science and Reality," Materials Science of Concrete II, American Ceramic Society, Westerville, OH. pp. 1-8.

Rhodes, James A. and ACI Committee 209. (1992). "Prediction of Creep, Shrinkage, and Temperature Effects in Concrete Structures," *Report No. ACI 209R-92.* American Concrete Institute, Farmington Hills, MI.

Sengul, O. and Gjørv, O. (2009). Effect of Embedded Steel on Electrical Resistivity Measurements on Concrete Structures. *ACI Materials Journal, 106(1),* 11-18.

Song, H., Jung, M., Lee, C., Kim, S., and Ann K. (2010). Influence of Chemistry of Chloride Ions in Cement Matrix on Corrosion of Steel. *ACI Materials Journal, 107(4),* 332-339.

Videla, Carlos C. and ACI Committee 209. (2008). Guide for Modeling and Calculating Shrinkage and Creep in Hardened Concrete. *American Concrete Institute.* Farmington Hills, MI.

Whiting, D.A. and Nagi, M.A. (2003). *Electrical Resistivity of Concrete - A Literature Review,* R&D Serial No. 2457. Portland Cement Association, Skokie, IL.

VITA

Kyle Marie Marlay was born in Fairfield, Iowa. She grew up in south central Iowa where she resided in Creston, Iowa until the age of 7 and then moved to Albia, Iowa. She moved to Clinton, Missouri at the age of 14 where she graduated in 2004 from Clinton Senior High School.

In the fall of 2004 she began her undergraduate career at University of Missouri – Rolla. She was a member of Kappa Delta Sorority, holding many executive council positions and a devoted musician to the band and orchestra program. She was also a member of the Kappa Kappa Psi National Honorary Band Fraternity where she helped with activities that supported the band program and also held many offices including president. For four years she helped welcome freshmen to campus and acquaint them with university programs as a Preview, Registration and Orientation (PRO) Leader. The professional societies in which she is a part of include: Architectural Engineers Institute (AEI); American Society of Civil Engineers (ASCE); and American Concrete Institute (ACI). In May 2009, she received her B.S. in Architectural Engineering from Missouri University of Science and Technology.

In December 2010 she was inducted into Chi Epsilon Honor Society. Her graduate studies were pursued at Missouri University of Science and Technology where she hopes to receive a M.S. in Civil Engineering in August 2011.